Predicting Preferential Flow and Mitigating Agrochemicals in the Vadose Zone

A Dissertation

Presented to the Faculty of the Graduate School

of Cornell University

in Partial Fulfillment of the Requirements for the Degree of

Doctor of Philosophy

by

Bahareh Hassanpour Guilvaiee

August 2019

Predicting Preferential Flow and Mitigating Agrochemicals in the Vadose Zone

Bahareh Hassanpour Guilvaiee, Ph.D.

Cornell University 2019

Nutrients and herbicides leach through drainage tiles to water bodies and degrade their quality. Denitrifying bioreactors reduce the nitrate from these tiles. In this dissertation, the removal of nitrate and atrazine by the denitrifying bioreactors is explored. Additionally, the preferential transport of herbicides in structured soils is examined and simulated.

In a 3-year field study, nitrate removal was examined in six bioreactors at three field locations. On average, bioreactors removed 50% of the nitrate. In each site, there was a critical hydraulic retention time (HRT), above which nitrate was removed entirely. Below this critical HRT, there was a linear relationship between nitrate removal and HRT, which varied with temperature and site locations.

Next, removal of atrazine by the woodchip (W) and woodchip amended with 50% biochar (WB) was studied in laboratory bioreactors in four HRTs. The first-order rate of the removal of atrazine for W and WB bioreactors were 0.007/h and 0.024/h, respectively. On average, biochar amendment increased atrazine removal by 40%. We determined that removal of atrazine was abiotic and hydroxyatrazine was the main degradation product in the anaerobic bioreactors.

In addition, we investigated the effect of biochar on the removal of nitrate by the woodchip bioreactors with 0%, 12.5%, 25%, and 50% biochar amendment. We measured nitrate, nitrite, carbon dioxide, and nitrous oxide and found that biochar, exposed to atmospheric oxygen, reduced nitrate removal by 9 to 13%, while increasing carbon dioxide production. We, thus, concluded that biochar acted as an electron acceptor.

Lastly, we tested a parameter efficient preferential flow model (PFM) to estimate the breakthrough of atrazine and 2,4-D in structured soils and compared it with field measurements from multiple samplers. The PFM divides soil profile to the top distribution zone which delivered the chemicals to the conveyance zone below, where several flow paths exist. Using chloride tracer, we estimated hydrological parameters of PEM. Then, by including adsorption and degradation rates, PFM successfully simulated the preferential flow of herbicides with R^2 varying from 0.59 to 0.99.

BIOGRAPHICAL SKETCH

Bahareh Hassanpour Guilvaiee was born in Rasht. She attended Urmia University where she received a Bachelor of Science Degree in Agricultural Engineering in 2007. Her mentors and professors at Urmia University helped Bahar follow her interests and encouraged her to pursue graduate studies. After taking fourth place in the national entrance exam for graduate school, Bahar worked for her master's degree at the University of Tehran. During this time, Bahar worked in a consulting firm where she estimated evapotranspiration in watersheds of Iran. Later in 2009 she was admitted to a Ph.D. program at the University of Tehran and became interested in transport phenomena in soils, especially preferential flows of chemicals.

Subsequently, Bahar contacted Professor Tammo Steenhuis, one of the pioneers of preferential flow modeling. She joined Cornell as a visiting scholar in 2013 during which time Bahar became interested in the advanced research in soil and water conducted under Professor Steenhuis' supervision. She found Professor Steenhuis' lab to be a welcoming place where she felt her scientific career could thrive. She applied for admittance into a Ph.D. program under Professor Steenhuis, was granted a research assistantship, and started her Ph.D. studies in January 2014. Bahar immersed herself in research on agricultural water quality, removal of nutrients and herbicides from agricultural tile waters, and chemical transport in soils. These new and exciting research experiences confirm her desire to pursue scholarly research in the future.

To Fardad

For his passion and his patience

For he is the pillar of my strength

ACKNOWLEDGMENTS

I would like to acknowledge my advisor, Prof. Tammo Steenhuis, and all my Special Committee members— Mr. Larry Geohring, Prof. Ludmilla Aristilde, Prof. Lawrence Cathles, and Prof. Len Lion—for offering guidance and support throughout my Ph.D. Specifically, I thank Tammo for giving me the opportunity and for giving me the independence to pursue my research interests. I thank him for helping me to grow personally and professionally. I could not have had a better supervisor. I thank Mr. Larry Geohring for supporting my research and directing me toward conducting applied research. I thank Prof. Aristilde for welcoming me into her lab, teaching me everything I know about liquid chromatography and mass spectrometry, and chemistry and providing me with future opportunities. I thank Prof. Cathles for contributing immensely to my professional development. Finally, I thank Prof. Lion for teaching me the chemistry with which I was able to construct my research.

I would like to express my gratitude to all members of the Soil and Water Laboratory. The Soil and Water Laboratory is a welcoming place of friendship and collaboration. I extend my special appreciation to Prof. Todd Walter, Dr. Brian Richard, Dr. Shree Giri, Mr. Steve Pacenka, for their advice, proofreading, and ideas. I would like to thank Sheila Saia, Chelsea Morris, Cathelijne Stoof, Christian Guzman, and Elizabeth Kreitinger for being sources of inspiration. I also would like to thank Daniel F. May for his help.

I thank the wonderful staff of the Department of Biological and Environmental Engineering for their kind assistance. I thank Doug Caveney and Karl Pendleton for their

help in constructing my experimental set-up. I acknowledge the help of Peggy Stevens, Jeff Carmichael, Theresa Lagasse, and Brenda Marchewka.

I wish to acknowledge funding from USDA NIFA Hatch Accession #231333, USDA NIFA Northeast SARE# GNE17-151-31064, USDA NIFA hatch Accession# 1004349, and NRCS- Conservation Innovation Grant (CIG) 67-3A75-13-215 which supported my research. Also, I wish to thank the Upper Susquehanna Coalition for their collaboration via NRCS CIG Grant 69-2C31-2-316.

Finally, I offer my sincere thanks to my family and friends who supported me throughout my life; to my late dad Ahmad Hassanpour, who always believed the world would be a better place for his daughters, to my mom, Razieh Javan, who taught me that with hard work and perseverance everything is within reach, and my sisters, Tahereh, Reyhaneh, and Mehraneh (Hamideh) for their care, love and support in every decision in my life. My appreciation for Lola and Alex Winter for their support and love during my Ph.D. studies. My deepest love and gratitude to my husband, Fardad, who left his job and came across the ocean with me, kept me going through the stressful moments and took long weekend trips with me to the field sites.

TABLE OF CONTENTS

LIST OF FIGURES

LIST OF TABLES

CHAPTER 1:

INTRODUCTION

1.1 Motivation

Nutrients (as fertilizers) and herbicides, used on agricultural lands, are transported to surface and ground waters (Gaynor et al., 1992; Burkart and James, 1999; Mayer et al., 2002; David et al., 2003; Guzzella et al., 2006; Malone et al., 2014). Agriculture is recognized as one of the main sources of nitrate in rivers and lakes (Mayer et al., 2002; Galloway et al., 2004). Excess nitrate in drinking water is tied to blue baby syndrome or methemoglobinemia and other health issues (Manassaram et al., 2006). In addition, excess nitrate can contribute to the production of algal blooms, which subsequently may produce toxins and unpleasant odors. Thus, excess nitrate adds to the cost of treatment for public water supplies (EPA, 2015). Furthermore, with the decomposition of the blooms oxygen depletes from water leading to hypoxia such as that in the Gulf of Mexico (Burkart and James, 1999; Smith et al., 1999). The low oxygen zones and their area in the oceans keep expanding (Breitburg et al., 2018), posing a great danger to marine habitats, impairing economic and food security of those who rely on fisheries and tourism. Indeed, nutrient pollution is the main reason for the degradation of water quality in the US (EPA, 2015).

Exposure to high levels of herbicides impacts the plant species in drainage ditches (Saunders et al., 2013), although the exposure may be short-lived. These plants play crucial ecosystem roles, including removal of nutrients through uptake or sediment deposition

(Kröger et al., 2011; Taylor et al., 2015). Additionally, herbicides can be detrimental in wetlands and reservoirs. Two of these herbicides are atrazine and 2,4-D.

Atrazine's impact on aquatic life was summarized in a review by Graymore et al. (2001). Even at low concentrations, atrazine can limit the growth of phytoplankton, zooplankton, and aquatic plants, as well as the development and swimming patterns of fish. In mammals and humans, atrazine causes chromosomal abnormalities. Some sources classified this herbicide as a possible carcinogenic compound (Sass and Colangelo 2006), although, the United States Environmental Protection Agency (EPA, 2006) recognized it as "not likely to be carcinogenic to humans". The EPA has set a drinking water standard as low as 3 µg L^{-1} for atrazine (EPA, 1995). Another widely used herbicide, 2,4-D, can also be detrimental to fish, amphibians, soil biota, and aquatic plants (Islam et al., 2018).

Given the harmful role that nitrate and herbicides play in the ecosystem functions, it is important to investigate their fate and removal. Since tiles are a distinct outlet point of groundwater to surface waters, measures can be implemented to mitigate the harmful effect of agricultural chemicals leached to groundwater (Clement, 2016). In the current study, we targeted the removal of nitrate and atrazine from the tile waters. In addition, the preferential transport of herbicides atrazine and 2,4-D to the lower layers in soils was investigated.

1.2 Objectives

Given the mobility of nitrate, and herbicides in the soils, we aimed to investigate their removal from tile effluents using woodchip denitrifying bioreactors. It is also important to predict the expected concentrations in the tile lines. With this information, **our first objective** was to characterize the nitrate removal by the field denitrifying

bioreactors. By constructing 6 bioreactors at three field locations, we investigated their removal of nitrate with respect to temperature and flow rate.

Second, we focused on atrazine removal by the woodchip denitrifying bioreactors. The co-removal of atrazine and nitrate requires a simple, low-cost, *in-situ* technique which secures their removal in short hydraulic retention times. For this purpose, we employed laboratory and field experiments using woodchip and woodchip+ biochar as substrate and investigated nitrate and atrazine removal.

Third, we conducted research to describe the discrepancies that were observed on the effect of biochar on nitrate removal in denitrifying bioreactors. We employed field and laboratory experiments to achieve this objective.

Finally, we modeled the preferential flow of herbicides, atrazine, and 2,4-D using a simple multi-region model. As a pathway for the chemicals to reach groundwater and tile lines, preferential flow plays an important role in the degradation of water resources. Although nowadays preferential flow is recognized amongst soil scientists, there is not a simple model to describe it with minimal input parameters.

In the next section, we introduce the dissertation, and briefly described the chapters that are included.

1.3 Background

Tile lines are important sources of the agrochemical contaminants such as nutrients and herbicides to the receiving water bodies (Blann et al., 2009; Williams et al., 2015; Tsaboula et al., 2019). After the application, these chemicals are transported with the flow of water to the lower layers in soil and to the tile lines. The transport of chemicals in soils

takes place through soil matrix and soil macropores. Nitrogen (N) is usually well distributed in soils. Thus is transported through the matrix typically as nitrate (Kladivko et al., 2004). While herbicides applied on the soil surface are transported through both matrix and preferential pathways, with preferential flow playing a crucial role (Shalit and Steenhuis, 1996; Vryzas, 2018). The following sections describe the appearance of nitrate and herbicides in tile lines.

1.3.1 Nitrate in Tiles

Nitrogen (N) is an essential nutrient for the crop's growth and function. Thus, to increase crop yield, it is supplied by fertilizer. The N not utilized by the plants leaches to deeper layers typically as nitrate, since it is mobile in soils. Nitrate is transported primarily through matrix flow from the root zone to the lower soil profile and therefore, to shallow groundwater (Mohanty et al., 1998; Gentry et al., 1998; Kladivko et al., 2004; Marjerison et al., 2016).

Installation of tiles is a common agricultural practice to prevent waterlogged conditions in the field. As a result, denitrification reduces. Thus, the streams of the tile-drained watersheds have greater nitrate concentrations (Jaynes et al., 1999; David and Gentry, 2000). Williams et al., (2015) found between 44 and 82% of the total nitrate export to the receiving waters was from the tile drains.

Tile drain nitrate-N concentrations (NO_3^-—N) are typically greater than 10 mg L^{-1} (Kladivko et al., 2004; Lavaire et al., 2017), varying with field management practices, crop, and season. Randall et al. (2003) observed concentrations of 10 to 40 mg L^{-1} over 4 years

in a field with corn-soybean rotation. Tile NO_3^-—N load can comprise 10-13% of the input N fertilizer (Ernstsen et al., 2015).

1.3.2 Atrazine in Tiles

Atrazine ($C_8H_{14}ClN_5$: 1-chloro-3-ethylamino-5-isopropylamino-3,4,6-triazines) is the second most commonly used herbicide in the United States (Atwood and Paisley-Jones, 2017). It kills broad-leaved weeds by attacking chloroplasts and inhibiting photosynthesis (Shimabukuro and Swanson, 1969). The usage of atrazine is banned in the European Union due to its contamination of groundwater (Sass and Colangelo, 2006). However, atrazine is still used in the United States where it is found in the groundwater throughout the year, especially in agricultural areas. In streams, the greatest concentration is detected in the spring season when heavy rain follows spraying (David et al., 2003; Gilliom, 2007). Atrazine is moderately mobile in soil because it has a soil organic carbon-water partition coefficient (K_{oc}) of ~ 100 $cm^3\ g^{-1}$. However, the K_{oc} can range from 26 to 1680 $cm^3\ g^{-1}$ depending on the type of organic matter present (Ma and Selim, 1996; Ahmad and Rahman, 2009). Literature suggests that degradation of atrazine is slow for two reasons: 1) atrazine is not a bioavailable source of organic carbon, and 2) atrazine is not a good source of nitrogen since agricultural drainage water contains bioavailable nitrogen sources (Chung et al., 1995; Ro and Chung, 1995; Katz et al., 2001). In soils, varied half-lives of atrazine were reported ranging from 22 d to 146 d (Issa and Wood, 2005; Gilliom et al., 2006). The common atrazine metabolites in soil and groundwater are hydroxyatrazine, atrazine desethyl, atrazine desisopropyl, and atrazine desethyl desisopropyl. Of these degradation

products, hydroxyatrazine is the only product that is not phytotoxic (Graymore et al., 2001; WHO, 2010).

Atrazine applied to agricultural lands percolates mainly through preferential pathways to shallow groundwater to agricultural tile lines (Steenhuis et al., 1990; Rothstein et al., 1996; Warnemuende et al., 2007; Shipitalo et al., 2016). In New York State, Rothstein et al., (1996) found that atrazine concentration in tile drains after the application was 34.5 μgL^{-1}. The annual mean concentration in tile drains in clay soils in Ontario, Canada varied from 6 to 16 $\mu g\ L^{-1}$ (Gaynor et al., 1992). In other studies, concentrations of atrazine in tile drains were observed ranging from 0.1 to 30 $\mu g\ L^{-1}$ (Steenhuis et al., 1990; Kladivko et al., 1991; Buhler et al., 1993; Gentry et al., 2010). David et al. (2003) showed that tile drains were one of the major contributors to atrazine in streams by finding concentrations of 15 and 17 $\mu g\ L^{-1}$ in streams of a predominantly tile-drained agricultural watershed.

1.3.3 2,4-D in Tiles

2,4-D (2,4-Dichlorophenoxyacetic acid) is one of the major herbicides used in the United States. It used for killing broad-leaved weeds in the agricultural field, sports grounds, and urban areas (Islam et al., 2018). The half-lives of 2,4-D vary from 7 d in terrestrial aerobic environments, to 45 d in aquatic environments 321 d in anaerobic aquatic environments (EPA, 2005). 2,4-D is mobile in soil with small affinity to soil organic matter (K_{oc} ~ 61.7; EPA, 2005). In addition, preferential flow impacts its transport to the tiles. Shalit and Steenhuis (1996) observed concentrations of 2,4-D in agricultural tile lines varied from 10 to 400 $\mu g\ L^{-1}$. The high concentrations were attributed to the

preferential flow in conventional till plots. Others also observed such high concentrations in lower layers. Tindall and Vencill (1995) observed 2,4-D concentrations up to 100 µg L^{-1} in suction cup samplers placed at 100-130 cm deep. King and Balogh (2010) reported concentrations from 0.07 µg L^{-1} to 75 µg L^{-1} in drainage channels, where direct spray may have contributed to the high concentrations.

1.3.4 Use of Organic Matter for the Removal of Nitrate and Atrazine in tiles

Adverse effects of spraying atrazine and the application of nitrogen have led to research to determine how to remove these compounds before they enter surface waters. Since atrazine and nitrate are often co-present in agricultural drains, simultaneous removal of both would be advantageous. Previous research focusing on the removal of both recommended two sequential bioreactors, anaerobic to remove nitrate, and a subsequent aerobic to degrade atrazine (Hunter and Shaner, 2010). Others suggested specific bacterial species to remove both atrazine and nitrate (Katz et al., 2001). The latter technique was not applicable due to contamination with other denitrifying bacteria. Thus, the simultaneous removal of both contaminants is challenging.

1.3.4.1 Nitrate Removal

The ideal way to remove nitrate from water is through denitrification since its final product is the harmless non-reactive N_2 gas. Denitrification is the reduction of NO_3^-—N through the following path: $NO_3^- \rightarrow NO_2^- \rightarrow N_2O \rightarrow N_2$. This process requires an organic carbon as an electron donor as followed:

$$4/5\ H^+ + CH_2O + 4/5\ NO_3^- \rightarrow CO_2 + 2/5N_2 + 7/5H_2O$$

Designing a self-sustained system to provide organic matter for the in-situ denitrification was a challenge until Boussaid et al. (1988) used a mixture of straw and maerl for groundwater nitrate removal. Six years later, Blowes et al. (1994), suggested woodchips as the electron donor for tile nitrate removal. Since then, woodchip has been a popular substrate because of its cost-effectiveness, hydrological properties, and longevity (Christianson and Schipper, 2016). Under saturated conditions, organic matter can provide an oxygen-deprived environment for denitrification (Greenan et al., 2009; Warneke et al., 2011b).

Woodchip denitrifying bioreactors were used successfully in the United States, Canada and New Zealand (Schipper and Vojvodić-Vuković, 1998; Driel et al., 2006; Christianson et al., 2011c, 2012b; Bock et al., 2016; Christianson and Schipper, 2016; Pluer et al., 2016). Research on the characterization of nitrate removal by these bioreactors and their environmental impacts continues until today. These studies include testing different organic substrates such as wheat straw, hardwood, softwood and biochar (Soares and Abeliovich, 1998; Warneke et al., 2011c; Bock et al., 2018; Coleman et al., 2019). In addition, research continues on their performance under varied field conditions such as under transient flow of stormwater (Pluer et al., 2019). In chapter 2 of this dissertation, we discuss the application of denitrifying bioreactors under varied field conditions.

1.3.4.2 Atrazine Removal

The adsorption of atrazine to natural soil organic matters and soil organic amendments is well documented (Dunigan and McIntosh, 1971; Hance, 1974; Lima et al., 2010). A wide range of organic matter including plants' remains such as woodchips and

humic substances or the product of pyrolysis of organic substances such as charcoal, biochar and activated carbon can adsorb atrazine (Cao et al., 2011; Chefetz, 2003; Delwiche et al., 2014; Ghosh et al., 2001; Ilhan et al., 2011; Lupul et al., 2015; Spokas et al., 2009). Although biochar has a great capacity for adsorption of atrazine, its surface can be altered by sorption of other organic matters, such as peat, and its atrazine adsorption capacity is reduced (Wang, 2005; Delwiche et al., 2014). Chapter 3 of this dissertation is dedicated to the reduction of agrochemicals nitrate and atrazine by denitrifying bioreactors using woodchip as substrate and biochar as an amendment to woodchip.

1.3.5 Modeling Preferential Flow of Herbicides

Transport models are important in that they provide information about the expected concentrations of agrochemicals in the tile lines or groundwater. This information is essential for the assessment of their environmental impacts and developing removal measures (Kladivko et al., 1991). It is now accepted that classical transport models assuming uniform flow are often incapable of describing the solute transport in soils. This is because natural soil has macropores and structural cracks, where water and chemical can transport with minimal resistant (Rothstein et al., 1996; Gerke, 2006; Zhang et al., 2015). Thus, preferential flow happens when flow through a portion of pores bypasses the soils matrix. It also happens in fine over course-textured sand as finger flow (Hill and Parlange, 1972; Selker et al., 1992; Steenhuis et al., 2013). The occurrence of preferential flow does not allow interaction of herbicide such as adsorption or degradation in soils. As a result, herbicides are often detected in groundwater and tile lines (Steenhuis et al., 1990; Kladivko et al., 1991; Shalit and Steenhuis, 1996; Torrentó et al., 2018).

Early preferential flow models described unstable wetting front such as in layered sandy soils (Hill and Parlange, 1972). Since then, researchers focused on models that can consider macropores. This has led to developing models that consider two flow domains. These models are called dual-porosity and dual-permeability models. The difference between these two types of models is that the latter considers water flow and chemical transport in both macropores and matrix, while dual-porosity models only consider flow and transport occurrence in macropores (Simunek et al., 2003; Gärdenäs et al., 2006). To date, most preferential flow models have been tested in laboratory columns, and field experiments are rare (Gärdenäs et al., 2006; Köhne et al., 2009a). Evidence, however, points to more than two flow paths in the soils (Gwo et al., 1995).

Multi-region models better represent the porous media. However, multi-region models require additional input data that are poorly defined (Wu et al., 2004; Zhang et al., 2018). Therefore, a basic simple-minded approach is needed for such conditions. In 2004, Kim et al. (2005) presented a multi-region model which described the preferential flow of chloride in laboratory columns. With some modification for adsorption and degradation, we fitted this preferential flow model (PFM) to field herbicide data in chapter 5.

1.4 Organization and Summary of Chapters

Following this introduction, in four chapters, we describe our field and laboratory experiments and modeling the transport of herbicides. Each chapter includes an introduction, material and methods, results, discussion, and conclusion.

Chapter 2 describes the field data obtained from six denitrifying bioreactors over three years. In this chapter, we aimed to characterize nitrate removal based on

environmental factors. A relationship between hydraulic retention time and the removal of nitrate for each site was presented. In addition, we discussed our observations unique to NY State.

In chapter 3, we investigate the removal of atrazine by denitrifying bioreactors. We presented the result of our laboratory experiment on the removal of atrazine by the woodchip and woodchip amended with biochar bioreactors. We conducted a kinetic study by considering four hydraulic retention times and varied influent nitrate concentrations and measured atrazine and its degradation products at the effluent. In addition, we report on the removal of atrazine in field woodchip bioreactors.

Chapter 4 is dedicated to the effect of biochar amendment on nitrate removal in the denitrifying bioreactors. Given the observed discrepancies in the literature regarding the effect of biochar on nitrate removal of the bioreactors, we used an integrated water and gas sampling approach to understand the effect of biochar on nitrate removal.

Finally, in chapter 5, we show how the preferential flow model (PFM) can describe the preferential flow of the atrazine and 2,4-D in field samplers. We compared the simulated and observed values and discussed the model's advantages and shortcomings.

CHAPTER 2:

SEASONAL PERFORMANCE OF DENITRIFYING BIOREACTORS IN THE NORTHEASTERN UNITED STATES: FIELD TRIALS

Adapted from: Hassanpour, B., S. Giri, W.T. Pluer, T.S. Steenhuis, and L.D. Geohring. 2017. Seasonal Performance of Denitrifying Bioreactors in the Northeastern United States: Field Trials. J. Environ. Manage. 202: 242–253.

2.1 Abstract

Denitrifying bioreactors are increasingly being used for nitrate (NO_3^-—N) removal from agricultural drainage water. Filled with carbon substrates, often woodchips, denitrifying bioreactors provide a favorable anaerobic environment for denitrification. Despite performing well in loess soils in the Midwestern United States, field bioreactors have not yet been evaluated in shallow soils over glacial till that are characteristic for the Northeastern United States. This study, therefore, investigates the performance of bioreactors and provides design criteria for shallow soil with flashy discharges.

Paired bioreactors, one filled with woodchips and one with a mixture of woodchip and biochar, were installed in tile-drained fields in three landscapes in New York State. The bioreactors were monitored for a three-year period during which, the flow rate, temperature, NO_3^-—N, sulfate ($SO_4^{2-} - S$) and dissolved organic carbon (DOC) were measured. Results showed that the average NO_3^-—N removal efficiency during the three years of observations was about 50%. The NO_3^-—N removal rate ranged from 0 in winter to 72 g d^{-1} m^{-3} in summer. We found that biochar was only effective during the first year

in enhancing denitrification due to aging. An index for carbon availability related to NO_3^-—N removal was developed. During winter, availability of the DOC was a limiting factor in bioreactor performance. Finally, to aid in the design of bioreactors, we developed generalizable relationships between the removal efficiency and hydraulic retention time and temperature.

2.2 Introduction

Anthropogenic nitrogen loading, especially from the use of excess fertilizers in agriculture, contributes to coastal hypoxia such as the dead zone in the Gulf of Mexico (Burkart and James, 1999). Some nitrogen is subject to denitrification or can accumulate as organic nitrogen in the root zone (Van Meter et al., 2016). However, it leaches to the streams with groundwater fluctuations (van Verseveld et al., 2009). To decrease the NO_3^-—N load from agricultural fields, denitrifying bioreactors are an economical, practical, and ecologically-friendly remediation approach to remove NO_3^-—N from agricultural drains by providing an anaerobic environment and organic carbon for the denitrification process (Elgood et al., 2010; Schipper et al., 2010; Christianson et al., 2013a). Original studies of this concept in Ontario, Canada (Blowes et al., 1994) and North Island, New Zealand (Schipper and Vojvodić-Vuković, 1998) formed the foundation for the use of denitrifying bioreactors, and the work in the United States during the last ten years has accelerated its implementation with a nearly exponential growth in published research (Addy et al., 2016; Christianson and Schipper, 2016).

Denitrifying woodchip bioreactors are made by routing drainage water through a buried trench filled with woodchips as a carbon source (Blowes et al., 1994; Bock et al.,

2016). The efficiency of bioreactors on NO_3^-—N removal depends on carbon availability, temperature, hydraulic retention time (HRT), and NO_3^-—N availability (Warneke et al., 2011b). Increasing temperature accelerates the denitrifying activity (Robertson et al., 2008; Elgood et al., 2010; Warneke et al., 2011c). In addition, dry periods in bioreactors have been reported to make more carbon available (Woli et al., 2010). In some cases, biochar has been added to bioreactors to enhance denitrification, although Christianson et al., (2011) found no significant difference in removal by adding biochar to woodchips. Biochar, a product of thermal decomposition of biomass (Singh et al., 2009; Lehmann et al., 2011), alters the nitrogen cycle by increasing the microbial population (Anderson et al., 2014b; Xu et al., 2014) through providing a "co-location" for carbon, microorganisms, and nutrients which leads to increased carbon use efficiency and microorganism activity (Lehmann, et al., 2011). Hence, additional research is warranted on the effect of biochar on the removal of NO_3^-—N in drainage water, especially under actual field conditions.

Although denitrifying bioreactors have been recommended for reducing NO_3^-—N losses in the Midwest (Christianson and Schipper, 2016), their efficiency is still being investigated in other regions with different soils and climatic conditions (Chun et al., 2009; Schipper et al., 2010; Christianson et al., 2011a, 2012a, 2013b; Warneke et al., 2011c). These conditions include those of the northeastern United States, where the presence of a hardpan at shallow depth in the glacial till limits the amount of water that the soil can hold (Neeley et al., 1965; Pearson et al., 1973; French et al., 1978). Due to limited water holding capacity, drainage discharge from these soils increases rapidly during times of large precipitation events compared with the Midwest (Lesaffre and Zimmer, 1989; Dahlke et al., 2012), affecting hydraulic retention time (HRT) and NO_3^-—N inputs. In addition, the

long winters limit the performance of the denitrifying bioreactors, but to what degree has not been studied well under field conditions in the Northeast US.

The design of denitrifying bioreactors should be fine-tuned to take the specific soil and climate factors into consideration. This study, therefore, field tests bioreactor performance for NO_3^-—N removal and discusses how the design should be tailored to soil and climatic conditions in the Northeast.

2.3 Materials and Methods

Six (in pairs) denitrifying bioreactors were constructed on farms in three counties, Tompkins, Chemung, and Steuben in upstate New York (Figure S2-1) to test their effectiveness in removing NO_3^-—N from agriculture tile lines.

2.3.1 Denitrifying Bioreactor Design

Bioreactors were excavated with the appropriate length, width, and depth dimensions to allow a retention time of 6 h for the estimated flow rate that would not be exceeded 80% of the time. This was followed by placing a plastic or geotextile liner around the bioreactors. Next, an AgriDrain® inline water level control structure with a weir was put in the inflow of the bioreactor to divert the flow to the bioreactor. In addition, the weir allowed the water to bypass the bioreactor (Figure S2-2). Thus, by measuring the water height above the gate, the bypass flow was calculated. The outflow structure was also used to maintain the water level in the bioreactor by setting the weir level. Similar to the inflow structure, a weir allowed measurement of the flow rate through the bioreactor (Christianson and Helmers, 2011). Solid plastic pipes connected the control boxes to the bioreactors,

where they transitioned to perforated pipes within the bioreactor (Figure S2-2). The bioreactors were then filled with wood chips or woodchips amended with biochar (Table 2-1) and covered with the liner and then leveled with the surrounding area by soil.

The woodchips used for all sites were obtained locally from a lumber mill and were primarily from ash (*Fraxinus ornus* sp.) trees. The average woodchip length was about 3 cm. The biochar was obtained from Biochar Now® and was a woody feedstock blended chip mostly of pine (*Pinus* sp.) origin with a particle length typically around 1-2 cm. The biochar was produced by slow pyrolysis at temperatures between 550 °C and 600 °C. To inoculate the media with denitrifying bacteria, the lower portion of the bioreactors was amended with 0.5 m^3 of soil taken from the hyporheic zones from the adjacent streambed. These zones are known to be enriched in denitrifying bacteria (Anderson et al., 2014).

2.3.2 Site Description

2.3.2.1 Tompkins County Site

The pair of bioreactors were installed in October 2012 at the Homer C. Thompson Vegetable Research Farm, Tompkins County, New York. Soils in the drainage area were mostly gravelly loam which received only inorganic fertilizer during the period of investigation. The bioreactors were 19 m^2 and filled with 1 m depth of woodchips and were enclosed with a polyethylene impermeable liner from North Plastics® (Table 2-1). In one of the bioreactors, the woodchips were amended with 10% biochar (WB) (Table 2-1).

A 250 m long interceptor drain at the base of a sloping area, drained groundwater into the two denitrifying bioreactors, although it may have drained from the root zone when it was saturated. Figure S2-3 shows the schematic of the field and the drain. The inlet weir

was set at a high elevation; therefore, high flows went to the bioreactor. Sampling began in March 2013 soon after the water level control gates, and V-notch weirs were installed to divert tile drain flow into the bioreactors. The outlet weir depth was set to maintain a minimum water depth of 0.5 m within the bioreactor.

Bi-weekly sampling and manual readings of water levels of the inlet and outlet started in April 2013. In 2014 (April to November), water temperatures at the inlet of the bioreactors were recorded every 5 minutes using a Watchdog ™ temperature logger fabricated by Spectrum Technologies, Inc. and water head was measured using a water level logger, Telog PR-31 from Telog Instruments Inc. Starting in April 2015 both temperature and water levels were recorded in the inlet and outlet structure with three HOBO® U20 water level loggers from Onset Computer Corporation. Water levels were used to calculate the flow rate with the standard weir equations (Table 2-1). Weather data was provided by a Cornell weather station on site.

2.3.2.2 Chemung County Site

Constructed in June 2013, the two bioreactors at the Chemung site received tile flow water from a cornfield on a dairy farm (Figure S2-4). Manure was applied in spring and late fall on the silty loam soils of the drainage area. The bioreactors were identical in construction to those at the Tompkins site, using the same source of woodchips, biochar, and impermeable liner (Table 2-1). However, the WB surface area was 1.8 times greater than the W bioreactor. In addition, the flow could bypass the bioreactor when the water level in the inlet control box exceeded the weir set at 1 m above the bottom of the bioreactor. The weir in the outlet was set to maintain around 0.5 m flow depth within the

bioreactor. Three HOBO® U20 water level loggers from Onset Computer Corporation were placed at the inlets and outlets of the bioreactors to measure temperature and water level in different periods (July to November 2014 and April to August 2015). At other times, the water head was measured during each bi-weekly sampling event. The discharge for the inflow and outflow was calculated using rating curves (Table 2-1). The water level at the inlet weir was used to calculate the bypass flow and the water level at the outlet weir was used for the discharge through the bioreactors. Weather data was obtained from a station 16 km away.

Table 2-1 Characteristics of the bioreactors

Site	construction date	Media+ %biochar by volume‡	Dimension L×U×D¶ (m^3)	Liner specification	Drainage area (ha)	n*	Weir type and equation H (cm) Q ($L\ s^{-1}$) †
Tompkins	Oct 2012	W	6.1×3.1×0.5	North Plastics® 5 mil polyethylene	4	62	V notch weir $Q = 0.0108H^{2.3151}$
		W+10%B	6.1×3.1×0.5				
Chemung	June 2013	W	6.1×3.1×0.5	North Plastics® 5 mil polyethylene	5	46	Rectangle weir $Q = 0.3255H^{1.4856}$
		W+10%B	7.6×4.5×0.5				
Steuben	July 2013	W	6.7×3.6×0.5	Woven Geotextile Fabric 200 liners	6	45	Rectangle weir $Q = 0.3255H^{1.4856}$
		W+2%B	7.6×4.5×0.5		9		

‡ the W is the woodchips only bioreactor, and WB is the biochar amended bioreactor
¶ Length (L), Width (U), and Depth (D) of the bioreactors. Depth of the trench for all bioreactors is 1.5 m, and the average drain depth in the field is 1 m.
* n is the number of sampling events
† H is the water head above the weir and Q is the discharge

2.3.2.3 Steuben County Site

The third set of two bioreactors was located at the outlets of two different drainage systems on the edge of a corn and forage field that received manure several times during the growing season. These two drainage systems collected water from a silt loam soil overlying shallow bedrock (Figure S2-5). The WB bioreactor at this site contained 2% biochar (Table 2-1). These bioreactors were lined with permeable W200 Geotextile from Granite Environmental® (Table 2-1). Therefore, surface water and shallow groundwater infiltrated into these bioreactors. High tile discharges bypassed the bioreactor when the water level was in excess of inlet weir height set at 1 m above the bottom of the bioreactor. The water level was recorded using Telog PR-31 from Telog Instrument Inc. at two different periods (June to November 2014 and April to November 2015). The weather data was obtained from a station 12 km away from the site. Manual water level recordings were taken during the biweekly sampling (Table 2-1).

2.3.3 Sampling and Analysis

Bi-weekly duplicate samples were collected in 125 ml low-density polyethylene bottles from both the inlet and the outlet of the bioreactors except during the coldest winter periods when the bioreactors were frozen. Table 2-1 shows the number of sampling events. The samples were transported to the laboratory in an iced cooler and immediately filtered. The filtered samples were stored at 4 °C and analyzed for NO_3^-—N, sulfate ($SO_4^{2-} - S$) and DOC concentrations. The NO_3^-—N and $SO_4^{2-} - S$ content was measured using a Dionex ICS-2000 Ion Chromatograph (Pfaff, 1993a). The DOC was analyzed using an O.I. analytical® TOC 1010 analyzer (Potter and Wimsatt, 2009).

For most of the sampling period, probes were used to report the water temperature flowing to the bioreactors, as stated in the previous sections. However, since these probes were not present throughout the entirety of the sampling period or at all sites, a temperature model by McCann et al., (1991) as adapted by Brisson et al., (1998) was used to estimate missing data. Additional description is reported elsewhere (Hassanpour et al., 2016). The snowmelt was estimated using "EcoHydRology package" in the R programming language (Fuka et al., 2015) and was added to the rainfall values obtained from the weather station data.

2.3.4 Data Analysis

The NO_3^-—N concentrations and the flow rate were used to calculate NO_3^-—N removal efficiency, HRT, and NO_3^-—N removal rate. The NO_3^-—N removal efficiency, ε_{NO_3} was calculated as

$$\varepsilon_{NO_3^- - N} = \frac{C_{NO_3,in} - C_{NO_3,out}}{C_{NO_3,in}} \quad (2\text{-}1)$$

where $C_{NO_3,out}$ is the NO_3^-—N concentration in the effluent and $C_{NO_3,in}$ is the NO_3^-—N concentration in the influent.

Hydraulic retention time (HRT) was estimated as

$$HRT = \rho \frac{Ad}{Q} \quad (2\text{-}2)$$

where A is the surface area of the bioreactor (m^2), d is the active height of water in the bioreactor (m), Q is the discharge ($m^3\ h^{-1}$), and ρ is the effective porosity of the media (Christianson et al., 2011a). Effective porosity of woodchips is 0.6 (Robertson, 2010). This media porosity was verified using subsamples of the woodchips. Occasionally at the

Tompkins and Steuben sites, the flow ceased during summer months. For those specific events, when no flow was observed, the number of days since the last day it rained was considered as the HRT. Such consideration was not pertinent for the Chemung site, since at this site, a continuous flow was observed.

The removal rate of $NO_3^- - N$, r_{NO_3} was calculated as

$$r_{NO_3^- - N} = \frac{C_{NO_3,in} - C_{NO_3,out}}{HRT} \quad (2\text{-}3)$$

Student's t-tests were used to test for significant differences between NO_3^-—N concentrations in the inlet and outlet of the bioreactors and between W and WB bioreactors. Confidence levels were set at 95% (p values <0.05). Small p-values indicate that there is strong evidence against null hypothesis. Null hypothesis is that the mean of the groups are not different.

2.4 Results

2.4.1 Rainfall and Discharge

The records combined precipitation and snowmelt, manually measured and continuously measured discharge at the Tompkins site bioreactors are shown in Figure 2-1a. The annual precipitation at the Tompkins site over the study period (2013-2015) varied between 858 mm y^{-1} and 990 mm y^{-1} with 2013 being the wettest, especially during the summer. The annual rainfall in 2015 was 47 mm less than the 100-year annual precipitation average. At the Tompkins site, the tile inflow (Figure 2-1a) was high during the spring and ceased in summer. Since the bypass weir in the inflow structure was set at a high elevation, and the bioreactors were in a flood-prone area, the bioreactors became occasionally

submerged (referred to as "*flooded*" in the Figure 2-1a) every year despite being a wet or dry year.

The annual amount of rainfall at in the Chemung site ranged from 888 to 911 mm y^{-1} throughout the period of investigation (2013 to 2015), with 2014 being the wettest year. At this site, the tile-drained the regional groundwater and interflow from adjacent hillslopes resulting in a relatively continuous flow year around, which increased during spring (Figure 2-2a). In spring, some of the increased flow bypassed through the inlet, thereby maintaining a more constant flow in the bioreactor. Thus, the amount of flow diverted into the bioreactors remained relatively uniform, typically less than 1 L s^{-1} (Figure 2-2a). Although, in 2014, the wettest year, a flood event was observed. The flow through the larger bioreactor, WB (Woodchips amended with biochar), was greater than that of the W (woodchips only) bioreactor but the average retention times for the WB and W bioreactors were 0.3 and 0.5 d, respectively (Table 2-2).

At the Steuben site, the year with the least amount of rainfall (933 mm y^{-1}) was 2014 (Figure 2-3a) and the wettest year was 2015, with 986 mm y^{-1}. The inflow to the bioreactors was highly variable, and bypass flow occurred more frequently than at the other two sites, bypassing 35% and 37% of the drain flow (Table 2-2 and Figure 2-3a). The limited water holding capacity of the shallow soil led to highly fluctuating flow, which bypassed frequently. Furthermore, surface runoff occasionally ponded near the bioreactors and this may have also infiltrated through the permeable geotextile liner used at this site. There were two flood events in 2015, the wettest year.

Table 2-2 Average discharge (Q), bypass(Q'), average hydraulic retention time ($\overline{\mathrm{HRT}}$), saturated volume ($\overline{\mathrm{SV}}$), NO_3^-—N concentration and removal efficiency ($\varepsilon_{NO_3^- - N}$), NO_3^-—N removal rate ($r_{NO_3^- - N}$), dissolved organic carbon ($\overline{DOC}$) and standard error (SE) at the inlets and outlets of the bioreactors.

Site and Bioreactor		Q ‡ L s^{-1} ±SE	Q'¶ (%)	$\overline{HRT}$ ¥ d	$\overline{SV}$ m^3	NO_3^-—N Concentration mg L^{-1} In ± SE	Out ± SE	$\varepsilon_{NO_3^- - N}$	$r_{NO_3^- - N}$† $gNm^{-3}d^{-1}$	$\overline{DOC}$ mgL^{-1} In± SE	Out± SE
Tompkins	W	0.2± 0.04	0	2.2	10.2	9.3 ± 0.4 a *	5.1 ± 0.5 b	42	3.8	4.9± 0.8 a	20± 7 b
	WB	0.1± 0.01		2.1	10.1		4 ± 0.4 c	55	4.7		6.4± 0.7 b
Chemung	W	0.29± 0.03	4	0.5	9.6	6.2 ± 0.5 a	2.7 ± 0.6 b	68	13.5	6.05± 1.4 a	8.8± 1.1 b
	WB	0.56± 0.03		0.3	17.6		2.6 ± 0.6 b	66	15.1		9.6± 1.8 b
Steuben	W	0.33± 0.08	35	2.8	12.2	18.4 ± 2.7 a	9.9 ± 2.7 b	58	4.7	13.7± 3.9 a	50.3± 10 b
	WB	0.44± 0.09	37	2.3	17.4	16.6 ± 1.4 a	6.4 ± 1.6 b	62	6.7	5.3± 0.5 a	34.1± 6 b

‡ Values are from the manually measured events and do not include the flood events
¶ From the continuous measurements
¥ Average of the individual events
†Removal rate values do not include flood and NO_3^-—N limited events (effluent NO_3^-—N < 0.5 mg L^{-1})
*Different letters in each row indicate statistically distinct groups (Paired *t*-test at $p < 0.05$)

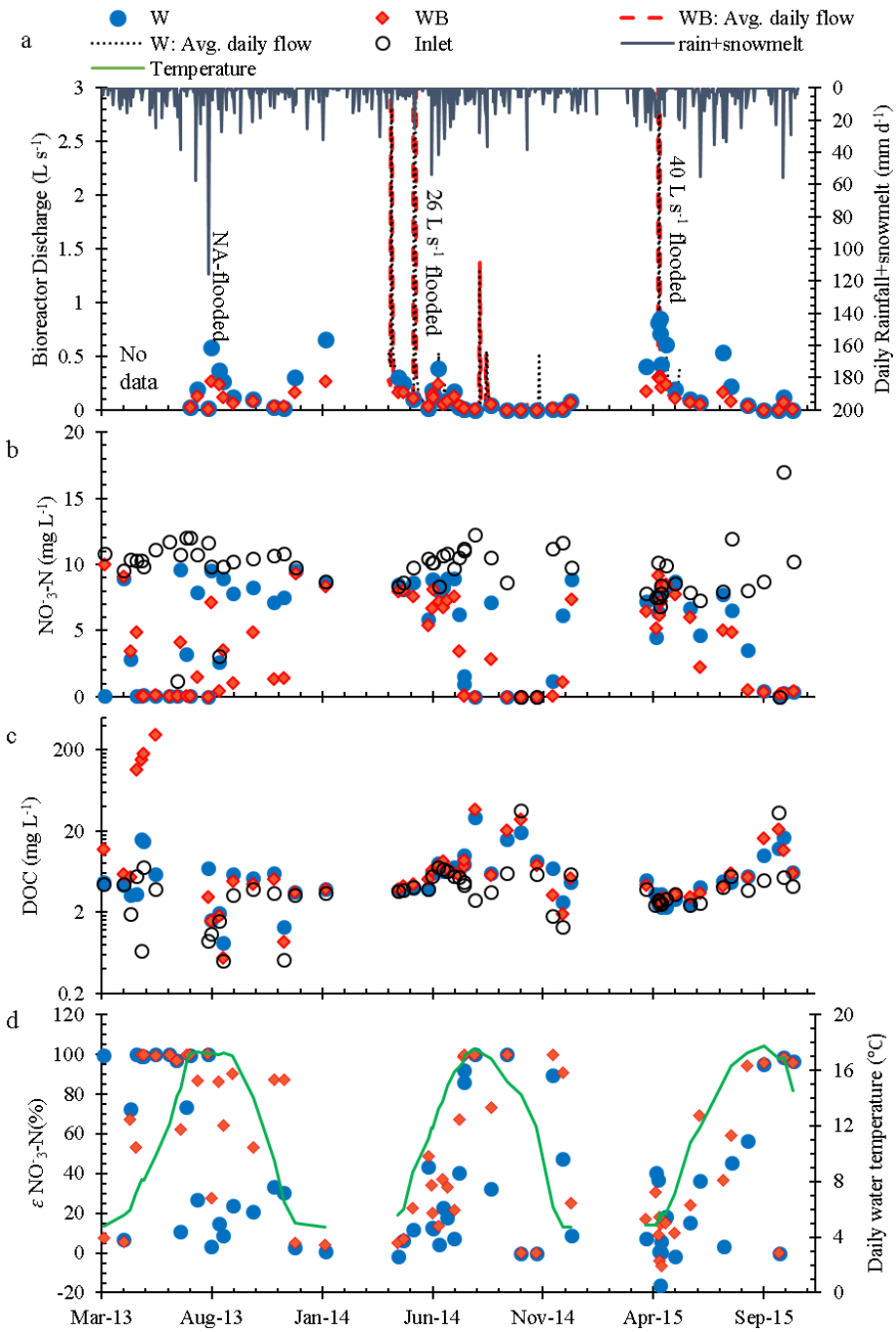

Figure 2-1 a) Discharge from the woodchips (W) and woodchips amended with biochar (WB) bioreactors and combined daily rainfall and snowmelt (blue hanging bars) at the Tompkins site. Both manually measured (symbols) and continuously measured (lines) are shown; b) NO_3^-—N concentrations in the influent (open black symbols) and effluent (closed blue dots and red diamonds) of the bioreactors; c) DOC concentrations in the influent (open black symbols) and effluent (closed blue dots and red diamonds) of the bioreactors; d) temperature (green line) and NO_3^-—N removal efficiency ($\varepsilon_{NO3^-—N}$) of the bioreactors (closed blue dots and red diamonds).

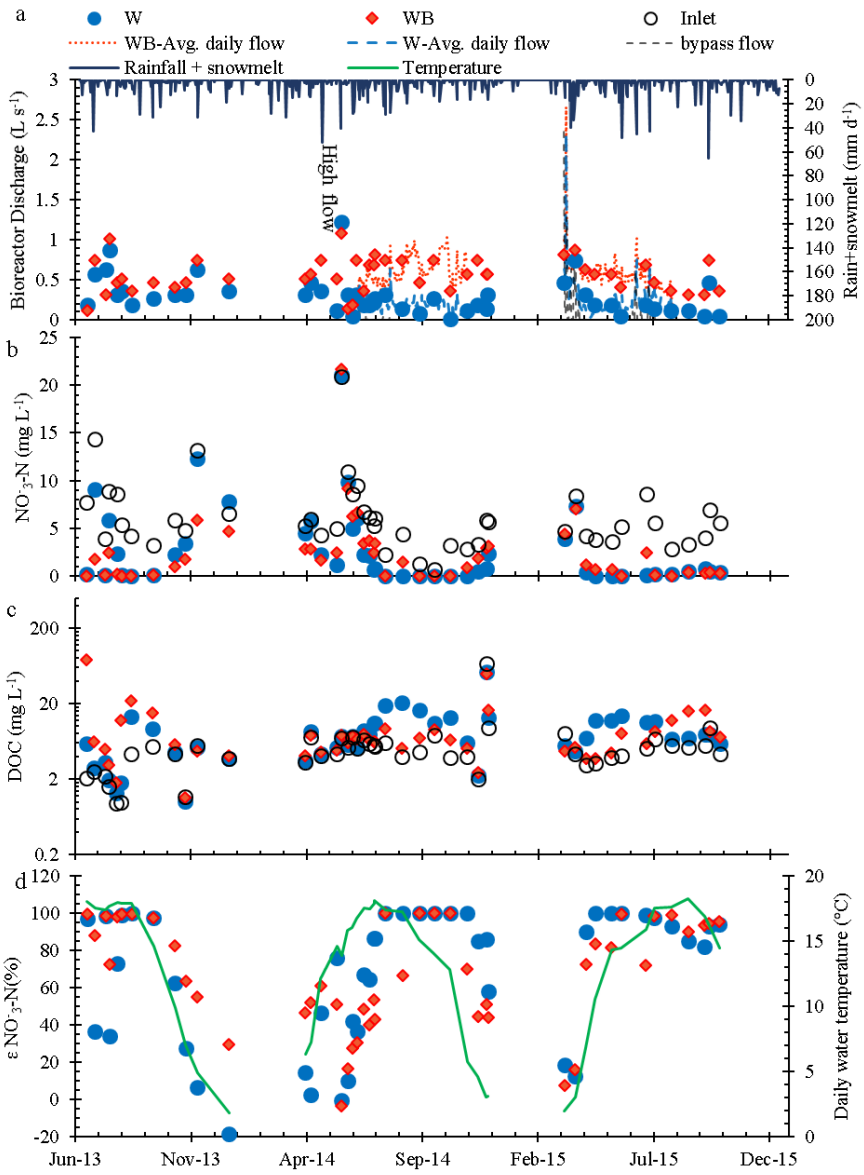

Figure 2-2 a) Discharge from the woodchips (W) and woodchips amended with biochar (WB) bioreactors and combined daily rainfall and snowmelt (blue hanging bars) at the Chemung site. Both manually measured (symbols) and continuously measured (lines) are shown; b) NO_3^-—N concentrations in the influent (open black symbols) and effluent (closed blue dots and red diamonds) of the bioreactors; c) DOC concentrations in the influent (open black symbols) and effluent (closed blue dots and red diamonds) of the bioreactors; d) temperature (green line) and NO_3^-—N removal efficiency ($\varepsilon_{NO3^-—N}$) of the bioreactors (closed blue dots and red diamonds).

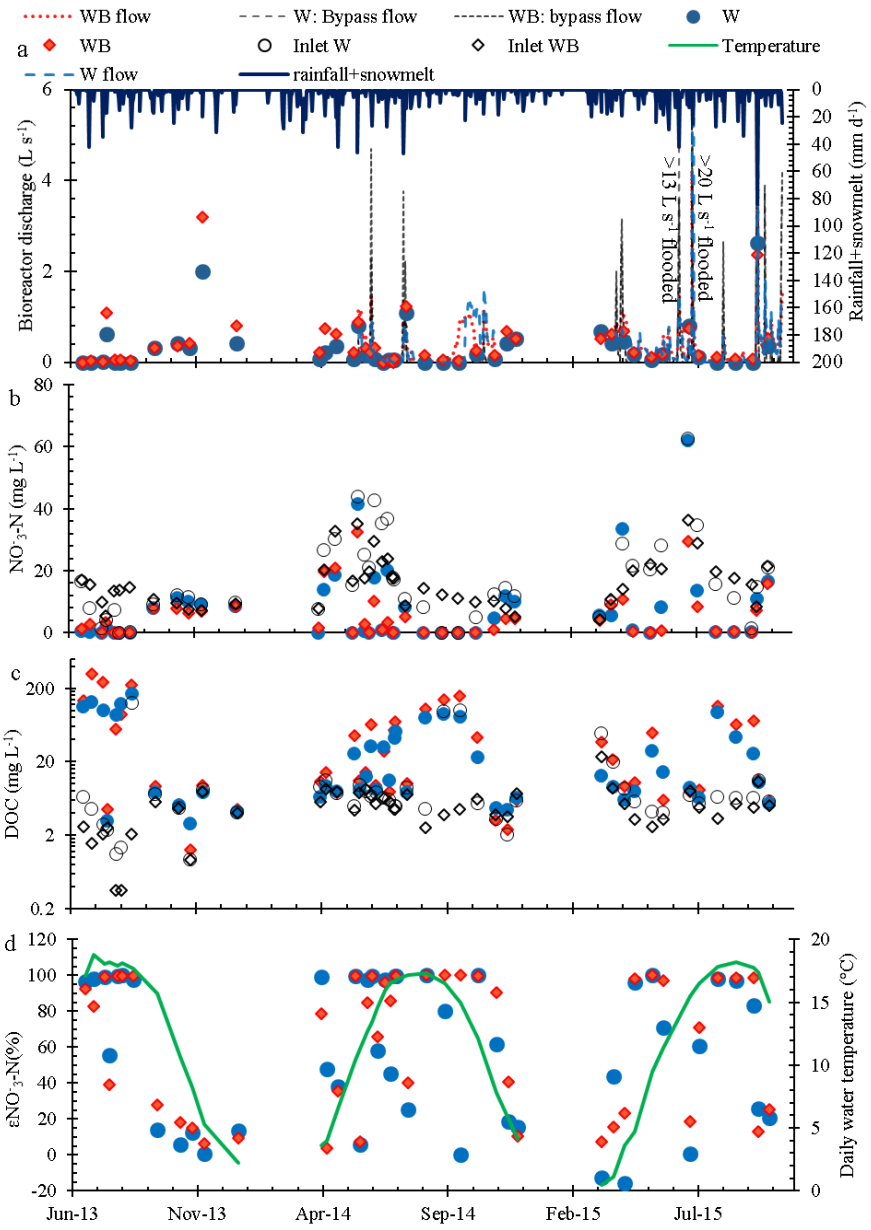

Figure 2-3 a) Discharge from the woodchips (W) and woodchips amended with biochar (WB) bioreactors and combined daily rainfall and snowmelt (blue hanging bars) at the Steuben site. Both manually measured (symbols) and continuously measured (lines) are shown; b) NO_3^-—N concentrations in the influent (black open symbols) and effluent (closed symbols) of the bioreactors; c) DOC concentrations in the influents (open symbols) and effluent (closed symbols) of the bioreactors; d) temperature (green line) and NO_3^-—N removal efficiency ($\varepsilon_{NO3^-—N}$) of the bioreactors (closed symbols).

2.4.2 Nitrate-N Concentrations

The NO_3^-—N concentrations in the tile water flowing to the bioreactors at the Tompkins site were generally about 10 mg L^{-1}, the least variable of all sites (Table 2-2; Figure 2-1b). They were insensitive to changes in temperature and discharge events. This implies that the source of the drain discharge at the Tompkins site was deep, old, and well-mixed groundwater (Van Verseveld et al., 2008). The effluent NO_3^-—N concentrations of the bioreactor ranged from 0 to 10 mg L^{-1} (Figure 2-1b). Both low temperatures (in winter) and early spring increased discharge caused effluent NO_3^-—N concentrations to increase to around 8 mg L^{-1}. Only during the summer and early fall when temperatures were elevated, and flow was generally low, effluent NO_3^-—N concentrations were close to zero. Shortly after starting up, the bioreactors were less effective in removing the NO_3^-—N after a high flow event in mid-August 2013, even with temperatures over 17 °C (Figure 2-1b). Despite this, the bioreactors at this site significantly reduced the NO_3^-—N concentrations ($p = 3.8\times10^{-14}$ for the Woodchips only (W) and 2.4×10^{-10} for the woodchips amended with biochar (WB)).

The average NO_3^-—N drain concentration at the Chemung location, 6 mg L^{-1}, was less than that of the other two sites (Table 2-2, Figure 2-2b). The influent NO_3^-—N concentrations ranged from 0.7 to 21 mg L^{-1} and increased when the flow peaked (Figure 2-2b). Regardless of the variation, the bioreactors at this site significantly reduced the NO_3^-—N concentrations ($p = 1.7\times10^{-14}$ and 6.6×10^{-14} for the W and WB bioreactors, respectively; Table 2-2, Figure 2-2b). The effluent NO_3^-—N concentrations ranged from 0 to 21 mg L^{-1} (Figure 2-2b), which elevated at early spring when the low temperatures

coincided with the high flow rates. They decreased with increasing temperatures except after a high flow event in June 2014.

Influent and effluent NO_3^-—N concentrations at the Steuben site were the greatest and the most variable among all bioreactors (Table 2-2, Figure 2-3b). Inlet NO_3^-—N concentrations increased from 4 mg L^{-1} in March, peaked to 62 mg L^{-1} in late spring and early summer, and decreased to 11 mg L^{-1} at the beginning of fall with manure application on the field and subsequent storm events (Figure 2-3b). The effluent NO_3^-—N concentrations, especially for the WB bioreactor, were high when both the influent concentrations and the flow rates were high (Figure 2-3b). Increased NO_3^-—N concentrations at the effluent of the reactors such as that observed in April of 2015 in W bioreactor were rarely observed. One of the complicating features of this site was the surface ponding and water might have infiltrated from the surface into the bioreactor, potentially diluting the concentration. Similar to the other two sites, Steuben site bioreactors had significantly lower effluent NO_3^-—N concentrations than in the influent ($p = 4.9\times10^{-8}$ and 4.5×10^{-12} for the W and WB bioreactors, respectively; Table 2-2, Figure 2-3b).

2.4.3 Organic Carbon Concentration

For all bioreactors, the effluent DOC concentrations were significantly greater than influent DOC concentrations (Table 2-2, Figures 2-1c, 2-2c, 2-3c), similar to the findings of Cameron and Schipper (2010) and Robertson (2010). Immediately after startup, the greatest DOC effluent concentrations were observed at all sites with the maximum concentrations of more than 200 mg L^{-1} at Tompkins and Steuben sites (Figures 2-1c and

2-3c). Under such conditions, all NO_3^-—N was removed from water (corresponding events in Figures 2-1d, 2-3d). For instance, at the Tompkins site on April 2013, when the water temperature was only 7 °C, and the DOC concentration in the effluent was 200 mg L^{-1}, the removal efficiency was 100% (Figures 2-1c, 2-1d).

After high concentration at the startup period, a seasonal pattern in DOC concentrations was observed in the effluent at all three sites. At the Tompkins site, the influent DOC concentrations generally remained below 5 mg L^{-1}, although they increased to more than 40 mg L^{-1} in September of 2014 and 2015, about the time of the first frost (Figure 2-1c). The effluent concentrations varied from 0.5 to 22 mg L^{-1} (Figure 2-1c). In winter and early spring, when temperatures were less than 10 °C (Figure 2-1d), inflow and outflow concentrations were nearly equal, and the removal efficiencies were low (Figure 2-1d). During the warm summer, the effluent DOC concentration was generally greater than the influent DOC concentrations and most influent NO_3^-—N was removed (Figures 2-1b, 2-1d), except for after the high flow events which were especially obvious in 2013 (Figures 2-1a, 3-1c).

Similarly, at the Chemung and Steuben sites, the amount of DOC released by the bioreactors was low in winter and early spring, peaked in the summer month, except during the times when the bioreactors were flooded (Figures 2-2c, 2-3c). Despite having the same woodchip media for all the bioreactors, the released DOC from the bioreactors at the Steuben site was greater than the other two sites (Table 2-2, Figure 2-3c).

2.4.4 Seasonal Pattern of the Nitrate-N Removal Efficiency

The water temperature at the Tompkins site varied from 3 °C in early spring and late fall to 20 °C during the summer (Figure 2-1d). Generally, the maximum NO_3^-—N removal efficiency ($\varepsilon_{NO_3^- - N}$; Eq 2-1) was near 100% when the temperatures were above 16 °C and usually below 30% when temperatures were below 5 °C (Figure 2-1d). Moreover, especially in 2014 and 2015, the bioreactor efficiency increased with increasing temperature. However, reduced NO_3^-—N removal efficiencies were observed in spring and summer when the bioreactors were inundated, described as flooded in Figure 2-1a. During some events in early spring 2015, high flow increased the NO_3^-—N coming out of the bioreactors, causing the $\varepsilon_{NO_3^- - N}$ to be less than zero. In summer 2013, after a high flow event, the woodchip (W) bioreactors' efficiency decreased and remained low until the following spring (Figure 2-1d). In that period, the advantage of biochar amendment (WB bioreactor) was noticeable with over a 50% or greater $\varepsilon_{NO_3^- - N}$ (Figure 2-1d). This difference between the W and WB reactor, however, did not occur in subsequent years.

At the Chemung site, the initial removal efficiency was 100% during the summer and decreased as temperature declined (Figure 2-2d). In the following years $\varepsilon_{NO_3^- - N}$ increased with increasing temperature, peaked to 100% in summer, and dropped as temperature decreased (Figure 2-2d). However, after a large storm in June 2014, the $\varepsilon_{NO_3^- - N}$ decreased. The data loggers were not installed at that time to measure the peak discharge through the bioreactors.

The $\varepsilon_{NO_3^- - N}$ of the bioreactors at the Steuben site (Figure 2-3d), similar to the other two sites, usually followed the temperature pattern. In early spring, $\varepsilon_{NO_3^- - N}$ increased with rising temperature, reached the maximum in summer, and decreased in the following

months. Like the other bioreactors, reduced $\varepsilon_{NO_3^- - N}$ was observed when the flow increased and after the occasional flooding events.

2.4.5 Nitrite-N Concentrations

In the Tompkins site, the nitrite (NO_2^-—N) concentration of at the influent of the bioreactors varied from 0 to 0.6 mg/L, averaging at 0.05 mg L^{-1} (Figure 2-4a). The effluent NO_2^-—N concentration of the W bioreactor was 0.15 ± 0.02 mg L^{-1} (mean ± Stnd Error), and that of the WB bioreactor was 0.15 ± 0.01 mg L^{-1}, both significantly greater than that of the influent ($p<0.05$).

Similar to the Tompkins site, the NO_2^-—N concentrations of the effluent of the bioreactors at the Chemung site were significantly greater than that of the influent ($p<0.05$). In this site, the influent NO_2^-—N concentration was 0.04 ± 0.02 mg L^{-1}, and that of the effluent of the W and WB bioreactors were significantly greater at 0.15 ± 0.03 and 0.21 ± 0.03 mg L^{-1}, respectively (Figure 2-4b).

At the Steubent site, in the first sampling event, the effluent NO_2^-—N concentration of the WB bioreactor was 17.3 mg L^{-1}, the greatest NO_2^-—N concentration observed among the bioreactors, possibly due to bioreactors being newly launched. For the rest of the period, the effluent NO_2^-—N concentrations were less than 1 mg L^{-1} (Figure 2-4c). Overall, the effluent NO_2^-—N concentration of the WB bioreactor was 0.56 ± 0.37 mg L^{-1}, greater than that of the influent at 0.13 ± 0.03 mg L^{-1}, although, the differences were not significant. Similarly, at this site, the differences between the influent and effluent NO_2^-—N concentration of the W bioreactor, 0.16 ± 0.02 and 0.18 ± 0.03 mg L^{-1}, respectively, were not significant (Figure 2-4c).

The observed NO_2^-—N concentrations were usually within those observed in the denitrifying bioreactors, ranging from 0 to 1.2 mg L^{-1} except for the NO_2^-—N concentration at the effluent of the WB bioreactor in Steuben site (Figure 2-4). Warneke et al. (2011c) and Warneke et al., (2011b) observed effluent NO_2^-—N concentrations below ranging from 0 to 0.95 mg L^{-1}.

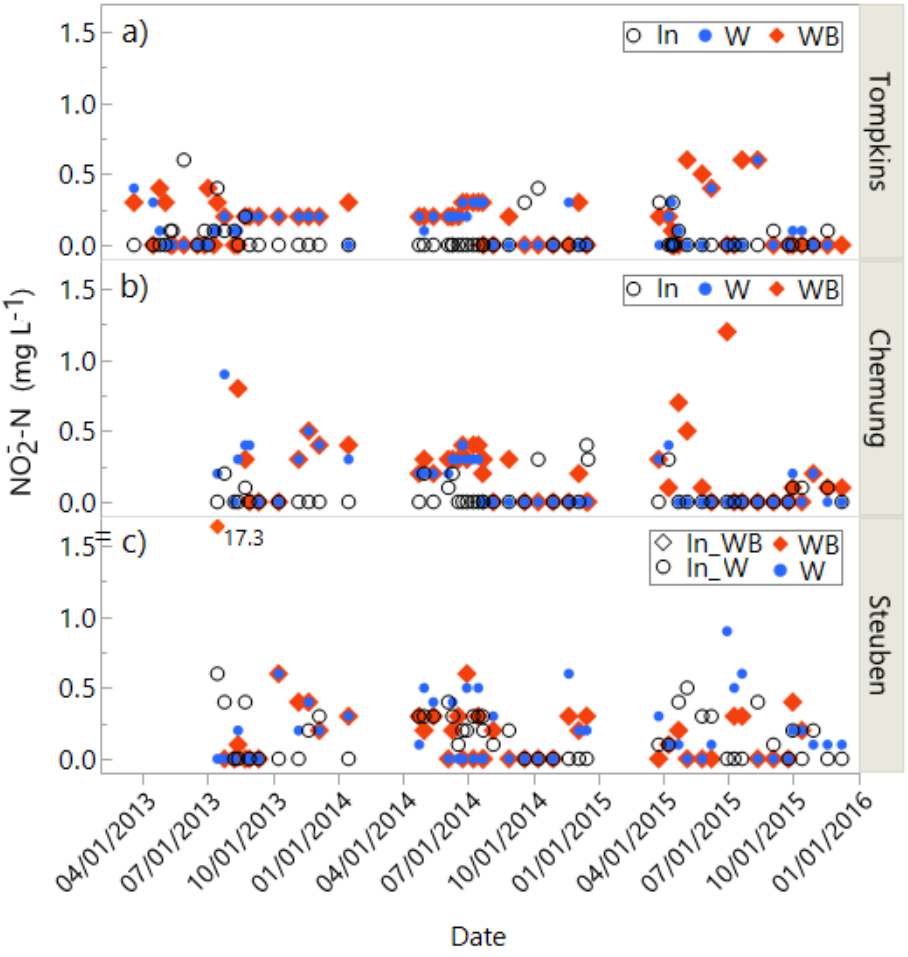

Figure 2-4 Nitrite (NO_2^-—N) concentrations at the influent (In) and effluent of the W (woodchip) and WB (woodchip+biochar) bioreactors at the a) Tompkins, b) Chemung, and c) Steuben sites.

2.5 Discussion

2.5.1 Temperature Dependent Nitrate-N Removal Rate

The NO_3^-—N removal rates ($r_{NO_3^- - N}$; Eq 2-3) for all six bioreactors are plotted as a function of the temperature of the input water in Figure 2-5. We plotted the NO_3^-—N limited events separately because in these cases, the rates were limited by the availability of NO_3^-—N.

Removal rates for the woodchip substrate usually remain less than 10 g N d^{-1} m^{-3} (Schipper et al., 2010), although in the current study, the $r_{NO_3^- - N}$ varied greatly from 0 to 73 g N d^{-1} m^{-3}. There were numerous events when the removal rates were greater than 10 g N d^{-1} m^{-3} at different temperatures. The maximum rates observed in this study were much greater than those for the woody media reported in a review by Schipper et al.(2010) of 22 g N d^{-1} m^{-3}. Nevertheless, the observed removal rates indicated a successful application of the denitrifying bioreactors.

Removal rates were not variable below 16 °C. However, they increased sharply at temperatures above 16 °C at all bioreactors, despite having been constructed in different landscapes. The sharp increase in removal rates at 16 °C could be attributed to seasonal change in the bacterial community. The seasonal variation of the microbial community may be linked to the organic carbon availability, which varies with temperature and moisture content of the bioreactors (Porter et al., 2015).

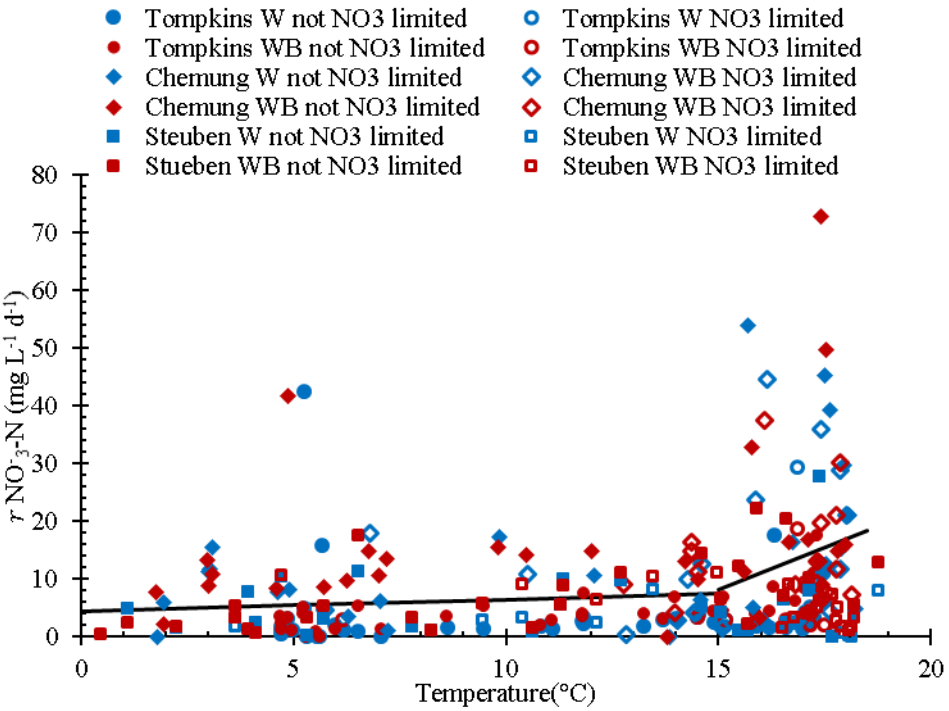

Figure 2-5 NO_3^-—N removal rate ($r_{NO_3^-—N}$) vs. temperature at all sites. "NO_3 limited events" (open symbols) are the events when the effluent NO_3^-—N concentration was less than 0.5 mg L^{-1}.

2.5.2 Carbon Availability on Nitrate-N Removal Indices

Denitrification is controlled by three factors; the presence of NO_3^-—N, presence of organic carbon as an electron donor and the absence of oxygen (Seitzinger et al., 2006; Schipper et al., 2010). For denitrification to take place, at the first step, the aerobic microorganisms use organic carbon as an electron donor to reduce the dissolved oxygen (DO) to obtain energy. By depleting DO, the anoxic environment is ideal for heterotrophic denitrification. Under these conditions, electron acceptor such as NO_3^- breaks down to oxidize organic matter and to produce energy (Korom, 1992). In both processes, organic carbon plays an important role. Indeed, a labile carbon source has a profound effect on the performance of bioreactors (Greenan et al., 2006; Cameron and Schipper, 2010). Bioavailable carbon sources appear in the forms of amino acids, carbohydrate, and other

simple organic compounds (Zou et al., 2005). Regardless, a young carbon source, such as that in the studied bioreactors, was bioavailable (Chapelle et al., 2009). Therefore, DOC concentrations were used as an indicator of the bioavailable carbon.

Figure 2-6 shows that NO_3^-—N removal efficiency ($\varepsilon_{NO_3^- - N}$) and DOC availability index are linked. In the abundance of nitrogen, DOC leachate decreased, whereas, in nitrogen-limited conditions, the DOC concentrations in the effluent were elevated (Figure 2-6). This is in agreement with the observation previously made in landscapes (Lai et al., 2016). Since the DOC is generated in the bioreactors and concentrations in the effluent were generally greater than those at the influent (Table 2-2, Figures 2-1c, 2-2c, 2-3c), the ratio of the DOC concentration in the inlet to that in the outlet was considered, and the DOC availability index was acquired as $1\text{-}C_{DOC,in}/C_{DOC,out}$.

Similar to temperature dependent removal rate, all six bioreactors behaved the same. When the DOC availability index was > 0.5, the released organic matter exceeded the amount needed to complete denitrification, and $\varepsilon_{NO_3^- - N}$ was greater than 0.8. The $\varepsilon_{NO_3^- - N}$ decreased sharply when the DOC availability index dropped from 0.5 to 0. Finally, sometimes when the inlet concentrations were greater than those of the outlet, which occurred following manure applications, NO_3^-—N removal improved possibly because inflow DOC was bioavailable to the denitrifying bacteria (Figure 2-6). This graph suggests that with sufficient carbon, NO_3^-—N was removed independently of other factors such as temperature. Indeed, at the start-up period at the Tompkins site, despite low temperature, complete removal of NO_3^-—N occurred (section 2.4.3). Elevated DOC concentration at the start-up period is because of the rapid decay of young organic carbon (Janssen, 1984). However, over time, differentiating between the effect of temperature and DOC is difficult

because the two factors are interconnected. The decomposition of organic matter increases with increasing temperature (Paré et al., 2006) and thus, the DOC availability index increased during warmer summer months.

It is also noteworthy that although the points from different sites overlapped closely, the Chemung site bioreactors (Figure 2-6), in comparison with the other sites, experienced greater removal efficiencies relative to the DOC availability index. This is attributed to the lower inlet NO_3^-—N concentrations and maintaining equilibrium due to the continuous flow in the bioreactors at this site. This suggests that the landscape characteristics of a site should be considered when designing the bioreactors.

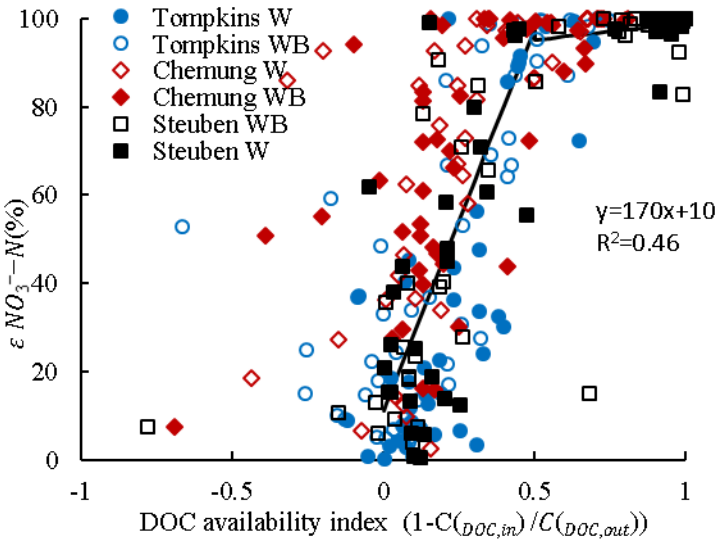

Figure 2-6 The relationship between the DOC availability index and the NO_3^-—N removal efficiency ($\varepsilon_{NO_3^-—N}$) at all sites.

2.5.3 Effect of Biochar Amendment

The size of the W and WB bioreactors were different in the Chemung site. At the Tompkins site, the discharge through the WB bioreactor was smaller, although both bioreactors had the same inlet water head (Table 2-2). Thus, the differences between the

outflow concentrations may have been due to the slower flow rate and consequently longer HRT (Figure 2-1a, Table 2-2). And the two bioreactors in the Steuben site received water from two different tiles. Therefore, the NO_3^-—N removal rate ($r_{NO_3^- - N}$; Eq. 2-3), was used to compare the W and WB bioreactors.

At all sites, the average $r_{NO_3^- - N}$ of the bioreactors containing biochar was greater than that of the woodchip bioreactors (Table 2-2). These differences, however, were not significant at all sites or during the whole period of investigation (Table 2-3). At the Tompkins site (10% biochar added to the WB bioreactor; influent NO_3^-—N concentrations of 9.3 mg L^{-1}) in the first two years of the bioreactor use, the $r_{NO_3^- - N}$ of the WB bioreactor was greater than that at the W bioreactor (paired t-test p-value < 0.002, Table 2-3). The differences were not significant during the third year and consequently, over the whole period of investigation, suggesting that the positive effect of biochar may only have been temporal. At the Chemung site (10% biochar added; influent NO_3^-—N concentrations of 6.3 mg L^{-1}) the difference was not significant during the years of investigation. However, at the Steuben site, where only 2.5% of biochar was added, the WB bioreactor had significantly greater $r_{NO_3^- - N}$ than the W bioreactor (Table 2-1). This site has the greatest influent NO_3^-—N concentrations of 18.4 and 16.6 mg L^{-1}. In general, the sites with greater NO_3^-—N concentrations benefited more from the biochar amendment.

Our finding was consistent with that of a plot scale experiment of Bock et al. (2016) that biochar was only effective in removing NO_3^-—N when the effluent concentrations exceeded 5 mg L^{-1} at lower temperatures and 10 mg L^{-1} at a higher temperature. According to Harter et al. (2014), biochar improves the NO_3^-—N removal in soils by altering pH, C:N ratio, and N and oxygen availability. The surface characteristics of biochar change in

response to a series of reactions referred as "aging" (Cheng and Lehmann, 2009; Harter et al., 2014), and evidently, this process diminished the beneficial effect of biochar amendment rather quickly. The aging process involves a decrease in carbon leachate from biochar coupled with the loss of ash and carbon content, decrease in pH and increase in cation exchange capacity (Cheng et al., 2006; Cheng and Lehmann, 2009; Heitkötter and Marschner, 2015). The abundance of organic matter in soil stimulates the aging process, likely due to an increase in biological activity (Heitkötter and Marschner, 2015). Considering the abundance of organic matter due to the presence of woodchips in denitrifying bioreactors, the aging process happened rapidly. However, Cheng et al. (2006) found that the aging of black carbon was mostly abiotic. We cannot rule out the fact that some biochar was lost through leachate since the bioreactors' effluent was dark after the initial start-up. Therefore, biochar's ash content decreased quickly after the start. Noting that the bioreactor performance was greatly influenced by the DOC concentrations and availability, the decrease in DOC availability due to the leachate of ash and aging process negatively impacted the advantage of the biochar.

Table 2-3 P-values of the t-test analysis of the NO_3^-—N removal rates between the W and WB bioreactors during the period of investigation.

Site	Whole period	2013	2014	2015
Tompkins	0.69	0.002	0.001	0.66
Chemung	0.17	0.66	0.08	0.42
Steuben	0.02	0.006	0.03	0.71

2.5.4 Effect of Hydraulic Retention Time on Nitrate-N Removal Efficiency

The relationship between NO_3^-—N removal efficiency ($\varepsilon_{NO_3^- - N}$) and hydraulic retention time, HRT, for the six bioreactors are shown in Figure 2-7 for events when the water temperature was above 16 °C and below 16 °C. Since the difference due to the addition of biochar was barely significant - section 2.5.3 - the points from the two bioreactors at each site were not separated. Less than 10% of the data were excluded from the calculations (Figure 2-7). These points comprised events when the bioreactors were flooded after which removal efficiencies were suppressed, and when some very high influent NO_3^-—N concentrations occasionally occurred. During the high and transient flow events, ammonification and nitrification of organic nitrogen may have occurred in the top portion of the bioreactors which was usually unsaturated and did not contribute to its performance, which finally lead to the negative removal efficiencies (van Verseveld et al., 2009).

A critical HRT, the minimum HRT required for reaching 100% $\varepsilon_{NO_3^- - N}$, was defined. Below this HRT, there is a linearly increasing relationship between HRT and $\varepsilon_{NO_3^- - N}$, which was observed with previous studies (Greenan et al., 2006, 2009; Chun et al., 2009; Robertson, 2010). The critical HRT was greater for low temperatures than for temperatures above 16 °C. The relationship between $\varepsilon_{NO_3^- - N}$ and HRT was similar for the Tompkins and the Steuben site (Figures 2-7a and 2-7c, both above or below 16 °C) with the Tompkins site having a larger critical HRT to reach the 100% NO_3^-—N removal than the Steuben site. At the Tompkins site, the critical HRTs were 48 and 79 h, for the temperatures above and below 16 °C, respectively. They were 24 and 61 h at the Steuben site for the temperatures above and below 16 °C, respectively. At the Chemung site, critical

HRTs were much less than the other two sites (compare Figure 2-7b with Figures 2-7a and 2-7c, note the change of scale). This suggests that the uniform flow at the Chemung site provided more stable conditions and equilibrium for the population of denitrifiers, which was accompanied with lower incoming NO_3^-—N concentrations than those at the other two sites (Hoover et al., 2016). Consequently, a wide range of the removal efficiencies was observed within a narrow range of HRT of about 4 h. The critical HRTs (to reach 100% NO_3^-—N removal) were within the range of those in other studies, such as in laboratory experiments by Greenan et al. (2009) of 5 d, and by Chun et al. (2009) of 24 h, or that in a field experiment by Christianson et al. (2013b) of approximately 31 h.

Finally, the average NO_3^-—N removal efficiency that was between 42% and 68% (Table 2-2) were within the range observed in previous field studies (Christianson et al., 2012), indicating that the bioreactors in New York state were able to perform reasonably well.

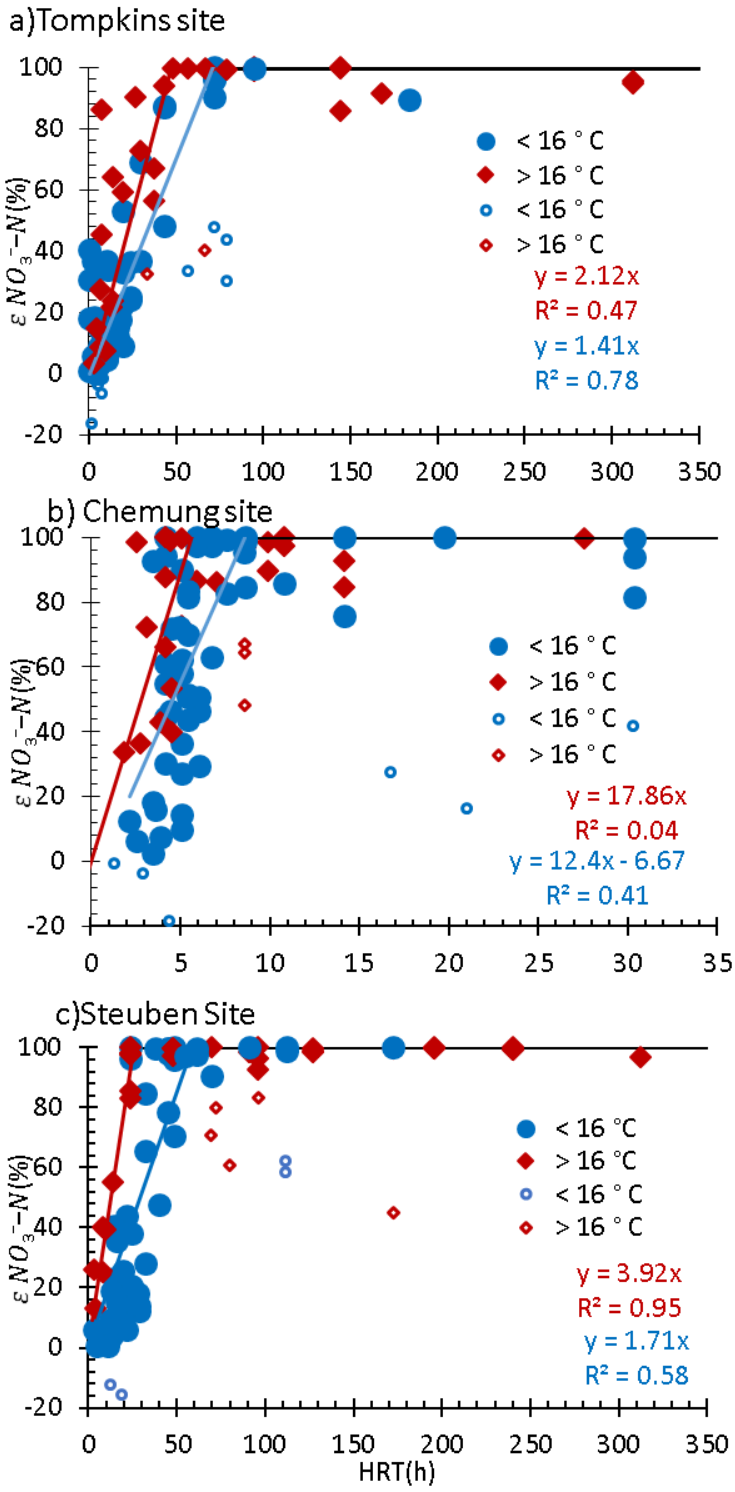

Figure 2-7 NO_3^-—N removal efficiency ($\varepsilon_{NO3^-\_N}$; %) at different HRTs at the bioreactors at a) Tompkins site, b) Chemung site, and c) Steuben site. The graphs did not separate W and WB bioreactors. The open circles were excluded from the calculations. Note that the scale of the X-axis for graph b, representing the Chemung site, is one-tenth of the other two graphs for the other two sits.

2.5.5 Performance Evaluation of Denitrifying Bioreactors in the Northeast

The design and application of denitrifying bioreactors requires an understanding of the landscape and hydrological setting of the field as well as understanding the relationship between the removal efficiency and HRT. For efficient removal of NO_3^-—N, the DO should be depleted from water. At short retention times, the DO may not be removed from the water and thus, sporadic removal of NO_3^-—N occurs. Figure 2-7 shows that at low retention times, a broad range of removal efficiencies was observed. At the Chemung site, when short retention times occurred, the sporadic NO_3^-—N removal was observed constantly (Figure 2-7). In the Tompkins and Steuben sites, the sporadic NO_3^-—N removal only occurred at shorter retention times. Therefore, to have a robust removal of NO_3^-—N, a sufficient HRT is required.

At retention times that are longer than the critical HRT, complete NO_3^-—N removal occurs. Since sulfate is usually present in the drainage water, it is a substitute for NO_3^-—N, as an electron accepter only in the absence of it (Moorman et al., 2010; Woli et al., 2010; Schipper et al., 2010). In the current study, too, the concentration of sulfate in the outflow was less than that at the inflow when NO_3^-—N was limited (Figure S2-6). In extreme reducing conditions, methane production may occur (Moorman et al., 2010). Moreover, the cost of the bioreactors increases with increase in HRT. Therefore, the complete removal of NO_3^-—N is not intended.

Christianson et al. (2013) suggested that the design procedure should use 10 to 20% of the peak flow at design HRT of 6 to 8 h, to ensure at least 30% removal at the time of peak flow. Previous to that, an HRT of 4 h was suggested as a design criterion (Christianson et al., 2011b). In the current research, the bioreactors were designed so that a discharge

equal to 20% of the estimated peak flow would be contained using the hydraulic retention time of 6 h. This design criterion was met at the Chemung site with continuous flow and lower NO_3^-—N concentrations. The continuous drain flow in deep soils (such as in the Chemung site and often in the Midwest US), help remove NO_3^-—N in the bioreactors throughout the growing season. Even at temperatures below 16 °C at the Chemung site, the critical retention time was less than 4 hours. However, at the other two sites, variable HRTs were observed (Figure 2-7). At the Steuben site, 30% of removal was acquired at 8 and 17 h at high and low temperatures, respectively. However, the steady removal of NO_3^-—N in colder temperatures occurred when the retention times were more than 21 h. At the Tompkins site, 14 and 38 h were required at high and low temperature to achieve 30% removal. These retention times were more than the retention times in which sporadic removal of NO_3^-—N was observed. The shallow soils over an impermeable glacial till or bedrock layer have a low storage capacity which leads to flow variation, high discharge during wet periods, and no flow during summer. The interceptor drain in the Tompkins site also received variable drain flows in response to seasonal fluctuations in the water table.

High flow events introduce dissolved oxygen to the bioreactors and, therefore, decrease the removal efficiency (Christianson et al., 2011c). Furthermore, extremely large flows (small observed HRT) could flush the biofilm, enzymes, and organic matter out of the media (Soares and Abeliovich, 1998; Chun et al., 2009; Bradford et al., 2013), which could have a long-term effect on the bioreactor performance. Thus, the removal efficiency was reduced for several days after high flow events (Figures 2-1, 2-2, 2-3 after each flooded event; section 2.4.4).

As an edge of field technique, constructing larger bioreactors to accommodate such variable flow events and to remove a sufficient amount of NO_3^-—N may not be applicable. Therefore, more efficient bypass or storage systems may be required to prevent damage to the bioreactors. However, more flow bypass means that the bioreactors will not be as effective overall for treating the drain discharge. This adds to the complexity of the design of the bioreactors in different landscapes. More research is required to quantify the threshold for the flow rate above which it would impair the performance of the bioreactors.

Seasonal variation of the bioreactor performance should be considered depending on the temperatures when the peak NO_3^-—N concentrations are observed. According to the Figures 2-1, 2-2, and 2-3, and an earlier study by van Es et al., (2004), the maximum NO_3^-—N concentrations from drain flows in this region usually occur during early spring or early fall, and when the temperatures were above 16 °C. Therefore, designing the bioreactor in accordance with the higher temperature relationship should be sufficient.

2.4 Conclusion

This study investigated the application of paired denitrifying bioreactors in three field sites in New York State. One of each paired bioreactor was amended with biochar. The results showed that to some extent, bioreactors could benefit from the addition of biochar. However, the biochar did not influence the bioreactor with low influent NO_3^-—N concentrations, and its effect on the bioreactor with high NO_3^-—N concentrations were only temporal.

Despite many variables in the field settings, the extensive sampling during three years of investigation at six individual bioreactors made it possible to investigate the

seasonal variation of bioreactor performance. This study provided relationships between removal efficiency and HRT for the bioreactors at different temperatures and inflow NO_3^-—N concentrations in New York.

During the study period, all the bioreactors maintained good NO_3^-—N reduction of about 50% and, therefore, the application of the denitrifying bioreactors was deemed successful. However, this study recommends more investigation on the performance of the bioreactors during and after high drainage flow. The bioreactors achieved a high removal rate and efficiency in summer, showing great potential to remove NO_3^-—N during the growing season. This could be attributed to the increased removal rate with temperature, seasonal variation in the microbial community, and availability of DOC to the denitrifiers. Following a seasonal pattern, the availability of DOC was a major factor controlling bioreactor performance.

This study found a correlation between removal efficiency and HRT. The relationships between the removal efficiency and HRT at the Tompkins site were similar to those of the Steuben site, as they both had variable discharge and high inflow NO_3^-—N concentrations. Whereas at the Chemung site, where the flow was constant at low rates and the inflow NO_3^-—N concentrations were low, the bioreactors achieved higher removal efficiency at lower HRTs. Due to these differences, a particular relationship was not found to govern all of the bioreactors. In addition, at temperatures above 16 °C, both the removal rate and efficiency in all bioreactors were elevated. Therefore, when designing new bioreactors for areas with predominantly cold temperatures, the current design standard (NRCS, 2015) might not be sufficient, as they may overestimate NO_3^-—N removal at lower temperatures. In addition, when designing bioreactors in New York State, it is essential to

consider the prevalence of extreme flow, due to the shallow soil profile and glacial tills, which overwhelms and flushes the bioreactor constituents out. A reduction of NO_3^-N removal was observed after each flooding event when the bioreactors' performance declined, sometimes for several weeks. Therefore, bioreactor design for these conditions should consider an effective bypass or additional storage system. Further investigation is needed to quantify the threshold of velocity above which bioreactor performance declines.

2.5 Acknowledgements

This research was made possible by funding from USDA NIFA Hatch Accession #231333 and NRCS- Conservation Innovation Grant (CIG) 67-3A75-13-215. Also, thanks to the Upper Susquehanna Coalition for their collaboration via NRCS CIG Grant 69-2C31-2-316, and especially to the cooperating farmers.

2.6 Supplementary Material

Figure S2-1 Location of the sites in Tompkins, Chemung, and Steuben counties in upstate New York, USA

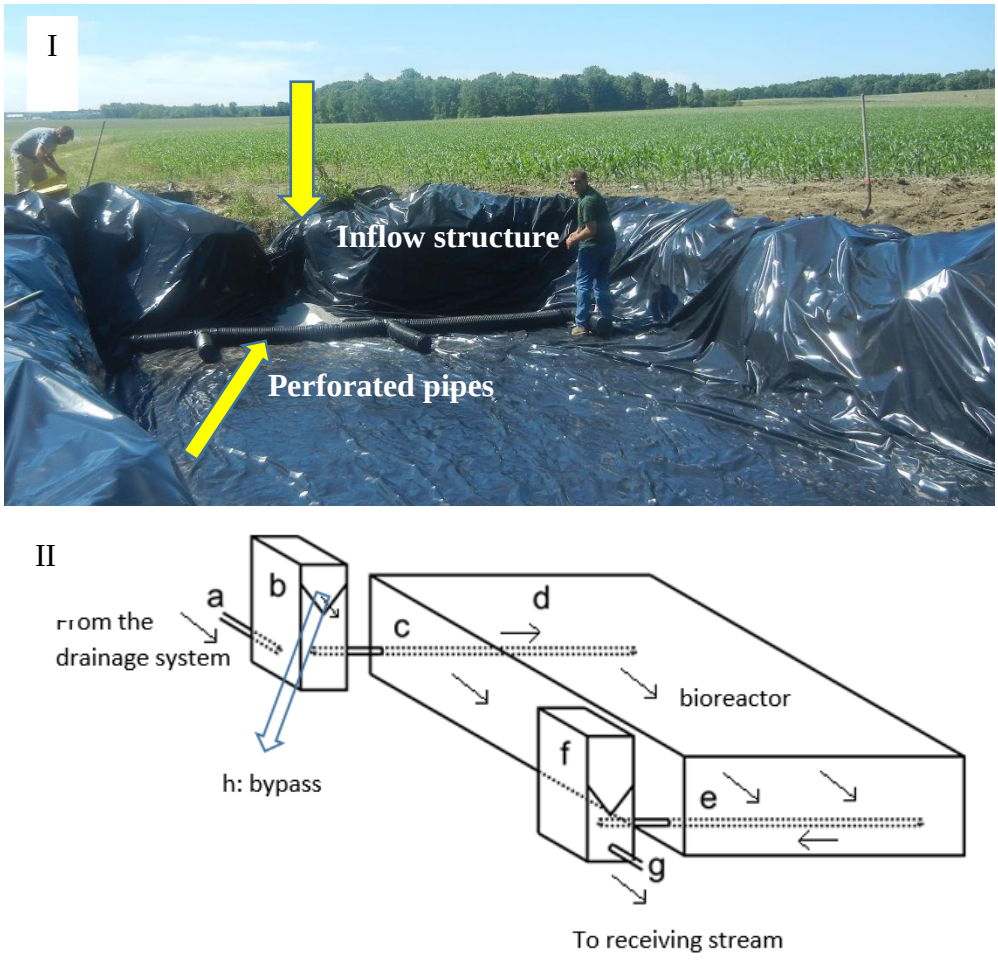

Figure S2-2 Photograph of a bioreactor before it was filled with woodchips. The plastic liner and perforated pipe through which the water enters the bioreactor can be seen. II) Schematic of the bioreactor(adapted from Pluer et al., 2016). The following elements can be distinguished: (a) drainage tile; (b) AgriDrain® groundwater table control boxes with weirs; (c) perforated pipes to distribute inflow; (d) denitrifying bioreactor; (e) perforated pipes for collecting outflow; (f) outflow control box with weir to control head at outflow; (g) outflow pipe to stream; (h) bypass to stream-water bypasses the bioreactor when water head exceeds the weir elevation. Arrows show the flow direction.

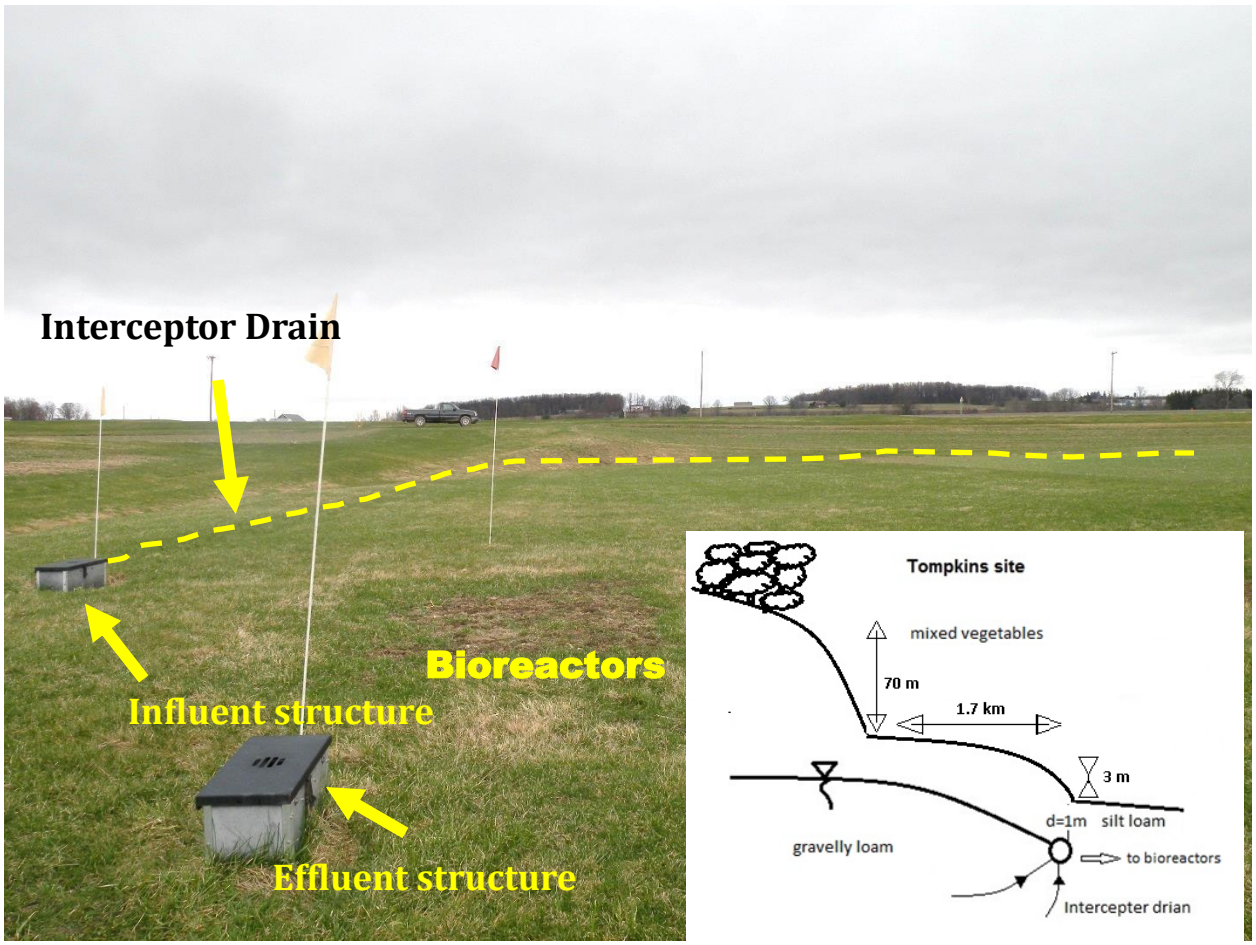

Figure S2-3 Tompkins bioreactor site overview and schematic cross-section (not to scale). The elevation difference between the woods in the background and the farm is 70 m.

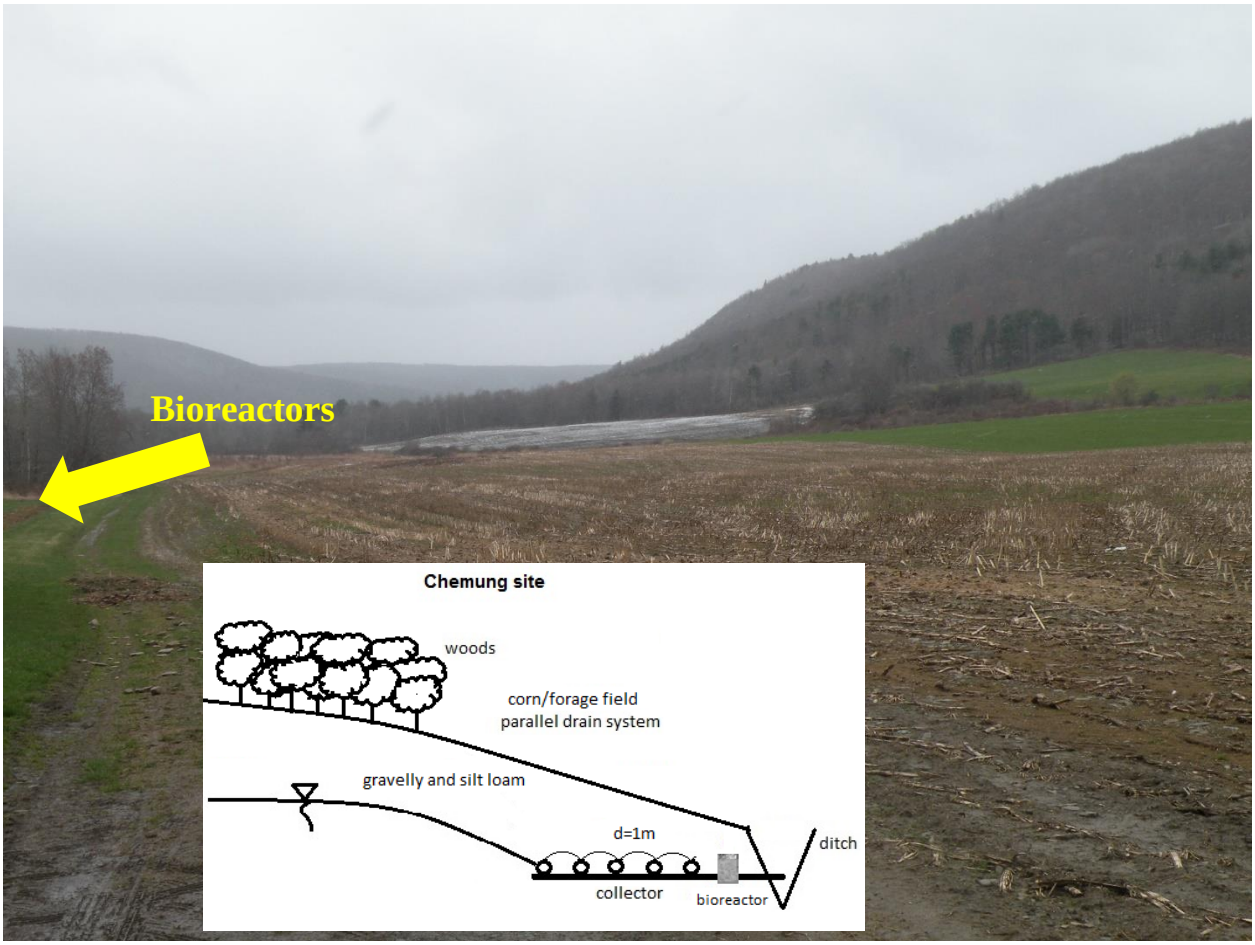

Figure S2-4 Chemung bioreactor site: overview and schematic cross-section (not to scale).

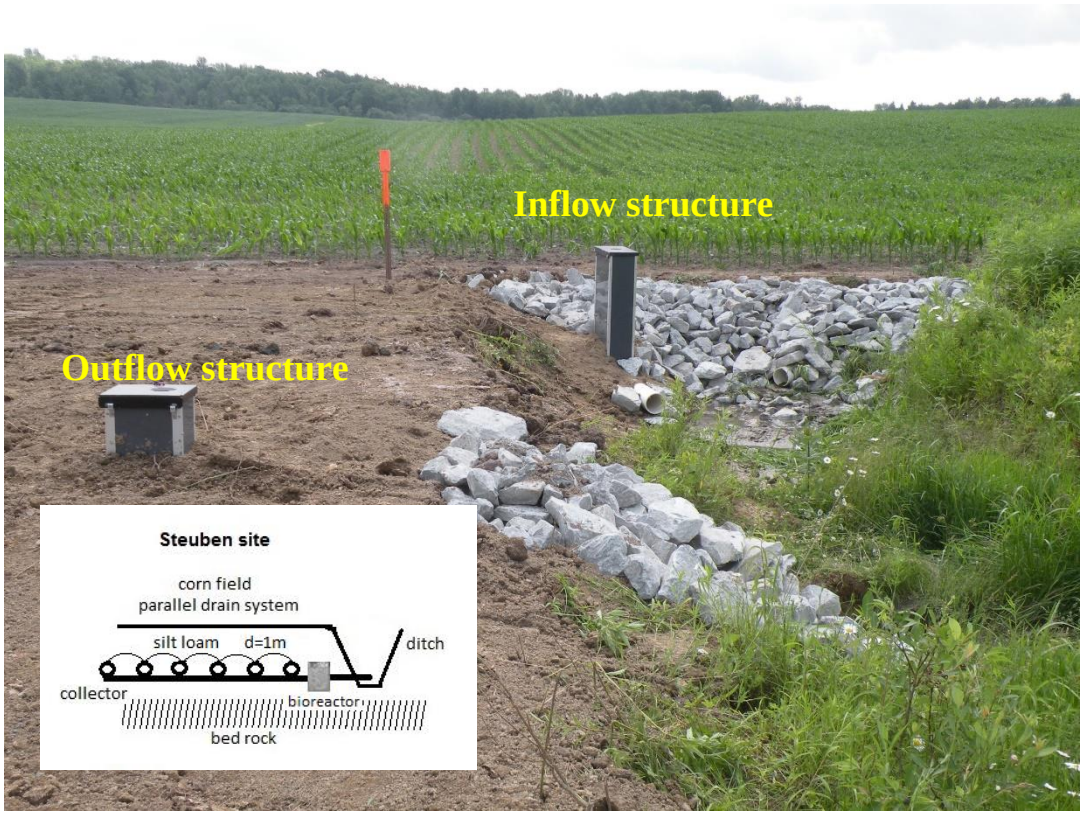

Figure S2-5 Steuben bioreactor site: overview and schematic cross-section (not to scale).

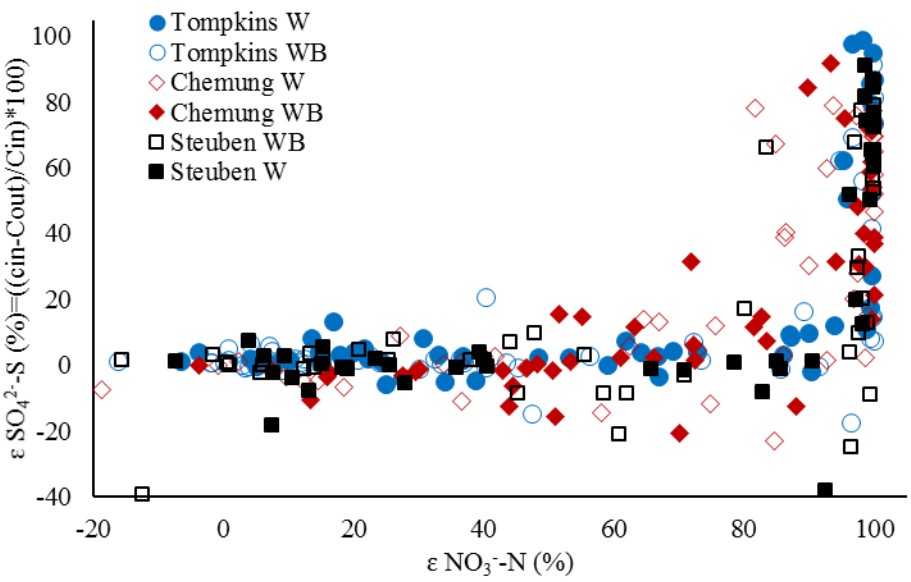

Figure S2-6 Sulfate removal vs. NO_3^-—N removal efficiency. This figure shows that the reduction sulfate (SO_4^{2-}—S) did not happen unless all NO_3^-—N was removed by the bioreactor

CHAPTER 3:

APPLICATION OF DENITRIFYING BIOREACTORS FOR THE REMOVAL OF ATRAZINE IN AGRICULTURAL DRAINAGE WATER

Adapted from: Hassanpour, B., L.D. Geohring, A.R. Klein, S. Giri, L. Aristilde, and T.S. Steenhuis. 2019. Application of denitrifying bioreactors for the removal of atrazine in agricultural drainage water. J. Environ. Manage. 239 (December 2018): 48–56.

3.1 ABSTRACT

Atrazine and nitrate (NO_3^-—N) are two agricultural pollutants that occur widely in surface and groundwater. One of the pathways by which these pollutants reach surface water is through subsurface drainage tile lines. Edge-of-field anaerobic denitrifying bioreactors apply organic substrates such as woodchips to stimulate the removal of NO_3^-—N from the subsurface tile waters through denitrification. Here, we investigated the co-removal of NO_3^-—N, and atrazine by these bioreactors. Laboratory experiments were conducted using 12-L woodchips-containing flow-through bioreactors, with and without the addition of biochar, to treat two concentrations of atrazine (20 and 50 μg L^{-1}) and $NO_3^- - N$ (1.5 and 11.5 mg L^{-1}), operated at four hydraulic retention time, HRT, (4h, 8h, 24h, 72h). Additionally, we examined the effect of aerating the bioreactors on atrazine removal. Furthermore, we tested atrazine removal by a field woodchip denitrifying bioreactor. The removal of both NO_3^-—N and atrazine increased with increasing HRT in the laboratory bioreactors. At 4 h, the woodchip bioreactors removed 65% of NO_3^-—N and 25% of atrazine but, at 72 h, the bioreactors eliminated all the NO_3^-—N and 53% of

atrazine. Biochar-amended bioreactors removed up to 90% of atrazine at 72-h retention time. We concluded that atrazine removal was primarily via adsorption because neither aeration nor NO_3^-—N levels had an effect. At 4-h retention time, the field bioreactors achieved 2.5 times greater atrazine removal than the laboratory bioreactors. Our findings thus highlighted hydraulic retention time and biochar amendments as two important factors that may control the efficiency of atrazine removal by denitrifying bioreactors. In sum, laboratory and field data demonstrated that denitrifying bioreactors have the potential to decrease pesticide transport from agricultural lands to surface waters.

3.2 Introduction

Agrochemicals such as nitrogen fertilizers and pesticides, which are applied to agricultural lands to increase crop yields, can be transported to surface and ground waters (Burkart and James, 1999; Mayer et al., 2002; Guzzella et al., 2006). Agricultural activities are recognized as one of the main sources of nitrogen in rivers and lakes (Mayer et al., 2002; Galloway et al., 2004). Excess nitrogen, which contributes to algal blooms in lakes and reservoirs, increases the cost of treatment for public water supplies (EPA, 2015). Decomposition of the blooms depletes oxygen from water and subsequently leads to low-oxygen zones worldwide (Burkart and James, 1999; Smith et al., 1999; Breitburg et al., 2018). Atrazine ($C_8H_{14}ClN_5$: 1-chloro-3-ethylamino-5-isopropylamino-3,4,6-triazines) is the second most commonly used herbicide in the United States (Atwood and Paisley-Jones, 2017). Although atrazine was banned in the European Union (Sass and Colangelo, 2006), it is still used in the United States where detection in shallow groundwater was found above the drinking water standard of 3 µg L^{-1} (EPA, 1995; Gilliom, 2007; Toccalino et al., 2014).

The soil half-life of atrazine varies from 22 to 146 d depending on the moisture and aeration (Issa and Wood, 2005; Gilliom et al., 2006). Even at low concentrations (1 to 10 µg L^{-1}), atrazine can limit the growth of phytoplankton, zooplankton, and aquatic plants, as well as the development and swimming patterns of fish (Graymore et al., 2001; Tillitt et al., 2010). The United States Environmental Protection Agency (EPA, 2006) classified atrazine as "not likely to be carcinogenic to humans," but this classification has been debated (Sass and Colangelo, 2006). Denitrifying bioreactors are effective in reducing NO_3^-—N discharged from agricultural tile lines (Christianson and Schipper, 2016), but a cost-effective in-situ technique to remove atrazine and other pesticides have not been developed. Here we investigate the potential of denitrifying bioreactors to achieve the co-removal of NO_3^-—N and atrazine from agricultural tile drain effluents.

The NO_3^-—N leaches through the matrix or preferential flow from the root zone to the lower soil profile (e.g., Ernstsen et al., 2015; Marjerison et al., 2016; Mohanty et al., 1998). The NO_3^-—N concentration varies depending on land use, and the amount of N-fertilizer applied. Reported NO_3^-—N concentrations in NY state varied from 0.7 mg L^{-1} at the end of the growing season in a vegetable farm with a perched water table to 62 mg L^{-1} in a cornfield with applied manure (Hassanpour et al., 2017). Atrazine applied to agricultural lands percolates mainly through preferential flow pathways to shallow groundwater, particularly in untilled soils (e.g., Malone et al., 2014; Rothstein et al., 1996; Warnemuende et al., 2007). Various studies reported atrazine concentrations in tile drains ranging from 0.1 µg L^{-1} to 49.2 µg L^{-1} (Steenhuis et al., 1990; Kladivko et al., 1991; Gaynor et al., 1992; Buhler et al., 1993; Rothstein et al., 1996; Rocha et al., 2008). After finding that atrazine concentrations ranged from 0.1 to 49 µg L^{-1} in the streams of a tile-drained

agricultural watershed in the spring season when heavy rain followed spraying period, David et al., (2003) concluded that tile drains were the major contributor of atrazine to streams. Therefore, as both NO_3^-—N and atrazine are transported via tile drain lines to surface waters, simultaneous removal of both would be valuable to mitigate surface water pollution.

Recently, fast removal of atrazine was achieved in sewage treatment systems with high chemical oxygen demand (Baghapour et al., 2013; Derakhshan et al., 2018b), but generally, biodegradation of atrazine takes months in wetland and natural systems and is reduced when nitrogen source is present (Chung et al., 1995, 1996; Ro and Chung, 1995). Therefore, Hunter and Shaner (2010) recommended two sequential bioreactors wherein the anaerobic bioreactor removes NO_3^-—N and a subsequent aerobic one to degrade atrazine in aqueous solution. Other researchers have suggested the addition of specific bacterial species to remove both atrazine and NO_3^-—N, but contamination with undesirable bacteria made this approach challenging (Katz et al., 2001). In-situ woodchip denitrifying bioreactors have been successful in removing NO_3^-—N in several countries (e.g., United States, Canada, New Zealand) (Schipper et al., 2005; Christianson et al., 2011a, 2012b; Bock et al., 2016; Pluer et al., 2016). The dissolved organic matter from woodchips serves as an electron donor for denitrification (Greenan et al., 2009; Warneke et al., 2011b). These woodchip bioreactors could also achieve removal of atrazine in the bioreactors through adsorption. The adsorption of atrazine to natural soil organic matters and soil organic amendments is well documented (Abate et al., 2004; Lima et al., 2010). A wide range of organic matter including woodchips, charcoal, and biochar has been shown to adsorb atrazine (Chefetz, 2003; Spokas et al., 2009; Cao et al., 2011; Ilhan et al., 2011; Delwiche

et al., 2014; Lupul et al., 2015). Biochar was reported to have a high capacity for atrazine adsorption, but this adsorption can be reduced when the biochar surface is modified by sorption of other organics (Wang, 2005; Delwiche et al., 2014).

Since woodchip denitrifying bioreactors have been shown to lower NO_3^-—N concentration in tile drains, it is worthwhile to evaluate whether these bioreactors are good candidates for atrazine removal. The present study investigated the co-removal of NO_3^-—N and atrazine from tile effluents in laboratory and field settings using anaerobic denitrifying bioreactors filled with woodchips without and with the addition of biochar (respectively, W and WB bioreactors). In addition, we operated these bioreactors under aerobic conditions to investigate the effect of aeration on atrazine removal. We targeted relatively short hydraulic retention times (HRT; 4h to 72h) because it is a limiting factor in the design of field denitrifying bioreactors.

3.3 Material and Methods

3.3.1 Laboratory Experiments

3.3.1.1 Flow-through Bioreactors

Twelve up-flow cylindrical reactors, with a 12-L volume each, were constructed with a diameter of 27 cm and a length of 21 cm. A perforated sheet was placed at the bottom of the column (at the entrance) to help distribute the flow evenly. Four of the bioreactors were filled with woodchips (W) and the remaining with woodchips and biochar (WB) at 1:1 v/v. Woodchips from ash trees (*Fraxinus ornus* sp.) were obtained locally from a lumber mill (Wagner Hardwoods, Cayuta, NY). The average woodchip length was 3 cm. The biochar, produced from pine (*Pinus* sp.) and commercially pyrolyzed at 550 to 600 ^{0}C,

was obtained from Biochar Now® and had a length of 1 to 2 cm. The porous medium (woodchips with or without biochar) was measured to have similar porosity of 0.61 cm^3 cm^{-3}. Figure 3-1 details the different investigated treatments, which includes the two organic media, under anaerobic and aerobic conditions with two different levels of NO_3^-—N. The aeration of the aerobic bioreactors was achieved by pumping air through two diffusers at the bottom. Although woodchip bioreactors establish anaerobic conditions if not aerated, we reduced the influent oxygen content to 3 mg L^{-1} via injection of argon gas (Airgas ®) to assure anaerobic conditions in the entire anaerobic bioreactors. These bioreactors were air-sealed.

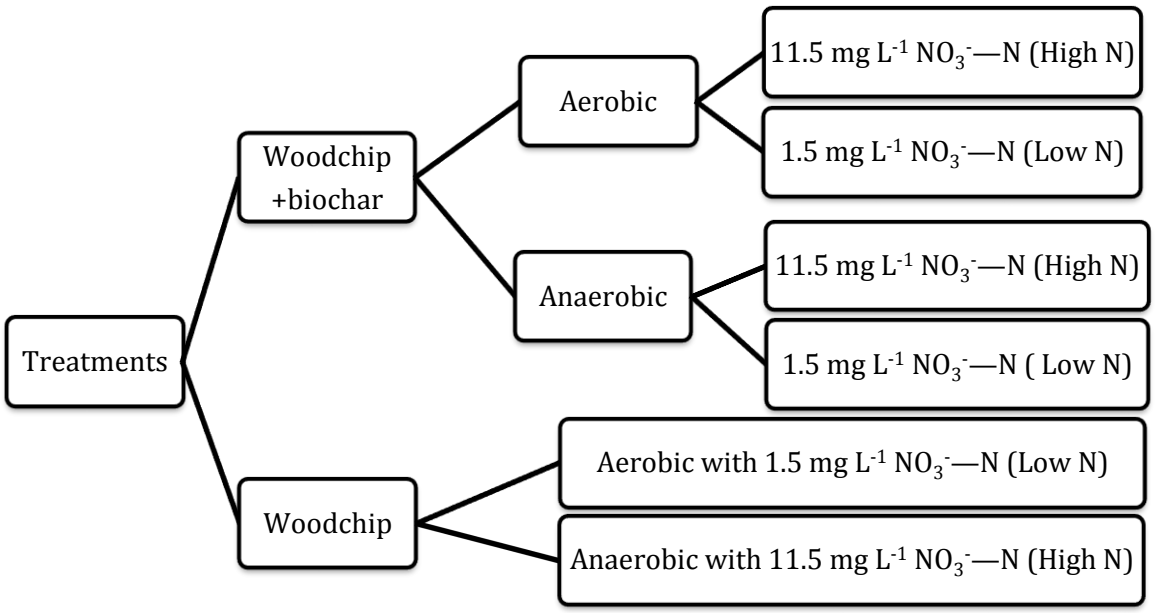

Figure 3-1 Experimental treatments, all in duplicates, consisted of treatments that included woodchips, woodchips, and biochar, under aerobic and anaerobic conditions at two levels of NO_3^-—N

3.3.1.2 Tile Drainage Water

The tile drain water was made from tap water which was sourced from Fall Creek near Ithaca, NY. The water had a constant NO_3^-—N concentration of 1.5 mg L^{-1}. To avoid side-reaction by chlorine in the tap water, the influent was stirred periodically in the influent reservoir for one day prior to each experiment. Then, based on our previous experiments at the Homer C. Thompson Vegetable Research Farm (Hassanpour et al., 2017) where the NO_3^-—N concentrations in the tile line was about 10 mg L^{-1} year around, NO_3^-—N concentrations were spiked to 11.5 mg L^{-1} for the treatments with elevated NO_3^-—N content using potassium nitrate (KNO_3). In addition, phosphate-P was supplied at a concentration of 2 mg L^{-1} by addition of monopotassium phosphate (KH_2PO_4) to the water for all treatments. Syngenta atrazine was from AAtrex ® Nine-O ®, which comes as water-dispersible granules and is 88.2% atrazine and 11.8% proprietary agent. Two atrazine concentrations, 20 and 50 µg L^{-1}, were used in the synthetic drainage water. These concentrations were within those observed in agricultural tile lines.

3.3.1.3 Experiments

The fabricated drainage water was pumped to the bioreactors using peristaltic pumps (Masterflex L/S ® from Cole- Parmer) at four different flow rates (30, 15, 5, and 1.7 mL min^{-1}) to achieve four different HRTs (4, 8, 24 and 72 h). For each HRT, at least 5 pore volumes of the influent were pumped through the bioreactors to ensure equilibrium was achieved. During the experiments, the water flow was measured at the effluent of each reactor to calculate the HRT for individual reactors accurately. The flow rates were 4 to

17% less than intended, thus indicating that the HRTs were only slightly longer than the targeted values.

The water in the influent tanks was kept in the dark and was monitored for NO_3^-—N, phosphorus, and atrazine content throughout the experiment. The experiments were conducted at an ambient room temperature of 21 ± 2° C. In the first two experiments with HRTs of 72 and 24 h, the bioreactors received synthetic drainage water with 20 µg L^{-1} of atrazine. Subsequent experiments with HRTs of 8, 4, 24 and 72 h used 50 µg L^{-1} of atrazine. There was no flow in the bioreactors for 1 to 5 days between experimental treatments. Before the experiments started, the tubing connections were tested for possible adsorption of atrazine. No atrazine adsorption was observed.

3.3.1.4 Chemical Analysis

Approximately 500 samples were taken from the influent and effluent of both laboratory and field bioreactors and were filtered through 0.45-µm filters. Laboratory samples were taken after 2 pore volumes had passed and were analyzed for NO_3^-—N and nitrite (NO_2^- — N) using ion chromatography (Dionex ICS-2000) within 48 hours (Pfaff, 1993a). The dissolved oxygen (DO) was measured in-line at the effluent using a YSI 550A probe. The pH of the influent and effluent samples was measured immediately after collection with an Accumet AR50 meter. Two series of samples at HRTs of 4 and 24 hours were analyzed for total dissolved phosphorus concentrations and cations using inductively coupled plasma optical emission spectrometry (ICP-OES; Thermo iCAP 6500 series). The samples were kept frozen until analyzed for atrazine. Atrazine concentrations were determined using both an enzyme-linked immunosorbent assay (ELISA) and high-

resolution liquid chromatography-mass spectrometry (LC-MS) (Smith et al., 2007). The LC-MS analysis was conducted using a Thermo Scientific Accela liquid chromatography system coupled to a Thermo Scientific TSQ Quantum Access triple quadrupole mass spectrometer.

Interference in the ELISA analysis of the effluent samples was a problem due to a high concentration of organic matter. Samples that showed interference were diluted up to 100 times to eliminate it as recommended by Koivunen et al., (2006). Solid phase extraction (SPE) clean-up was used prior to LC-MS analysis. The SPE was performed using HyperSep™ C18 Cartridges (ThermoFisher scientific) as proposed by Mills and Thurman (1992) with some modification. The 200-mg bed cartridges were preconditioned sequentially with 2 mL each of methanol, ethyl acetate, methanol, and milli-Q water. This was followed by the addition of 2 mL of each sample spiked with atrazine internal standard (atrazine-d_5). Finally, 3 mL ethyl acetate flowed through the cartridges and was collected. Along with the ethyl acetate eluent, about 0.5 mL water which was trapped in the cartridges was collected in the test tube. This water and ethyl acetate were mixed thoroughly using a vortex mixer. After settling, the ethyl acetate fraction was collected from the test tube and evaporated until dry under nitrogen gas. The evaporated sample was resuspended in 2 mL of Milli-Q water, vortexed and sonicated, then analyzed using LC-MS (full method available in section 3.8.1, and Tables S3-1 to S3-3). The samples were analyzed for atrazine and its four common degradation products (hydroxyatrazine, atrazine desethyl, atrazine desisopropyl, and atrazine desethyl desisopropyl). The compound standards were acquired from Sigma-Aldrich with more than 98% purity. Figure S3-1 shows the calibration for the SPE cleaned standards. Contrary to chemical analysis via ELISA, LC-MS analysis of

woodchips leachate with a high concentration of organic matter spiked with atrazine, and its metabolite showed no matrix interference. Based on comparative analysis of the two analytical methods (presented in section 3.8.1, Figure S3-2), we only present the data of the ELISA-determined atrazine concentrations for the influents and for the effluent of the WB bioreactors after adjustment.

3.3.1.5 Statistical Analysis

Statistical analysis was performed using JMP (Statistical Discovery™ from SAS). F-Statistics were performed on the data points to characterize the performance of the reactors based on the measured parameters and treatments evaluated in this study.

3.3.2 Field Bioreactor

In June 2017, the influent and effluent of a field bioreactor in Onondaga County in New York State were monitored for atrazine shortly after application to the fields. The W bioreactor at the Onondaga site was constructed in October 2016 at the outlet of a subsurface drainage collector in a field where corn, soybeans, and wheat are grown in contoured strips. This bioreactor is 1 m deep, 3 m wide, and 13.5 m long. Atrazine was applied on the cornfield shortly before corn emergence, in June 2017. In three sampling events, on June 6th, 10th and 12th, 2017, atrazine was detected at the influent and effluent of this bioreactor.

3.4 Results

3.4.1 Nitrate-N Removal in the Bioreactors

At the high influent NO_3^-—N concentration of 11.5 mg L^{-1}, there was NO_3^-—N removal in both anaerobic and aerobic bioreactors (Figure 3-2). It is of note that NO_2^-—N was not detected at the effluent of the bioreactors. The NO_3^-—N removal increased with increasing HRT and followed first-order kinetic rates for both aerobic and anaerobic bioreactors (Figure 3-2a and Figure 3-2b). In both bioreactors, the NO_3^-—N removal ranged from 50% (C/C_0 = 0.5) to 80% (C/C_0 = 0.2) at the 4-h HRT and increased to 80 to 98% (C/C_0 = 0.2 to 0.02) at 8-h retention time (Figure 3-2a and Figure 3-2b). At 72-h HRT, all NO_3^-—N was removed from the bioreactor effluent. We note that at the low influent NO_3^-—N concentration of 1.5 mg L^{-1}, the NO_3^-—N removal was erratic due to N-limiting conditions (Figure 3-2c and Figure 3-2d). Previously, it was determined that in anaerobic woodchip bioreactors, denitrification is responsible for NO_3^-—N removal (Warneke et al., 2011b; c). In aerobic bioreactors, however, NO_3^-—N removal coincided with the uptake of phosphorus and potassium (Figure S3-3) and likely occurred through cellular assimilation of NO_3^-—N (Mclatchey and Reddy, 1998; Reddy and Delaune, 2008; Saia et al., 2017).

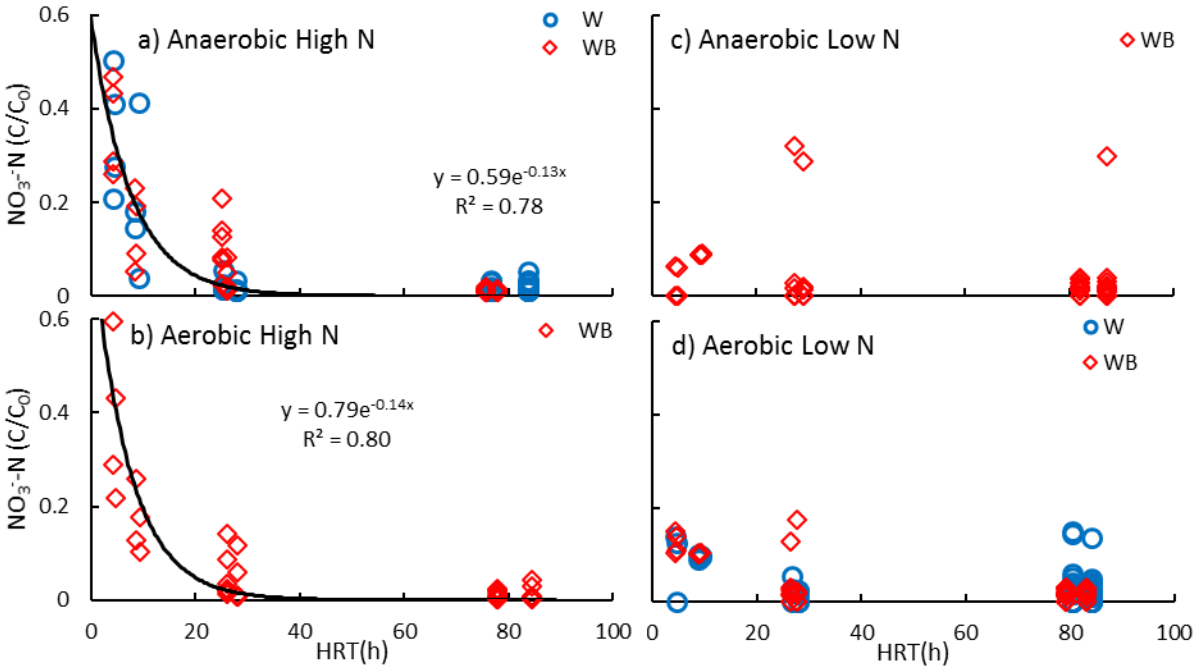

Figure 3-2 The C/C_0 (effluent concentration/influent concentration) of NO_3^-—N in the different HRTs in both W (woodchips; blue circles) and WB (woodchips and biochar; red diamonds) a) anaerobic bioreactors with high level of NO_3^-—N, b) aerobic bioreactors with high level of NO_3^-—N, c) anaerobic bioreactors with the low level of NO_3^-—N, and d) aerobic bioreactors with the low level of NO_3^-—N.

3.4.2 Atrazine Removal As A Function of Hydraulic Retention Time and Biochar Amendment

The bioreactors achieved atrazine removal from the influent for all treatments, but the WB bioreactors were more efficient than the W bioreactors (Table S3-4). In the experiments with influent atrazine concentration of 20 µg L^{-1}, atrazine concentrations in the effluent were less than 3 µg L^{-1} (2.7 ± 0.2 µg L^{-1}) in WB bioreactors for both 24-h and 72-h HRTs (Figure 3-3a). However, at the corresponding HRTs, the atrazine concentration in W bioreactors was, respectively, 13 ± 0.9 µg L^{-1} and 7.3 ± 1.2 µg L^{-1} (Figure 3-3a). We also evaluated atrazine removal from higher influent atrazine concentration of 50 µg L^{-1} through both types of bioreactors at four HRTs: 4h, 8h, 24 h, and 72h. We found that, at

the higher influent atrazine concentration, the WB bioreactors removed more atrazine than the W bioreactors (Table S3-4, Figure 3-3a). The atrazine concentrations in the effluent of the WB bioreactors were 18 ± 0.8 µg L^{-1} and 3.7 ± 0.6 µg L^{-1} at HRTs of 4 h and 72 h, respectively, whereas the corresponding concentrations in the effluent of the W bioreactors were respectively, 39 ± 1.4 µg L^{-1} and 23 ± 1.5 µg L^{-1} (Figure 3-3a).

The atrazine removal as a function of the variation in HRTs is shown in Figure 3-3b. Overall, the C/C_0 for the W bioreactors was 0.63 ± 0.03 (atrazine removal = 37%) compared to 0.25 ± 0.04 (atrazine removal = 75%) for the WB bioreactor (Figure 3-3b). In 4 h, the W bioreactor removed 24% (C/C_0 = 0.76 ± 0.03) of the inflow atrazine while the WB bioreactors removed 63% (C/C_0 = 0.37± 0.02) of atrazine (Figure 3-3b). By increasing HRT from 4 h to 8 h, the removal of atrazine increased to 29% (C/C_0 = 0.71 ± 0.02) for the W bioreactor and 72% (C/C_0 = 0.28 ± 0.02) for the WB bioreactors (Figure 3-3b). In 24 h, the W bioreactors removed 36% (C/C_0 = 0.64 ± 0.04) of atrazine while the WB bioreactors removed 83% (C/C_0 = 0.17 ± 0.01) (Figure 3-3b). In 72 h, the W and WB bioreactors removed 55% (C/C_0 = 0.45 ± 0.03) and 93% (C/C_0 = 0.07 ± 0.01), respectively (Figure 3-3b). The atrazine removal followed a first order reaction rate with a constant of 0.024 h^{-1} (or 0.58 d^{-1}) for the WB medium and 0.007 h^{-1} (or 0.17 d^{-1}) for the W medium (Figure 3-3b). This finding agreed with previous findings whereby the removal of atrazine by adsorption to organic matter followed first order reaction kinetics (Liu et al., 2015).

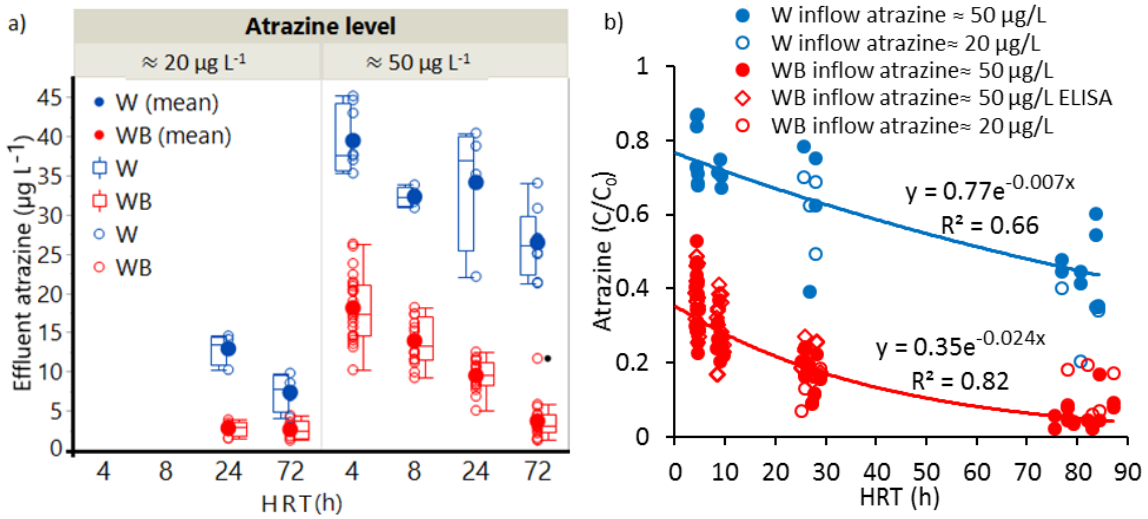

Figure 3-3 Atrazine concentration in the laboratory bioreactors. a) Concentrations of atrazine in the effluent of the W (woodchips; blue open dots) and WB (woodchips and biochar; red open dots) bioreactors at different HRTs (Hydraulic Retention times) at the two atrazine levels. Each line on the box plot from top to bottom shows maximum, the first quartile, median, third quartile, and minimum concentrations of atrazine. The closed dots next to each box is the average concentration of atrazine. b) The relationship between atrazine C/C_0 (effluent concentration/influent concentration) versus HRT for both levels of atrazine in the W and WB bioreactors.

We performed F- test on the measured atrazine concentrations in the effluent to determine the role of each variable: the substrate, HRT, influent atrazine concentration, NO_3^-—N concentration and aeration (Table 3-1). The results showed that atrazine concentrations in the effluent responded to substrate, HRT, and influent atrazine concentrations ($p<0.0001$ and large F values), whereas influent NO_3^-—N concentrations and aeration did not affect effluent atrazine concentrations ($P>>0.05$). This indicated that the removal of atrazine was primarily abiotic. Additionally, we have conducted separate assay experiments to confirm that biodegradation did not contribute to the removal of atrazine in anaerobic and aerobic conditions with wood as a substrate (section 3.8.5 and Figures S3-5, S3-6).

Table 3-1 The influencing parameters on atrazine concentrations at the effluent. N is the number of parameters, DF is the degree of freedom, Sum of squares, F ratio, and the P-value for the effect test. HRT is the hydraulic retention time

Variable	Number of parameters	DF	Sum of Squares	F Ratio	Prob > F
Substrate	1	1	5619	216	<.0001*
HRT	1	3	3306	127	<.0001*
Influent atrazine	1	1	1802	69	<.0001*
Influent nitrate	1	1	2.06	0.08	0.7790
Aeration	1	1	1.09	0.04	0.8377

We monitored the presence of common atrazine degradation products in the effluent of the laboratory bioreactors, and only atrazine desethyl and hydroxyatrazine were found at appreciable levels (Figure 3-4). It is important to note that there was a small concentration of atrazine desethyl in the influent tanks, but the amount generated inside the bioreactors was greater (Figure S3-4). Unlike the atrazine concentration in the effluent, the effluent concentration of the degradation products depended on the aeration of the bioreactors (Figure 3-4). Atrazine desethyl, which was present in the effluent of the aerobic bioreactors, had a greater concentration in the W bioreactors than the WB bioreactors (Figure 3-4). The maximum concentration of atrazine desethyl was 3.7 $\mu g\ L^{-1}$ in the aerobic W bioreactors at an HRT of 72 h (Figure 3-4). In the aerobic WB bioreactor, atrazine desethyl was found at concentrations of $0.6 \pm 0.1\ \mu g\ L^{-1}$ for both HRTs of 24 h and 72 h (Figure 3-4). Hydroxyatrazine was found in the anaerobic bioreactors and one aerobic bioreactor that became anaerobic due to a failure with an oxygen diffuser (shown with arrows) (Figure 3-4). The hydroxyatrazine concentrations varied from 0 to 3.4 $\mu g\ L^{-1}$ in the bioreactor effluents (Figure 3-4). Hydroxyatrazine first started to appear at an HRT of 24 h in the effluent of the W bioreactors and its concentrations amounted to 5% of the atrazine

applied at the influent in 72 h (Figure 3-4). Atrazine transformation to hydroxyatrazine is important because hydroxyatrazine is less toxic than the chlorinated metabolites of atrazine and is not phytotoxic (Graymore et al., 2001; WHO, 2010). The increased concentration of atrazine degradation products in the reactors with increasing retention times agreed with the previous studies that atrazine degradation and the appearance of the degradation products follows the first order kinetics (Jones et al., 1982; Seybold et al., 2001a).

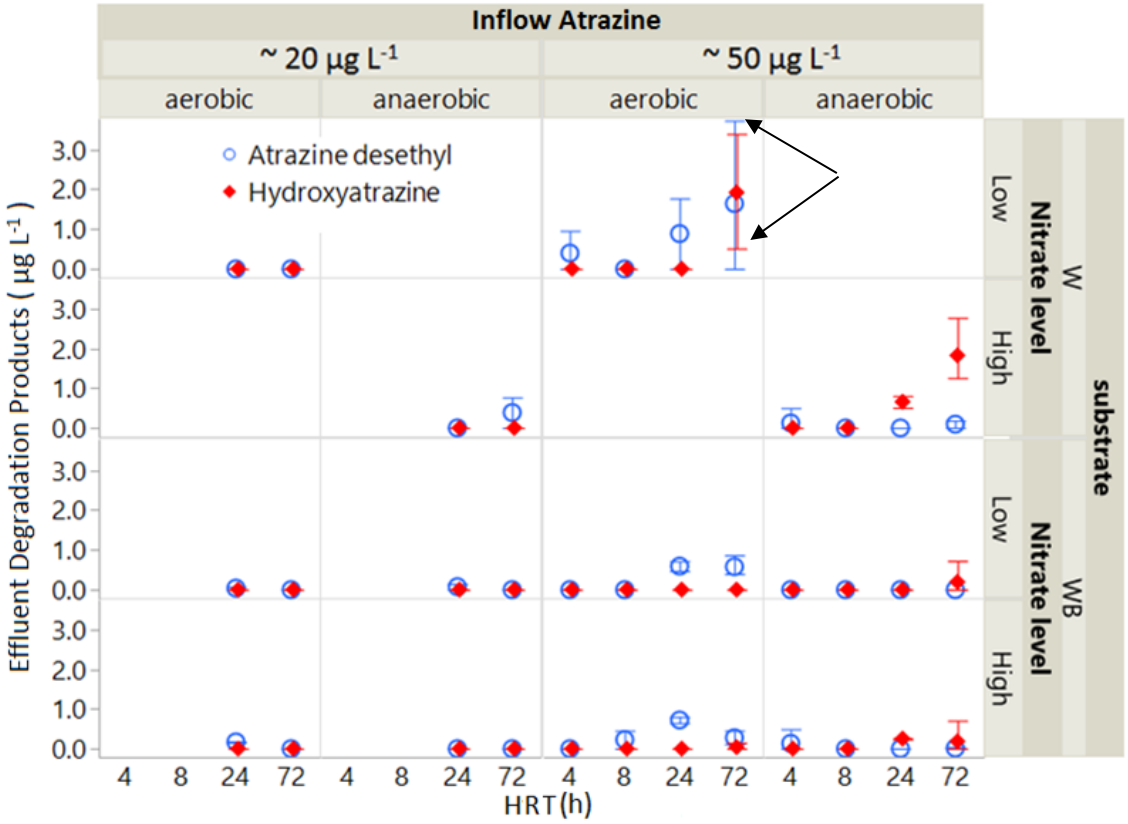

Figure 3-4 Degradation products of atrazine, atrazine desethyl (blue dots) and hydroxyatrazine (red diamonds), at the effluent of the W (woodchips) and WB (Woodchips and Biochar) bioreactors at different HRTs (Hydraulic Retention Times). The error bars show the observed range of the concentrations of the degradation product. Note that one of the two air inlets in one W aerobic bioreactor plugged and that bioreactor behaved like an anaerobic bioreactor (shown by the arrows at 72 h HRT).

3.4.3 Field Bioreactor

Results with the field bioreactor supported the findings of the laboratory experiments (Figure 3-5). For the three sampling events (on June 6th, June 10th, and June 12th, 2017), the removal of NO_3^-—N recorded in the W bioreactor effluent at the Onondaga site was, respectively, 32%, 88%, and 55% (Figure 3-5a). Moreover, we found that the removal of NO_3^-—N was coupled with atrazine removal (Figure 3-5). With respect to atrazine removal, on June 6th, 2017, the Onondaga W bioreactor achieved 62% atrazine removal (C/C_0 = 0.38) at 4-h HRT, by reducing influent atrazine from 9.5 µg L^{-1} to 3.8 µg L^{-1} (Figure 3-5b). At the subsequent sampling dates, however, the effluent atrazine concentration was slightly greater than that in the influent (Figure 3-5b). On June 10th, 2017, at an HRT of 13.4 h, the atrazine concentration increased from 0.4 µg L^{-1} in the influent to 1.37 µg L^{-1} in the effluent (Figure 3-5b). In the last sampling event, on June 12th, 2017, when the HRT was 8.7 h, the atrazine concentration increased from 0.3 µg L^{-1} in the influent to 0.9 µg L^{-1} in the effluent (Figure 3-5b). These results with higher atrazine concentration in the effluent than in the influent thus indicated that desorption of atrazine from the woodchips had occurred. The desorption of atrazine from woodchips and other organic matter was reported in previous studies (Lima et al., 2010; Ilhan et al., 2011). Atrazine desethyl was observed in the influent of the field bioreactor (Figure 3-5c). Given that the tile drain collected water from an agricultural field, observing atrazine desethyl in its effluent was expected (Gilliom, 2007; WHO, 2010). Figure 3-5c shows that the bioreactors removed atrazine desethyl. It is worthy of note that atrazine degradation products can adsorb to the organic matter (Krutz et al., 2003; Abate et al., 2004). Hydroxyatrazine, however, is greater in the bioreactor effluent than in the influent,

indicating the occurrence of atrazine hydrolysis inside the bioreactors (Figure 3-5d). Overall, in the field site, about 10% of the removed atrazine exited the field bioreactor as hydroxyatrazine (Figure 3-5d).

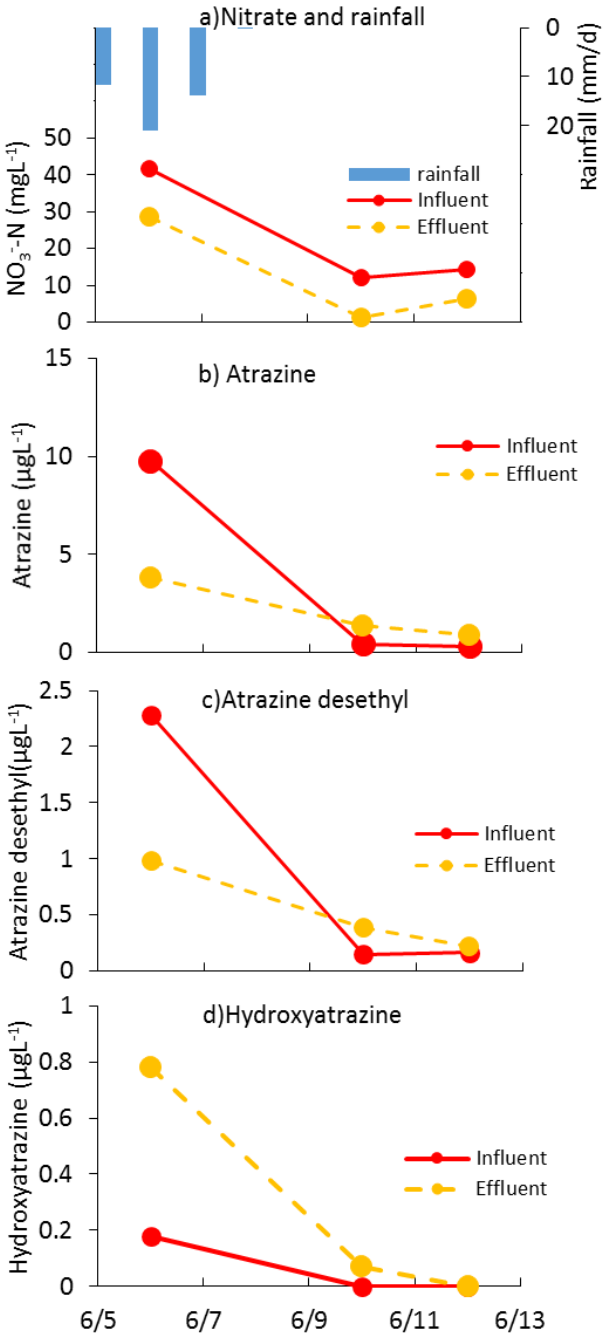

Figure 3-5 a) daily rainfall and inflow and outflow of NO_3^-—N, b) atrazine, c) atrazine desethyl, and d) hydroxyatrazine in Onondaga W (woodchips) denitrifying bioreactor. Note the change in scale of the Y-axis of the graphs.

3.5 Discussion

3.5.1 Mechanism of the Atrazine Removal

The difference between the adsorption of atrazine onto woodchips versus biochar is related to their surface characteristics. The two most efficient sorption sites for atrazine on the organic matter are the aromatic compounds for π-π interactions (Lima et al., 2010; Zhang et al., 2011, 2013) and carbonyl/carboxylic acid groups for hydrogen bonding interactions (Mackay and Gschwend, 2000; Kulikova and Perminova, 2002). Hardwood is made of cellulose, hemicellulose, and lignin. Lignin, with its aromatic components, has strong adsorption capacity for atrazine (Dunigan and McIntosh, 1971). Adsorption of monoaromatic carbon to wood was proportional to the lignin content (Mackay and Gschwend, 2000). During pyrolysis for biochar production, at temperatures below 360 ^{0} C lignin chars, whereas cellulose and hemicellulose degrade to volatile compounds (Blasi, 1993; Mohan et al., 2006). Therefore, for pyrolysis at 550 to 600^{0}C, the biochar used here would be comprised mostly of aromatic compounds (Jindo et al., 2014) as confirmed by infrared spectroscopy (spectra presented in Figure S3-7). The infrared spectroscopic data highlighted the abundance of aromatic compounds as well as carboxyl and keto groups on the biochar surface. Thus, we attributed the lower adsorption capacity of woodchips for atrazine compared to biochar to the aromatic-enriched surface of the biochar compared to that of the wood.

Atrazine degradation products were detected at the effluent of the bioreactors (Figures 3-4 and 3-5). However, the lack of influence of aeration or NO_3^-—N level on atrazine removal led us to conclude that adsorption was the predominant mechanism, especially when removal occurred within hours (Ilhan et al., 2011). In urban wastewater

treatment plants with chemical oxygen demand of 1-10 g L^{-1}, rapid co-metabolism was suggested to be responsible for 61 to 90% atrazine removal in 6 to 24 h (Baghapour et al., 2013; Derakhshan et al., 2018b; c; a). In our study, however, in anaerobic W bioreactors filled with drainage water with generally relatively low chemical oxygen demand, the assay tests revealed that atrazine removal was primarily abiotic.

Our field observations show a greater atrazine removal in a short HRT compared to the laboratory bioreactors. Taking into consideration that the field bioreactor was older, this difference might be caused by the aging of the wood, resulting in a higher percentage of lignin and a lower percentage of cellulose and hemicellulose (Ghane et al., 2018), which lead to an increase in the capacity of the woodchips to adsorb atrazine.

3.5.2 Nitrate -N Removal Rate

To compare our research findings with the research reported in the literature (Schipper et al., 2010; Warneke et al., 2011a; Addy et al., 2016; Pluer et al., 2019), we converted the reduction in NO_3^-—N concentrations in the bioreactors in Figure 3-2 to the removal rates defined as $(C_0\text{-}C)/HRT$ where C_0 is the inflow concentration (mg L^{-1}), C is the effluent concentration (mg L^{-1}), and HRT is the hydraulic retention time (d). The results are plotted in Figure 3-6. The removal rate of the reactors varied between 0.1 mg L^{-1} d^{-1} and 52 mg L^{-1} d^{-1} with the maximum in bioreactors with high N level and short HRTs. The NO_3^-—N removal rates in long HRTs and in bioreactors with low N level were less because of the rate-limited conditions (NO_3^-—N content < 1 mg L^{-1}; Robertson, 2010).

In the anaerobic bioreactors, the influent dissolved oxygen level was reduced (DO ~ 3 mg L^{-1}) with a temperature of 21 ± 2° C. Thus, in short HRTs, the NO_3^-—N removal

rates of the bioreactors with high N level were in the upper ranges of those reported in the literature due elevated NO_3^-—N concentrations and temperature, and readily available anaerobic conditions (Warneke et al., 2011a; Addy et al., 2016; Hassanpour et al., 2017; Pluer et al., 2019). In aerobic bioreactors NO_3^-—N removal rates were similar to those in anaerobic bioreactors (Figure 3-6c, d). Due to the presence of dissolved oxygen, cellular assimilation of nitrogen with the uptake of other nutrient and micronutrients was responsible for NO_3^-—N removal (Myrold and Posavatz, 2007; Geisseler et al., 2010), especially in the abundance of organic matter (Rice and Tiedje, 1989; Mclatchey and Reddy, 1998; Reddy and Delaune, 2008).

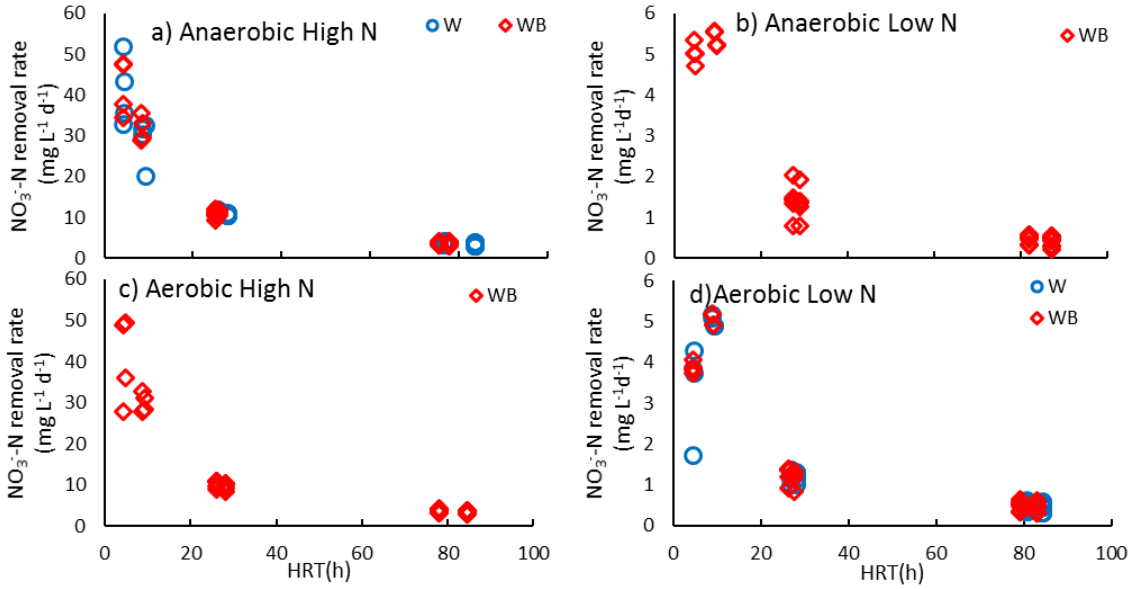

Figure 3-6 The NO_3^-—N removal rate the different HRTs in both W (woodchips; blue circles) and WB (woodchips and biochar; red diamonds) in a) anaerobic bioreactors with the high level of NO_3^-—N, b) aerobic bioreactors with the high level of NO_3^-—N, c) anaerobic bioreactors with the low level of NO_3^-—N, and d) aerobic bioreactors with the low level of NO_3^-—N.

3.5.3 Atrazine Removal in Aerobic vs. Anaerobic Conditions

There was a difference between the produced atrazine degradation products in aerobic and anaerobic conditions. We found that about 5% of the influent atrazine appeared as atrazine desethyl in the effluent of aerobic W bioreactors after 72 h. However, hydroxyatrazine was the degradation product of atrazine in the anaerobic bioreactors, although a trace amount of atrazine desethyl was still observed in these reactors (Figures 3-4 and 3-5). Degradation of atrazine to atrazine desethyl and other dealkylated metabolites, which is known to be microbially mediated (Gilliom et al., 2006), has been reported in the soil, riverine systems, and in groundwater (Gilliom et al., 2006; Gilliom, 2007). These dealkylated atrazine metabolites are almost as toxic as atrazine (Graymore et al., 2001). Degradation of atrazine to hydroxyatrazine under anaerobic conditions is consistent with the finding of earlier studies (Chung et al., 1996; Seybold et al., 2001a). Hydrolysis of atrazine to hydroxyatrazine has been attributed to chemical degradation through adsorption of atrazine to organic matters, sediments and particles (Armstrong et al., 1967; Stevenson, 1972; Lerch et al., 1999; Seybold et al., 2001a). Armstrong et al. (1967) suggested that the enhanced hydrolysis of atrazine in soils can occur due to the presence of catalytic metals on the surface of soil mineral particles, in addition to a low soil pH that can facilitate acid hydrolysis. In equilibrium with atmosphere, the pH of the aerobic bioreactors remained the same as the influent at about 7.5, while in anaerobic conditions the pH dropped to an average of 6.5 (Table S3-4), which could have contributed in atrazine hydrolysis to hydroxyatrazine (Armstrong et al., 1967; Geller, 1980; Gamble and Khan, 1985; EPA, 2006). Mandelbaum et al. (1993) provided evidence that microbial activity, such as the production of enzymes, enhanced atrazine hydrolysis at neutral pH

values in both aerobic and anaerobic conditions. Both the aerobic and anaerobic bioreactors in the current study allowed bacterial growth, therefore, the contribution of microbial activity may not have been substantial in the production of hydroxyatrazine as it was pointed out by Jones et al. (1982).

3.6 Conclusion

The results of this study showed that both field and laboratory woodchip containing anaerobic bioreactors, also known as denitrifying bioreactors, can achieve co-removed of atrazine and NO_3^-—N from tile waters according to first-order kinetics. In anaerobic conditions, atrazine removal was abiotic and primarily through adsorption. Hydroxyatrazine, a non-phytotoxic degradation product of atrazine, was also produced in such conditions. Contrary to the previous proposal by Hunter and Shaner, (2010), we showed here that, aeration did not increase atrazine removal and, thus, the application of aerobic bioreactors may not be necessary.

One of the challenges in the treatment of agricultural tile waters is handling the peak flow of water and concentrations. With the addition of biochar, which represents a simple adjustment to the substrate of the woodchip denitrifying bioreactors, we found that atrazine removal was improved, particularly at short retention times. In the HRT of 8 h, a previously suggested criterion in bioreactor design (Christianson et al., 2011b), we found that the WB bioreactors could achieve 65% atrazine removal, more than two-fold higher atrazine removal than the W bioreactors.

3.7 Acknowledgment

This research was supported by USDA NIFA Hatch Accession [grant numbers 231333 and 1004349], NRCS- Conservation Innovation Grant (CIG) [grant number 67-3A75-13-215]. This work made use of the Cornell Center for Materials Research Shared Facilities, which are supported through the NSF MRSEC program [award number DMR-1719875]. We would like to thank cooperating farmers. Special thanks to Steven Pacenka and Dr. Brian K. Richards for their help in various aspects of his work. The assistance of Seyed Fardad Riazi with sample analysis is gratefully acknowledged.

3.8 Supplemental Material

3.8.1 LCMS Analysis of Atrazine and Its Degradation Products

The LCMS analysis of atrazine (and degradation products) in this study followed the method of Smith et al., (2007) with some modifications, specifically to the chromatography.

Liquid Chromatography Parameters:

Separation of atrazine and degradation compounds was achieved using an Agilent ZORBAX Eclipse Plus 95Å C18, 4.6 x 100 mm, 5 µm column coupled with a gradient elution employing 5 mM ammonium acetate and methanol (MeOH) at a flow rate of 1 mL min^{-1}. The autosampler chamber was kept at 4^{o}C. The sample injection volume was 100 µL.

Table S 3-1 Gradient Program

Time (mins)	% 5 mM Ammonium Acetate	% MeOH
0.0	98	2
2.5	98	2
4.0	70	30
6.5	70	30
11.0	10	90
15.0	10	90
15.1	98	2
19.0	98	2

Table S3-2 Mass spectrometry parameters

Ionisation mode	Positive
ESI voltage (V)	3500
Sheath gas pressure (arbitrary units)	30
Ion sweep gas pressure (arbitrary units)	0
Aux gas pressure (arbitrary units)	10
Capillary temperature (^{o}C)	350
Scan width (m/z)	0.1
Scan time (s)	0.1

Table S3-3 Parent-daughter transitions measured

Compound	Parent ion (m/z)	Daughter ion (m/z)	Collision Energy	Quan/Qual transition[#]	Retention Time (mins)
Atrazine-d_5	221	105	34	Qual	4.45
Atrazine-d_5 (IS)*	221	179	18	Quan	4.45
Atrazine	216	104	24	Qual	5.80
Atrazine	216	174	18	Quan	5.80
Hydroxyatrazine	198	114	20	Qual	6.85
Hydroxyatrazine	198	156	16	Quan	6.85
Atrazine desethyl	188	104	28	Qual	7.20
Atrazine desethyl	188	146	19	Quan	7.20
Atrazine desisopropyl	174	68	28	Quan	10.10
Atrazine desisopropyl	174	132	11	Qual	10.10
Atrazine desethyl desisopropyl	146	68	32	Quan	10.10
Atrazine desethyl desisopropyl	146	104	26	Qual	10.10

[#]Qual/Quan transition: The two most common fragments for each parent ion were measured. The fragment with strongest intensity was used for quantitation (quan). The

second (qual) transition was used as a quality control measure to ensure correct peak identification and quantification for each compound.
*IS = internal standard

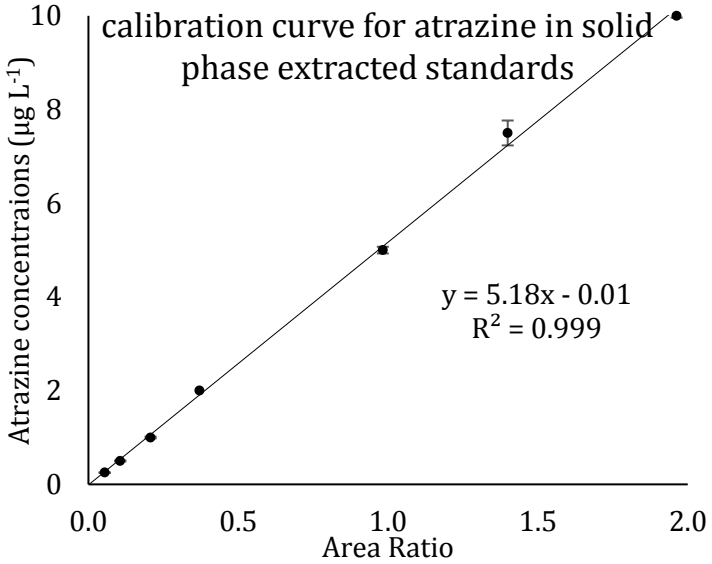

Figure S3-1 Atrazine standard calibration for two sets of standards after solid phase extraction clean-up, 0.25-10 µg L^{-1}. The range of observations is shown by error bars.

3.8.2 Comparing Chemical Analysis by ELISA versus LC-MS

To account for the interference of atrazine ELISA analysis by dissolved organic matter, we diluted by 20 to 100 times prior to analysis by ELISA of the effluent samples containing high concentrations of organic matter at long hydraulic retention times. However, this dilution either reduced the atrazine concentrations below to the limit of quantitation or did not improve quantitation when the organic matter concentration remained high even after dilution (for instance, at 72 hydraulic retention time). Therefore, the samples taken at 72-h hydraulic retention times were only analyzed by LC-MS. For LC-MS analysis, the samples were diluted 0 to 10 times and went through SPE clean-up.

Select samples (72 samples total) samples from the influent and effluent of the reactors were analyzed by both methods for comparison (Figure S3-2). We obtained a 1:1 linear relationship between the atrazine concentrations in the influent tanks determined by ELISA and those determined by LCMS (slope = 1.04; R^2 = 0.92) (Figure S3-2). The effluent samples, however, were colored and interfered with ELISA. The atrazine concentrations in the effluent of the WB bioreactors correlated well between the two analytical methods (slope = 1.00; R^2= 0.76), but the ELISA analysis underestimated the values by 5.8 µg L^{-1}. In the effluent of W bioreactors, the two analytical methods did not agree (R^2=0.09). Therefore, based on this comparative analysis, we only present the data of the ELISA-determined atrazine concentrations for the influents and for the effluent of the WB bioreactors after adjustment.

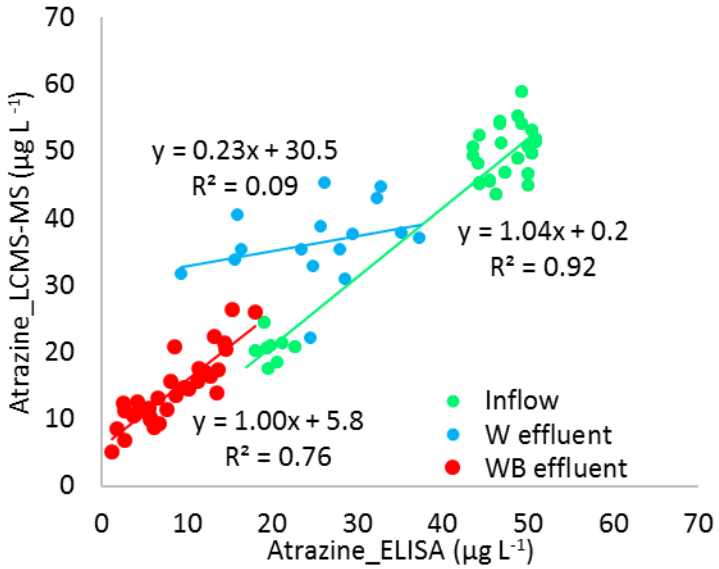

Figure S3-2 Atrazine concentrations in the influent and effluent of the bioreactors determined by ELISA vs. those by LCMS. This figure shows atrazine in the inflow with green dots, atrazine in the effluent of the woodchip bioreactors (W effluent) with blue dots, and atrazine in the effluent of the biochar amended bioreactors (WB effluent) with red dots

3.8.3 Uptake of Nutrients in Anaerobic and Aerobic Bioreactors

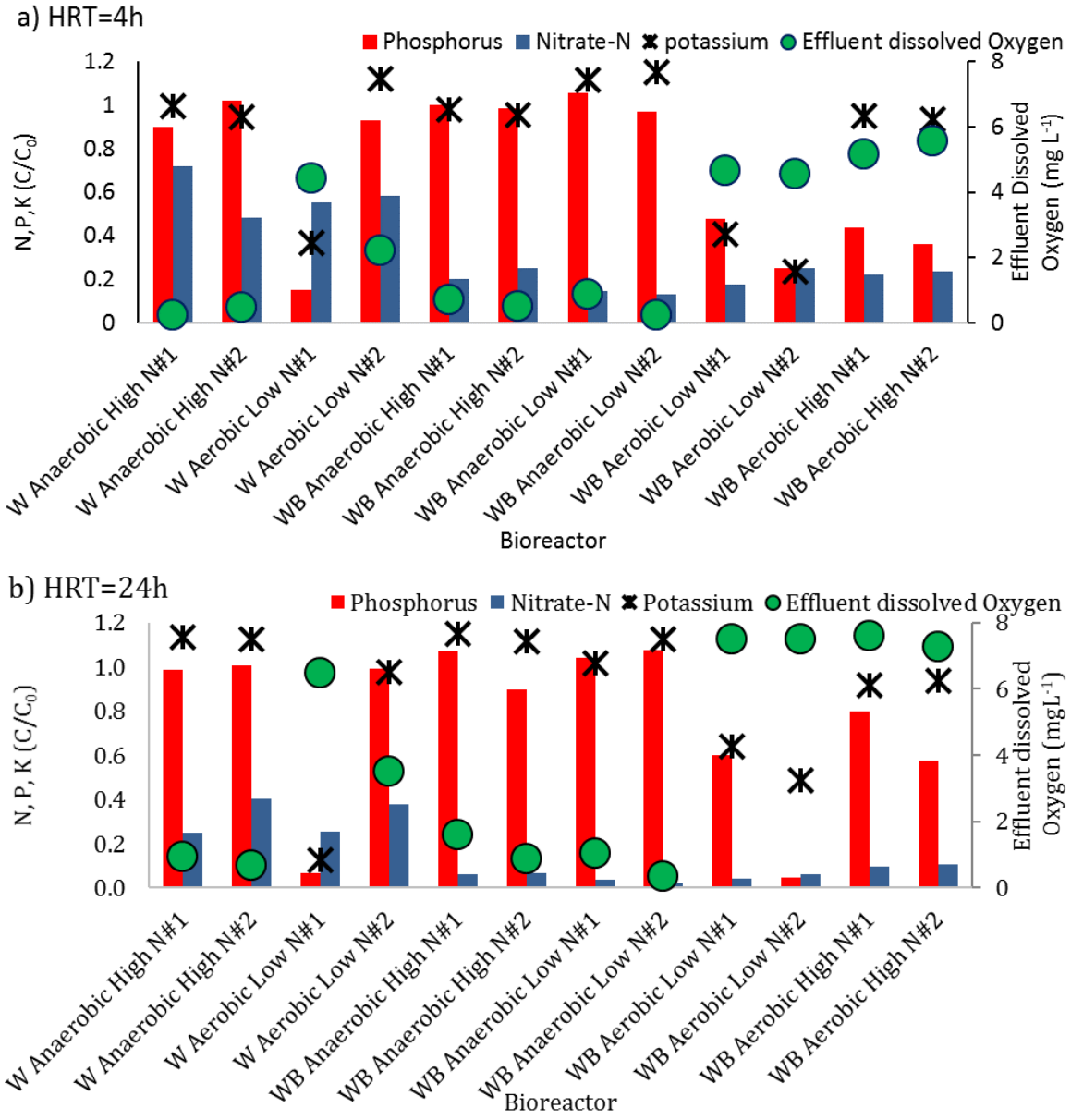

Figure S3-3 The uptake of phosphorus(P), nitrate (N) and potassium(K) in the anaerobic and aerobic conditions in woodchips (W) and Woodchips and biochar (WB) bioreactors in a) Hydraulic retention time of 4 h and b) Hydraulic retention time of 24h. Note that one of the air inlets in woodchips aerobic bioreactor, W aerobic low N#2, was clogged and the bioreactor acted similarly to anaerobic bioreactors.

3.8.4 Atrazine in the Influent and Effluent of the Laboratory Bioreactors

Table S3-4 Atrazine concentrations at the inflow and outflow of the W and WB bioreactors, hydraulic retention time (HRT), atrazine C/C_0 (effluent concentration/ influent concentration), pH, and the dissolved oxygen (DO) of the outflow at different hydraulic retention times.

Bioreactor	**HRT (h)**	**Inflow atrazine (µg L^{-1})**	**Outflow atrazine ± SE (µg L^{-1})**	**atrazine ratio (C/C0) ± SE**	**Average atrazine (C/C0)**	**pH**	**DO (mg L^{-1})**
W Aerobic Low N	24	20.5	13.4±0.7	0.65±0.03	0.46±0.11	7.3	NA
	72	20.1	5.5±1.4	0.27±0.07		6.8	3.5
W Anaerobic High N	24	20.7	12.4±0.1	0.59±0.11	0.49±0.08	6.5	NA
	72	24.3	9.2±0.6	0.38±0.03		6.0	0.33
WB Aerobic Low N	24	20.5	2.4	0.11	0.09±0.03	7.8	NA
	72	20.1	1.2	0.06		7.8	4.61
WB Aerobic High N	24	21.3	3.5±0	0.16±0	0.12±0.02	7.8	NA
	72	20.8	1.6±0.14	0.08±0.01		7.9	5.36
WB Anaerobic Low N	24	17.5	2.3±0.8	0.18±0.05	0.16±0.02	6.3	NA
	72	18.3	3.3±0.2	0.18±0.02		6.4	0.55
WB Anaerobic High N	24	20.7	2.7	0.13	0.15±0.02	6.5	NA
	72	24.3	4.4	0.20		6.5	0.59
W Aerobic Low N	4	51.4	40.1 ± 2.2	0.78 ± 0.05	0.58±0.06	7.5	NA
	8	45.1	32.8 ±1.1	0.72±0.02		7.4*	3.52*
	24	56.3	28.7±6.5	0.51±0.11		7.1*	4.53*
	72	60.5	23.7±1.4	0.39±0.02		7.4*	3.51*
W Anaerobic High N	4	51.1	38.8±2.2	0.74±0.03	0.65±0.03	7.1	NA
	8	45.9	31.6±1	0.69±0.02		7.0	0.33
	24	51.3	39.6±0.8	0.76±0.01		6.7	0.77
	72	56.5	29.2±2.0	0.52±0.03		6.20	0.98
WB Aerobic Low N	4	51.1	18.7±2.0	0.36±0.04	0.23±0.04	7.8	NA
	8	46.2	14.9±1.7	0.32±0.04		7.6	4.61
	24	52.9	8.9±0.9	0.17±0.02		7.8	6.86
	72	60.5	1.9±0.1	0.03±0.00		8.0	5.45
WB Aerobic High N	4	47.8	18.6±1.3	0.39±0.03	0.27±0.03	7.8	NA
	8	49.8	16.3±1.0	0.32±0.02		7.7	5.35
	24	46.6	10.6±0.65	0.22±0.02		7.8	6.71
	72	65.7	5.2±2.2	0.08±0.03		7.8	4.97
WB Anaerobic Low N	4	45.5	14.6±1.1	0.32±0.02	0.2±0.02	6.7	NA
	8	49.1	10.7±0.7	0.22±0.01		6.5	0.54
	24	50.4	7.4±0.8	0.14±0.02		6.6	0.90
	72	65.2	4.3±0.8	0.07±0.01		6.2	0.39
WB Anerobic High N	4	51.1	20.4±1.8	0.40±0.03	0.28±0.13	7.0	NA
	8	48.1	13.7±1.2	0.28±0.02		6.7	0.59
	24	51.3	11.1±0.7	0.22±0.01		6.7	1.13
	72	56.5	3.4±0.7	0.06±0.01		6.4	0.44

* One of the two bioreactors went under anaerobic condition

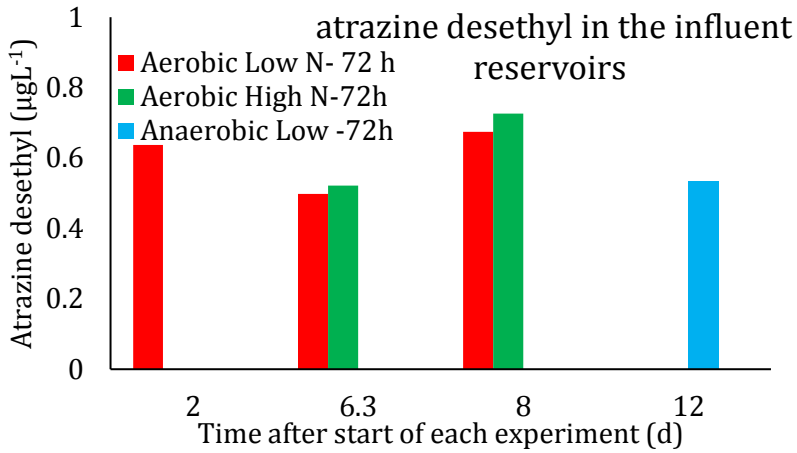

Figure S3-4 Atrazine desethyl concentrations at the influent reservoir.

Figure S3-4 shows that a small amount of atrazine desethyl was observed at the influent of some of the bioreactors when the 72h retention time experiment started. The inlets of other experiments did not show atrazine desethyl or other metabolites of atrazine. No change of water took place while each experiment was ongoing.

3.8.5 Adsorption Test

Batch Experiment #1

Methods: To make a distinction between adsorption of atrazine to woodchips or biochar and biodegradation, an assay test was performed. For this test, nine Erlenmeyer flasks contained 10 g woodchips and nine other contained 5 g biochar. Before starting the experiment, 100 mL of deionized water was added and kept overnight to fill the internal porosity of the woodchips and biochar. The treatments included the assays that did not

allow bacterial growth by 1) sterilizing (autoclaving) and 2) adding copper and the assays that allowed bacterial growth.

For the first type of essays, six Erlenmeyer flasks, three with woodchips and three with biochar, all containing 150 mL deionized water were autoclaved for 45 minutes at 125 °C. The water was then filtered out using a sterilized screen, and the flask was weighed to count for the deionized water left in the Erlenmeyer flasks. This was followed by adding 150 mL sterilized solution of tap water containing 60 µg L^{-1} atrazine and 30 mgL^{-1} glucose to the essays. The Flasks were topped with sterilized stoppers. Then, the air was evacuated and was replaced with sterilized helium gas. The second series of essays comprised the same media with the difference that the essays were not autoclaved. Instead, the solution contained 150 mg L^{-1} $CUSO_4$-Cu. These two essays aimed to prevent bacterial growth (Ilhan et al., 2011; Ochoa-Herrera et al., 2011).

Bacterial growth was desired for the third assays. Therefore, the assays contained water from the effluent of the lab bioreactors (1:15) to inoculate them. Apart from that, the same procedure as for the other two assays was followed. Controls were considered for each essay that was without the addition of woodchips and biochar. All the essays were kept in the dark and were shaken simultaneously for 18 hours on an orbital rotator shaker at a slow rate.

Results: The difference in atrazine removal in the three woodchips treatments was not significant (Figure S3-5). This indicated that atrazine removal by the bioreactors was attributed to abiotic processes. It is noteworthy that the biochar lost its structure and was powdered due to the shaking and thereby, by increasing its surface area, all atrazine adsorbed. Thus, the comparison between treatments was not possible for biochar essays.

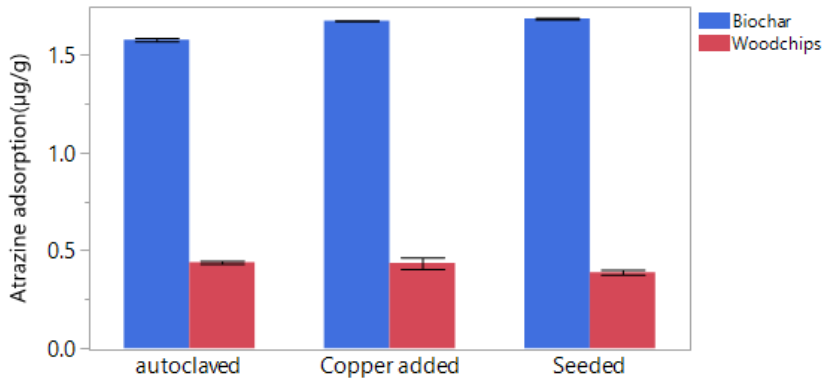

Figure S3-5 the removal of atrazine in the essay test. The error bars show the standard error.

Batch Experiment #2

Methods. This essay test included testing two pH levels (6.2 and 7.7) observed at the effluent of the flow-through bioreactors. We compared atrazine removal in sterilized solutions with and without wood in aerobic and anaerobic conditions. We also tested the effect of microorganisms (inoculated from the denitrifying bioreactors) on atrazine removal. All treatments had three replicates.

The sawdust from ash tree was sieved with the final size of 105- 596 µm, rinsed with deionized water, and air dried. We weighed 0.2 g portions and sterilized by autoclaving at 120° C for 30 minutes in VOA vials. The solutions were prepared using tap water containing 100 mg L^{-1} glucose-C, 20 mg L^{-1} NO_3^-—N, and 2 mg L^{-1} $PO_4^{3-} - P$, and 200 µg L^{-1} atrazine. The pH of the solutions was buffered at 7.7 using MOPS buffer and 6.2 with MES buffer; both acquired from Research Products International. Such buffers were shown not to interfere with atrazine (De Souza et al., 1996). In addition, controls at pH=6.6 were used to investigate the effect of these two buffers on atrazine removal, and they did not influence atrazine concentrations in the essays (both with and without wood and both in aerobic and anaerobic conditions). For the sterilized treatments, the solution

was sterilized by passing through 0.2-micron glass fiber filters. Otherwise, the solutions were inoculated with 10% effluent of the atrazine-free lab bioreactors.

The solution (35 ml) was added to each vial. For the aerobic conditions, vials were covered with porous caps made of PTFE membranes with pore sizes of 0.2 µm. For anaerobic conditions, 5 ml air was drawn from inside of the vials through the caps made of PTFE septa and was replaced with N_2 gas. This was repeated three times to ensure an anaerobic condition was achieved. The samples were put on a shaker at medium speed for 336 h in the dark. The solutions were then filtered through 0.2-micron PTFE syringe filters. It is noteworthy that there was a visible indication of bacterial growth in the intended treatments.

For extraction, wood from each vial was collected in a centrifuge tube and was centrifuged for 30 min in 6800 g. The supernatant was collected from above the wood. Then the wood fraction was extracted two times with 20 ml of methanol/water (80/20, v/v) solution. At each step, the mixture was shaken on the shaker for 30 min followed by centrifuging at 6800g for 15 min, which was followed by the collection of the supernatant. Finally, the collected samples from the two steps were mixed and dried under a flow of nitrogen gas and resuspended with deionized water. The samples were analyzed for atrazine using LC-MS without purification.

Results. The normalized atrazine concentrations C/C_0 (final concentration/initial concentration) for the different treatments are shown in Figure S3-6. The C/C_0 of atrazine after 336 h in the essays without wood was 0.93 ± 0.02 while the addition of wood significantly reduced it to 0.67 ± 0.01. Neither the pH level nor microbial activity significantly influenced atrazine removal (Table S3-5). Previously, Shirmardi et al., (2016)

similarly observed that pH did not influence atrazine adsorption to mineral and organic surfaces. The aerobic essays had statistically significant less removal of atrazine than the anaerobic assays by 6% (Table S3-5), and this difference was only observed when wood was present. Thus, it can be inferred that air or lack thereof may have impacted the surface of the wood. The extracted atrazine from the wood comprised of the 2.5 % to 6% of the initial atrazine concentrations. Thus 60 to 90% of the atrazine was recovered from the wood essays. In summary, this assay experiment confirmed that atrazine removal was not influenced by the growth of microorganisms from the denitrifying bioreactors.

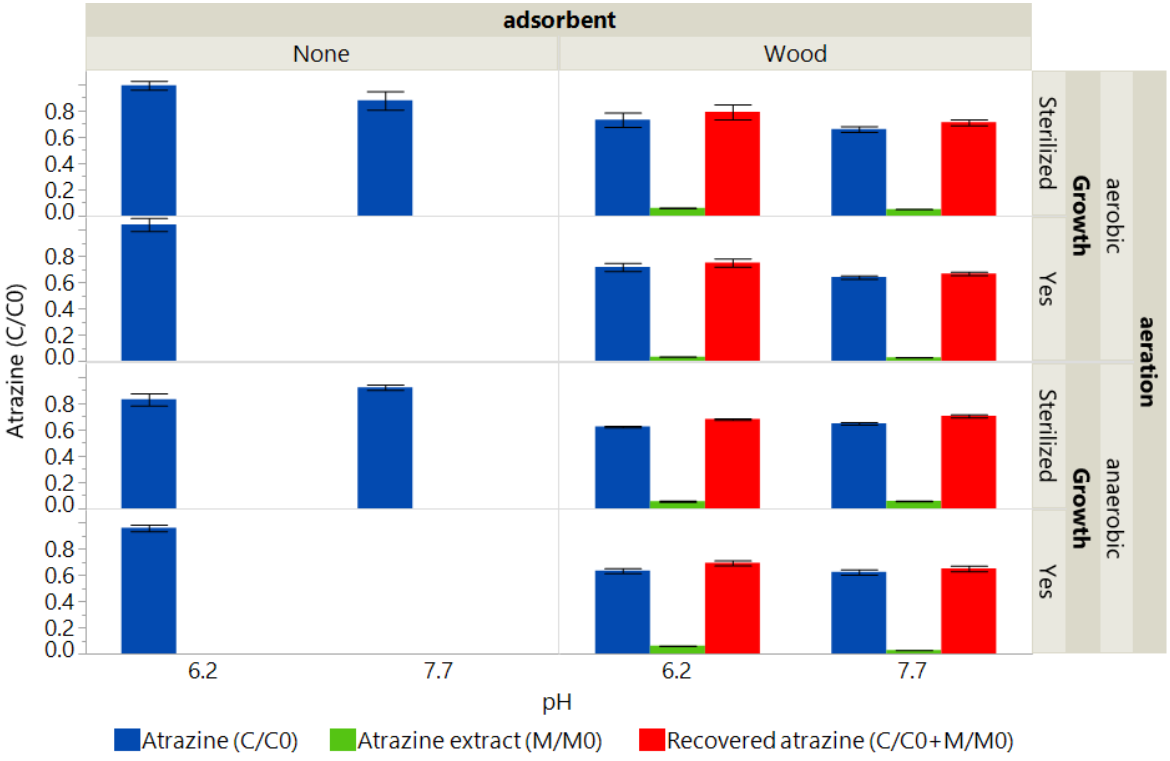

Figure S3-6 the relative atrazine concentration of atrazine remained in the solution (Atrazine (C/C_0)), the mass of the atrazine extracted from wood to initial mass of atrazine (Atrazine (M/M_0)), and the sum of two which is the recovered atrazine. The error bars show standard error.

Table S3-5 the influencing parameters on atrazine C/C_0 (final concentration/initial concentration). N is the number of parameters; DF is the degree of freedom, Sum of squares, F ratio, and the P-value for the effect test.

Source	N parm	DF	Sum of Squares	F Ratio	Prob > F
pH	1	1	0.014	3.07	0.0879
Bacterial Growth	1	1	0.007	1.52	0.2253
Media	1	1	0.727	159.59	<.0001*
aeration	1	1	0.038	8.42	0.0062*

3.8.6 Fourier-Transform Infrared Spectroscopy of Wood and Biochar

Methods: Fourier-Transform Infrared Spectroscopy (FTIR) for woodchip and biochar provides valuable information about the structure of the organic matter through evaluating the strength of bonds in the compounds. For FTIR measurements of woodchips, they were grated and further powdered using a ball mill. This was followed by recording FTIR Attenuated Total Reflection (ATR) spectra of milled wood using a Bruker Tensor 27 IR (Bruker Optics, Ettlingen, Germany) with a resolution of 10 cm^{-1} from 600 to 4000 cm^{-1}. The number of scans for each measurement was 32. A background measurement was made before gaining the sample spectra. For each sample, three measurements were recorded, then averaged.

Potassium bromide (KBr) pallet method was used for biochar since it is not transparent. The mixture of 0.1 grams of biochar and 3 grams of KBr were pressed under vacuum and pressure (Liu et al., 2015). Subject to pressure, KBr becomes transparent and does not absorb light in the infrared spectrum range. A background measurement was measured before acquiring the sample spectra to account for any interferences or any IR spectra losses by the KBr pellet. The same number of scans and measurements were taken

for biochar as they were taken for the woodchips. Finally, a baseline correction of spectra was done by utilizing software OPUS for both spectra of woodchips and biochar.

Results: The FTIR spectrum provides information about the constituent of each medium (Figure S3-7). Specifically, it characterizes the bonds on the surface of each material. This is crucial in assessing the potential of each organic matter in adsorbing atrazine. The more aromatic compound an organic matter has, the more it is capable of adsorbing atrazine. The FTIR spectra showed that woodchips consisted primarily of cellulose (1153 and 896 cm^{-1}), hemicellulose (1735 and 1051 cm^{-1}) and lignin (1593 and 1506 cm^{-1}) (Blue line in Figure S3-7; Rana et al., 2010). Biochar spectra (red line in Figure S3-7), showed a pronounced peaks for the aromatic compounds such as aromatic skeleton vibration at 1593 cm^{-1} (Rana et al., 2010), aromatic ether at 1124 cm^{-1} (Hergert, 1960), C-H and CH_2 out of plane deformation for aromatic rings at 871 cm^{-1} 829 cm^{-1}, respectively (Hergert, 1960). In addition, multiple peaks between 600 to 800 indicate the presence of aromatic bonds. Finally, the presence of polar, aliphatic compounds are indicated by the peaks at 1384cm^{-1} , 2852 cm^{-1}, and 2922 cm^{-1} which are originating from the C-H in aliphatic carbon, and the peak at 1697 cm^{-1} that reflects the presence of C=O bond for carboxylic carbon and traces of ketones and esters (Kimetu and Lehmann, 2010; Jindo et al., 2014; Sánchez-Sánchez et al., 2013).

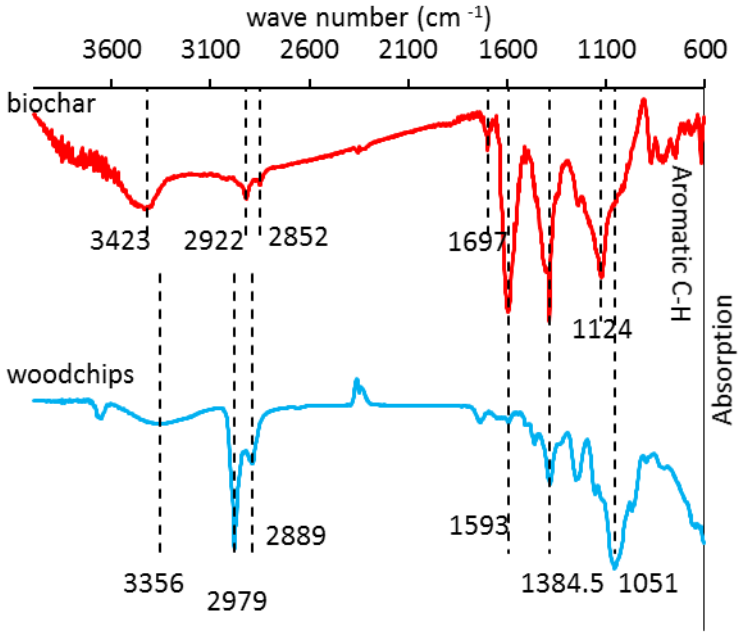

Figure S3-7 FTIR spectra for woodchips and biochar

CHAPTER 4:

EVIDENCE OF BIOCHAR ACTING AS AN ELECTRON ACCEPTOR IN WOODCHIP DENITRIFYING BIOREACTORS

Manuscript prepared for the Journal of Ecological Engineering.

By: Bahareh Hassanpour, Seyed Fardad Riazi, Erin Pluer Menzies, Larry D. Geohring, Christian D. Guzman, Ludmilla Aristilde, Tammo S. Steenhuis

4.1 Abstract

Woodchip denitrifying bioreactors mitigate nitrate load from agricultural tile effluents. Biochar is added occasionally to enhance their performance. However, research findings contradicted its effect on nitrate removal. In the current study, we, therefore, aimed to investigate the effect of biochar on the removal of nitrate in denitrifying bioreactors. For this purpose, laboratory and field experiments were carried out. In the laboratory, we used cylindrical up-flow bioreactors filled with woodchip and oxidized biochar at rates of 0%, 12.5%, 25%, 50%. The removal of nitrate was investigated at two stages: unaged and aged for 16 weeks. The bioreactors were operated at four hydraulic retention times of 2, 4, 8, and 24 h. In the field, nitrate removal over a 6-year period was investigated in two denitrifying bioreactors, one of which amended with 10% fresh biochar.

The laboratory experiments showed that, on average, oxidized biochar (OB) amendment reduced nitrate removal by 9% in unaged to 13% in aged bioreactors. This occurred despite OB bioreactors having the same or more respiration, which led us to conclude that oxidized biochar acted as an electron acceptor. In the field bioreactors, fresh

biochar initially increased nitrate removal. However, biochar became less effective over six years. In the final year, biochar-amended bioreactor removed less nitrate than the woodchip bioreactor, which can be ascribed to the electron-accepting ability of biochar due to aging. In summary, our study showed that biochar's role as an electron acceptor could significantly reduce denitrification in denitrifying bioreactors.

4.2 Introduction

Excess nitrogen load from fertilizer application is ,in part, responsible for eutrophication and ultimately hypoxia in freshwater lakes and the oceans (Galloway et al., 2004; Boyer et al., 2006). Woodchip bioreactors are employed for reducing nitrate load from agricultural tile drains (Schipper et al., 2010; Christianson and Schipper, 2016). It is well established that denitrification is responsible for the removal of nitrate in denitrifying bioreactors (Warneke et al., 2011a; c). These bioreactors use an organic substrate as an electron donor for denitrification (Blowes et al., 1994; Warneke et al., 2011b). As a substrate, wheat straw, green waste, sawdust (Warneke et al., 2011c), woodchip (Blowes et al., 1994; Driel et al., 2006; Hoover et al., 2016) or woodchip amended with biochar (Bock et al., 2014) have been used. Woodchip is the most widely used substrate because of its low cost, availability, hydrological properties, and ability to provide a long-lasting carbon source. Biochar is a good sorbent for organic pollutants found in tile lines (Ashoori et al., 2019; Hassanpour et al., 2019).

Biochar is a mediator for biogeochemical reactions in natural and engineered systems due to its role as an electron shuttle and can be both electron acceptor and donor (Lehmann et al., 2011; Clough et al., 2013; Kappler et al., 2014; Klüpfel et al., 2014). As

a result, studies show the contradictory role of biochar in the nitrogen cycle in soils (Singh et al., 2009; Cayuela et al., 2013; Chen et al., 2015; Bayabil et al., 2016). Similarly, in denitrifying bioreactors, biochar's effect is mixed. Some studies showed an increase in nitrate removal with the addition of biochar to woodchip (Bock et al., 2014; Coleman et al., 2019; Pluer et al., 2019) which agreed with our preliminary experiment with fresh biochar (see section 4.8.1). In other studies, however, biochar did not affect nitrate removal (Christianson et al., 2011d; Ashoori et al., 2019). In a three-year field study, Hassanpour et al. (2017), found biochar only temporarily increased nitrate removal in the bioreactors during the first two years of the bioreactor's application.

Coleman et al. (2019) and Bock et al. (2018) investigated the effect of biochar on nitrate removal, carbon dioxide, and nitrous oxide emissions in 120-h long experiments. They observed that biochar slightly increased nitrate removal, while increased carbon dioxide and nitrous oxide emissions considerably. Emission of nitrous oxide is unfavorable since it is a greenhouse gas that contributes to climate change (Montzka et al., 2011). Therefore, investigating the emission of nitrous oxide from the denitrifying bioreactors has been of interest (Spokas et al., 2009; Elgood et al., 2010).

The general objective of the current study was to investigate the effect of biochar amendment on the removal of nitrate in the woodchip denitrifying bioreactors. In this study, we improved on the Bock et al. (2018) and Coleman et al. (2019) experiments by measuring the dissolved concentrations of carbon dioxide than the emissions, and we monitored dissolved oxidizing anions such as nitrate, nitrite, and sulfate. Additionally, we examined the unaged and aged bioreactor conditions, as suggested by (Coleman et al., 2019). Finally, we investigated how aging impacted nitrate removal in the biochar amended

bioreactor in comparison to that of the woodchip bioreactor in field conditions over a 6-year period. Our findings have direct implications in water treatment systems under varied redox conditions where biochar may be applied.

4.3 Material and Methods

4.3.1 Biochar

Biochar used for all experiments in the current study was commercially supplied from Biochar Now® and was mostly of pine (Pinus sp.). This biochar was produced by slow pyrolysis at temperatures between 550 °C and 600 °C. The product had a length of 1–2 cm. For clarity, the terms used for fresh and oxidized biochar are described in Table 4-1. Fresh and oxidized biochar are distinguished due to their different characteristics as a result of the oxygen chemisorption to biochar. The oxidized biochar was from the same batch as the biochar used in the supplemental experiment (section 4.8.1). Fresh biochar was used in the field bioreactors and for the laboratory experiment described in the supplemental experiment. Biochar used in the laboratory experiment described in the following sections was exposed to the atmospheric oxygen for 2.5 years, thus, was oxidized (Bradbury and Shafizadeh, 1980; Bourke et al., 2007).

Table 4-1 Description of the terms for biochar used in the current study

Term	Description
Fresh biochar (FB)	Biochar that was recently purchased and kept in sealed plastic bags until use in the bioreactors. Fresh biochar was used for the supplemental experiment (section 4.8.1) and field bioreactor
Oxidized biochar (OB)	Biochar that was exposed to the atmosphere for 2.5 years in the laboratory until used for the current study

4.3.2 Laboratory experiment

4.3.2.1 Bioreactor preparation

Eight up-flow bioreactor chambers with a volume of 12 L (Figure 4-1) were filled with the mixtures of woodchip and oxidized biochar. Woodchip from ash trees (Fraxinus ornus sp.), was locally supplied and was 1-5 cm long and 5-6 mm wide. Woodchip (W), then, was mixed with oxidized biochar (OB) at four levels; woodchip only (0% biochar; W), and woodchip with oxidized biochar at rates of 12.5% (OB12.5), 25% (OB25) and 50% (OB50). A hole was drilled in the top of each bioreactor, and a septum was placed for drawing water samples for gas analysis (Figure 4-1). Finally, the bioreactors were air sealed.

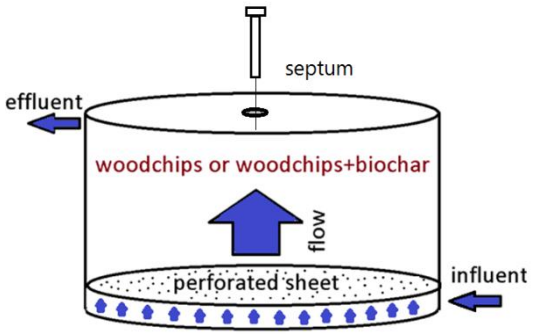

Figure 4-1 Schematic of the up-flow laboratory bioreactor. A septum was placed at the top of the bioreactors to draw water samples for gas analysis using a syringe.

4.3.2.2 Bioreactor operation and sampling

After construction, the bioreactors were flushed upward during a four-day start-up period with tap water at the rate of 1.8 L/h. The bioreactors, then, were inoculated with 6 L of the field woodchip bioreactor effluent. A detailed description of the field bioreactor is provided in the following sections. After two days of idling for inoculation, the first series of experiments began. The influent solution for the experiment was synthesized using tap

water, which is originated from a nearby creek, spiked with 11.5 mg/L NO_3^-—N. This concentration is close to the NO_3^-—N concentrations in the field bioreactor at about 10 mg/L year-around (Hassanpour et al., 2017). Prior to each experiment, the influent solution was stirred periodically overnight to avoid side reactions due to chlorine gas. The influent solution had a dissolved oxygen concentration (O_2) of ~ 6.1 mg/L.

The influent was introduced sequentially to the bioreactors at four different flow rates of 3.8, 1.8, 9.2, and 3 L/h. At each flow rate, 5-7 pore volumes of water were added to the bioreactors. After this initial "unaged" experiment, the bioreactors aged for 16 weeks. During these 16 weeks, tap water flowed to the bioreactors biweekly for 24 h at the rate of 1.8 mL/h to mimic the transient flow conditions in the field. Then, the experiments on the aged bioreactors began. The same experimental procedure as the unaged bioreactors were repeated for the aged bioreactors. The experiments on unaged and aged bioreactors were conducted in an average ambient room temperature of 22 °C.

In each pore volume, water samples were taken from the influent and effluent of the bioreactors during each experiment and were filtered through 0.45-micron filters. Then, they were stored in polypropylene test tubes and were refrigerated at 4 °C until analysis. The pH of the samples was measured immediately after collection with an Accumet AR50 pH probe. During the experiments, the effluent dissolved oxygen was measured in-line using a YSI 550 A dissolved oxygen meter. The samples were analyzed for nitrate (NO_3^-—N), nitrite (NO_2^-—N) and sulfate (SO_4^{2-}—S) using a Dionex ICS-2000 ion chromatograph (Pfaff, 1993b).

For gas analysis, water samples at all HRTs were taken using 60 mL syringes with 2.5 cm-long needles from the septum located at the top of the bioreactors (Figure 4-1). The

headspace equilibrium was carried out using 15 mL of the water sample and 45 mL helium gas as recommended by Jahangir et al. (2012). The obtained gas samples were stored in evacuated sealed serum vials and were analyzed for N_2O—N and CO_2 by an Agilent Technology 6890N gas chromatograph. The EPA method, with some adaption, was used to calculate the concentration of N_2O—N and $C_T^{CO_2}$ (CO_2 and equivalent HCO_3^-) (Wilhelm et al., 1977; Hudson, 2004). Since CO_2 is in equilibrium with HCO_3^- at environmental pH range, it was crucial to take both CO_2 and HCO_3^- into account. Details are provided in section 4.8.1.

4.3.2 Field Bioreactors

Paired bioreactors were constructed in October 2012 at Homer Thompson Vegetable Farm 10 km NE of Cornell University, by excavating two pits with dimensions of 6.1×3.1×1 m^3. One of the bioreactors was filled with woodchip, and the other was filled with woodchip (W) mixed with 10% fresh biochar (FB10). In March 2013, both bioreactors began to receive tile water from an interceptor which drained the vegetable farm and surrounding land. These bioreactors did not allow the tile flow to bypass; thus, tile effluent was entirely converted to the bioreactors. A full description of these bioreactors is provided in Pluer et al. (2016) and Hassanpour et al. (2017). Biweekly to monthly grab samples were collected from the influent and effluent on the bioreactors for 6 years from 2013 to 2018. In March 2018, before the start of the sampling period, the bioreactors went under a drying cycle to improve its performance as suggested by Maxwell et al. (2018).

In addition to monthly sampling, in May 2018, three ISCO-3700 autosamplers were used to take samples from the bioreactor's influent and effluents for two weeks at two-hour

intervals. Each sample composed of four 150 mL sips, which were taken 30 minutes apart. In this period, 123 samples were analyzed. Two HOBO® U20 water level loggers were placed at the effluent's water structure to measure the water head through the V notch weirs. The discharge from each bioreactor was calculated using the Weir equation calibrated for the weir in accordance with Hassanpour et al. (2017).

4.3.3 Calculations and Statistical Analysis

The performance of the denitrifying bioreactors was assessed using NO_3^-—N removal, R_{NO_3} (mg/L/h), which is calculated as (Pluer et al., 2019):

$$R_{NO_3} = \frac{C_{in}^{NO_3} - C_{out}^{NO_3}}{HRT} \qquad (4-1)$$

where $C_{in}^{NO_3}$ the inflow NO_3^-—N concentrations (mg/L) $C_{out}^{NO_3}$ is the effluent NO_3^-—N concentration. The hydraulic retention time (HRT) was calculated for each bioreactor as:

$$HRT = \rho \frac{V}{Q} \qquad (4-2)$$

where ρ is the porosity of the substrate, V is the volume of the bioreactor chambers (L), and Q is the flow rate (L/h). The porosity of the substrate for all four levels of biochar additions was 0.6 ± 0.01 cm^3/cm^3 measured by water displacement method, which is consistent with Robertson, (2010). For the four flow rates used in this study, the HRTs were 2,4, 8, and 24 h.

Our preliminary analysis of the results showed that respired CO_2 was in excess of the respiration of the influent oxygen, and oxygen from breaking down nitrate and sulfate.

Thus, we calculated the CO_2 mass balance, through which, we obtained the oxygen source which was required to produce the excess CO_2. The CO_2 mass balance of the bioreactors for one pore volume (PV) of the influent can be written as:

$$M_{bio}^{resp}/PV = M_{in}^{resp}/PV + M_S^{CO_2}/PV \qquad (4-3)$$

The M_{bio}^{resp}/PV is the respired CO_2 in the bioreactors per pore volume (mg), $\frac{M_S^{CO_2}}{PV}$ is the source term representing the excess CO_2 (mg) in one pore volume, and $\frac{M_{in}^{resp}}{PV}$ is the respired CO_2 (mg) by the reduction of influent in one pore volume. Assuming the production of nitrite is negligible, $\frac{M_{in}^{resp}}{PV}$(mg) is calculated by the stoichiometry of the respiration reactions (Table S4-2). According to Table S4-2, one mole of CO_2 is produced from the respiration of one mole of O_2, reduction of 4/5 mole of NO_3^- to nitrogen gas (N_2), and reduction of 1/2 mole of SO_4^{2-} to hydrogen sulfide (H_2S). Thus, the $\frac{M_{in}^{resp}}{PV}$(mg) is calculated as followed:

$$M_{in}^{resp}/PV = Qt\left\{\left(C_{in}^{O_2} - C_{out}^{O_2}\right) + \frac{4}{5}\left[C_{in}^{NO_3^-} - \left(C_{out}^{NO_3^-} + \frac{1}{2}C_{out}^{N_2O}\right)\right] + \frac{1}{2}C_{out}^{N_2O} + \frac{1}{2}\times\left(C_{in}^{SO_4^{2-}} - C_{out}^{SO_4^{2-}}\right)\right\} \times 44.01 \qquad (4-4)$$

Where Q is the flow rate (L/h), t is the HRT (h), $C_{in}^{O_2}$ and $C_{out}^{O_2}$ are the inflow and outflow O_2 concentrations (mM), $C_{in}^{NO_3^-}$ is the influent nitrate (mM), $C_{out}^{NO_3^-}$ is the effluent nitrate (mM), $C_{out}^{N_2O}$ is the effluent nitrous oxide (mM), and $C_{in}^{SO_4^{2-}}$ and $C_{out}^{SO_4^{2-}}$ are the influent and effluent sulfate concentrations (mM). The M_{bio}^{resp}/PV which is the respired CO_2 in the bioreactors per pore volume was calculated as:

$$M_{bio}^{resp}/PV = Qt\left\{C_{T,resp}^{CO_2}\right\} \quad (4-5)$$

, and $C_{T,resp}^{CO_2}$ is the respired (produced) CO_2 (mg/L) in the bioreactors as followed:

$$C_{T,resp}^{CO_2} = C_{T,out}^{CO_2} - C_{T,in}^{CO_2} \quad (4-6)$$

where $C_{T,out}^{CO_2}$ is the effluent [CO_2+ equivalent HCO_3^-] concentration (mg/L) and $C_{T,in}^{CO_2}$ is the influent [CO_2+HCO_3^-] concentration (mg/L). Finally, oxygen source per pore volume, M_S^O/PV (mg), which is the oxygen required to produce the $M_S^{CO_2}/PV$ was calculated as:

$$M_S^O/PV = M_S^{CO_2}/PV \times \frac{16}{44.01} \quad (4-7)$$

The Statistical analysis was performed using F-test for the comparison of the effects of the treatments by employing JMP package from Statistical Discovery™ (SAS). The paired comparison was performed by Student's t-test.

4.4 Results

4.4.1 Laboratory Bioreactors

The following describes the performance of the bioreactors amended with oxidized biochar (OB) and compares it with the woodchip only (W) bioreactors. Section 4.8.1 provides information about the application of fresh biochar in the denitrifying bioreactors. The supplemental experiment showed that fresh biochar (FB) increased NO_3^-—N removal by chemisorbing the influent dissolved oxygen.

4.4.1.1 Effluent Dissolved Oxygen

Establishing anoxic conditions is crucial for NO_3^-—N removal by the bioreactors. The dissolved oxygen concentrations of the effluent with the exception of the unaged W bioreactors at the 2-h hydraulic retention time (HRT) was less than 2 mg/L (Figure 4-2), thus, were anoxic (Gilham and Cherry, 1977; Korom, 1992).

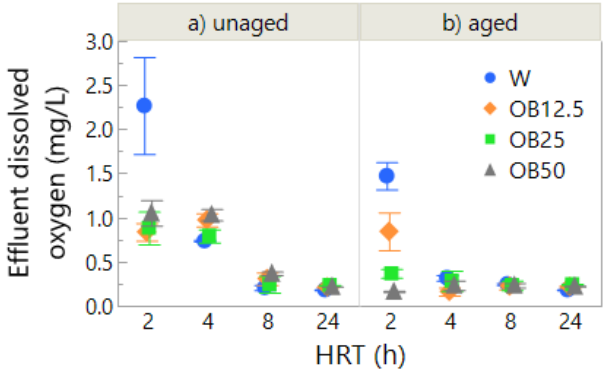

Figure 4-2 The effluent dissolved oxygen of the bioreactors containing W (woodchip), OB12.5 (woodchip with 12.5% oxidized biochar), OB25 (woodchip with 25% oxidized biochar), and OB50 (woodchip with 50% oxidized biochar) in four hydraulic retention times (HRT) for the a)unaged and b)aged conditions.

4.4.1.2 Nitrate-N Reduction In the Bioreactors

The concentrations used for analysis were measured in the samples taken during the last pore volume of water applied to the bioreactors when the equilibrium was achieved. The ratio of bioreactors' effluent and influent NO_3^-—N concentrations (C/C_0) as a function of HRT of the bioreactor are plotted in Figure 4-3. The HRTs were calculated for each bioreactor by measuring flow rate and were within 8% of the targeted values (Figure 4-3). Nitrite (NO_2^-—N) concentrations were below the detection limit of 0.1 mg/L.

The NO_3^-—N removal in the bioreactors was significantly impacted by HRT, substrate, and the age of the bioreactors (Table 4-2). The effect of the substrate was related to the HRT (Table 4-2). At short HRTs, the unaged bioreactors contained statistically similar concentrations of NO_3^-—N ($p > 0.05$), removing 6% of NO_3^-—N at 2 h (C/C_0= 0.94± 0.01; mean ± Std error) and 15% of NO_3^-—N at 4 h (C/C_0= 0.85± 0.01). At the HRT of 8 h, the W bioreactors removed 47% of the influent NO_3^-—N (C/C_0= 0.53) which was significantly greater than the bioreactors with the oxidized biochar (OB) bioreactors. The removal in the woodchip (W) bioreactors was 18 % greater than the OB12.5 and OB25 bioreactors ($p < 0.001$), and 24% greater than the OB50 bioreactors ($p=0.0002$; Figure 4-3). When the HRT increased to 24 h, the OB50 bioreactors had 20% less removal than W, OB12.5, and OB25 bioreactors which were NO_3^-—N limited (effluent NO_3^-—N < 0.5 mg/L; $p < 0.01$). On average, unaged OB bioreactors removed 9% less NO_3^-—N than the W bioreactors ($p<0.05$, Table 4-2).

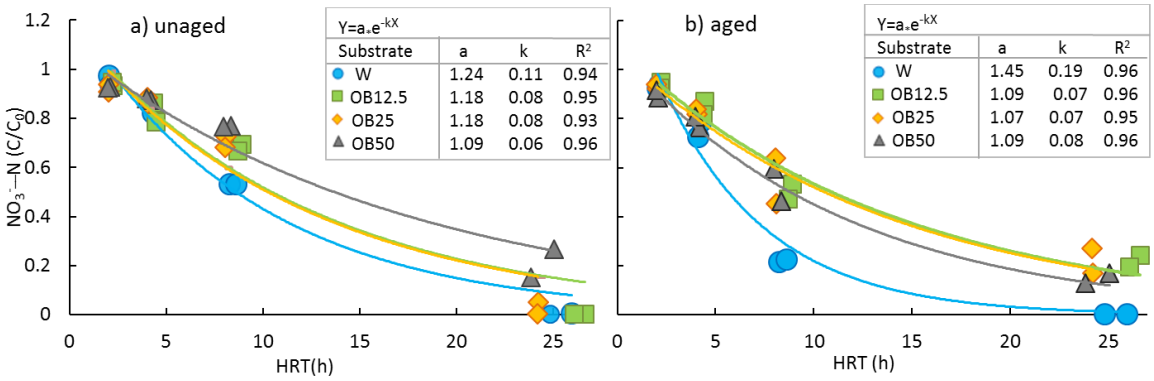

Figure 4-3 C/C_0 (effluent concentration/influent concentration) of NO_3^-—N for bioreactors containing W (woodchip), OB12.5 (woodchip amended with 12.5% oxidized biochar), OB25 (woodchip amended with 25% oxidized biochar), and OB50 (woodchip amended with 50% oxidized biochar) at different hydraulic retention times (HRT). a) C/C_0 of NO_3^-—N in the unaged bioreactors, b) C/C_0 of NO_3^-—N in aged bioreactors.

The NO_3^-—N removal of the aged bioreactors was greater than that of the unaged bioreactors (Figure 4-3). In aged bioreactors, like the unaged bioreactors, there was not a significant difference between NO_3^-—N removal of different substrates in short HRTs of 2 and 4 h (Figure 4-3 b; $p > 0.05$). For the 8 h HRT, the W bioreactors removed 80% of the NO_3^-—N which was significantly greater than the OB bioreactors ($p < 0.03$), while there was not a significant difference between the OB bioreactors with different levels of biochar amendment. For 24 h HRT, only W bioreactors removed the NO_3^-—N completely, about 20% more than the OB bioreactors ($p < 0.05$; Table 4-2, Figure 4-3b).

It is evident in the removal of NO_3^-—N followed first-order kinetics (Figure 4-3a, b). This agrees with the earlier findings of Schipper et al. (2010) for low inflow NO_3^-—N concentrations. When unaged, the OB50 bioreactors had the lowest first-order rate of 0.06/h while the W bioreactors had the greatest rate of 0.11/h. The aged W bioreactors had the greatest first-order rate of 0.19/h in comparison to the OB12.5 and OB25 bioreactors with the rate of 0.07/h and OB50 bioreactor with that of 0.09/h (Figure 4-3 a, b).

For comparison with other published studies, the NO_3^-—N removal rate of the bioreactors was calculated using Eq. 4-2. The NO_3^-—N removal rates varied between 5.7 and 22.7 mg/L/d and averaged at 10.4± 0.45 mg/L/d (Figure S4-3). These values were within those observed in the field (Schipper et al., 2010; Warneke et al., 2011a) and laboratory experiments (Warneke et al., 2011c; Hassanpour et al., 2019).

Table 4-2 Summary of statistical analysis of the NO_3^-—N removal, N_2O-N, $C_{T,resp}^{CO_2}$, and source of oxygen M_S^O/PV in the bioreactors.

parameters	NO_3^-—N (C/C_0)		NO_2—N		$C_{T,resp}^{CO_2}$ (mg/L)		M_S^O/PV mg	
	DF	P > F	DF	P > F	DF	P > F	DF	P > F
substrate	3	0.0005	3	0.0004	3	0.0054	3	0.0029
age	1	0.0218	1	0.0112	1	0.0019	1	0.0013
HRT(h)	3	<.0001	3	0.6822	3	<.0001	3	0.0793
age*substrate	3	0.0535	3	0.0003	3	0.1488	3	0.2353
HRT(h)*substrate	9	0.0237	9	0.8319	9	0.9703	9	0.9410

4.4.1.3 Nitrous Oxide

Dissolved nitrous oxide (N_2O—N) concentration in the water near the outlet in the top of bioreactors was used as a proxy for the potential of N_2O—N emission (Figure 4-1). The level of oxidized biochar (OB) amendment and the age of the bioreactors impacted N_2O—N concentrations (Figure 4-4, Table 4-2). The aged OB50 bioreactors had the greatest N_2O—N concentrations, which were two orders of magnitude greater than the concentrations of other bioreactors in all conditions. The N_2O—N concentrations of the aged OB50 bioreactors were variable ranging from 5.2 to 345 µg/L. Overall, the N_2O—N concentrations of the aged OB50, OB25, OB12.5, and W bioreactors were 125.9 ± 43.3, 1.1 ± 0.3, 0.7 ± 0.3, and 0.8 ± 0.3 µg/L, respectively (p=0.0004, Table 4-2).

In unaged bioreactors, a significant difference did not exist between N_2O—N concentrations of bioreactors with different levels of OB (p> 0.05), except for the bioreactors at the 2-h HRT. In this HRT, the N_2O—N concentration of the W bioreactors was 9.2 ± 1.6 µg/L while that was 2.9 ± 0.4, 2.6 ± 0.5 and 0.9 ± 0.9 µg/L for the OB12.5, OB25, and OB50, respectively (p< 0.01; Figure 3a). This was likely due to the presence of oxygen, which was not entirely reduced in W bioreactors in 2 h (Figure 4-2).

Ideally, N_2O—N would not be produced in the bioreactors since it is a greenhouse gas. However, the concentrations of N_2O—N produced in this experiment, were within those observed in previous studies. The N_2O—N concentrations in aged OB50 bioreactors comprised 1% of the inflow NO_3^-—N and 6% of the removed NO_3^-—N. In other unaged and aged bioreactors, N_2O—N concentrations were less than 0.02% of the influent NO_3^-—N. Such a transformation to N_2O—N was within those observed in the previous studies. Warneke et al. (2011) observed N_2O—N concentrations ranged from 0 to 1472 µg/L in laboratory bioreactors with different substrates, which comprised up to 10% of the influent NO_3^- — N. In another study, Warneke et al. (2011a) observed that 4.3 % of the inflow NO_3^-—N in field bioreactors was released as N_2O—N, however, Greenan et al. (2009) observed negligible N_2O—N emission.

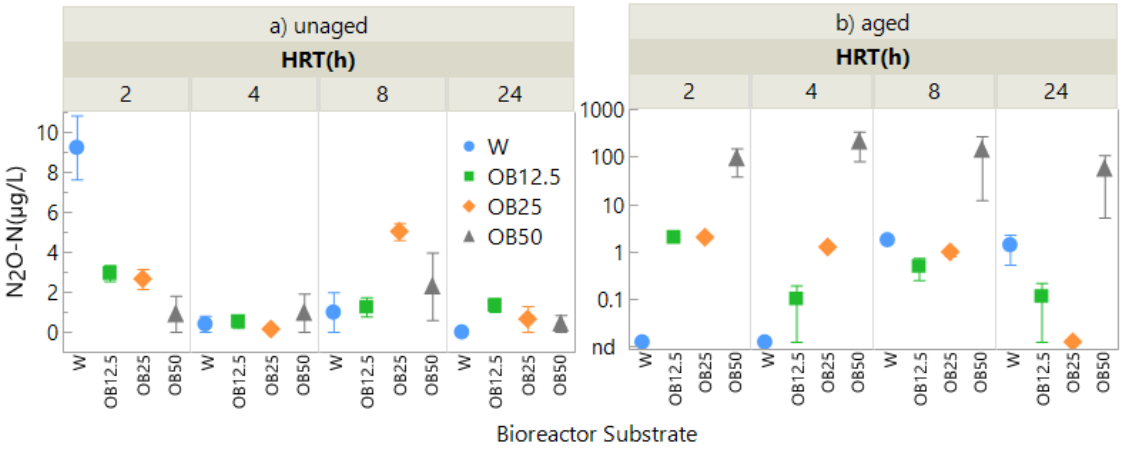

Figure 4-4 N_2O—N concentrations in bioreactors containing W (woodchip), OB12.5 (woodchip amended with 12.5% oxidized biochar), OB25 (woodchip amended with 25% oxidized biochar), and OB50 (woodchip amended with 50% oxidized biochar) at the four hydraulic retention times (HRT). a) N_2O—N in unaged bioreactors, b) N_2O—N in aged bioreactors. Note that the Y-axis for graph b is in logarithmic scale.

4.4.1.4 Bioreactor Respiration

Carbon dioxide (CO_2) is the product of respiration (Bridgham et al., 2014). The respired CO_2 ($C_{T,resp}^{CO_2}$) varied between 20 mg/L and 161 mg/L in the bioreactors (Figure 4-5a,b), with the substrate, age, and HRT (Table 4-2). The $C_{T,resp}^{CO_2}$ of the unaged bioreactors (mean ± Std error) was 86.2 ± 6.6 mg/L (Figure 4-5a). The W bioreactors had significantly less $C_{T,resp}^{CO_2}$ of 58.5 mg/L in comparison to the OB bioreactors, which respired 94.2 to 96.6 mg/L CO_2 ($p < 0.05$; Figure 4-5a,b). All unaged OB bioreactors have the same $C_{T,resp}^{CO_2}$ ($p > 0.05$).

The $C_{T,resp}^{CO_2}$ of the aged bioreactors was 64.0 ± 5.3, significantly less than that of the unaged bioreactors (Figure 4-5a). Except for the 2h HRT, the $C_{T,resp}^{CO_2}$ of the aged bioreactors increased with increasing oxidized biochar amendment level (Figure 4-5b). In 2h HRT, $C_{T,resp}^{CO_2}$ of the W bioreactors was more than that of the OB12.5 bioreactors, while it was not different from the OB25 and OB50 bioreactors.

The similar or increased $C_{T,resp}^{CO_2}$ of the OB bioreactors occurred despite less reduction of NO_3^-—N in these bioreactors in comparison to that of the W bioreactor. The respired CO_2 calculated from the reduction of the one pore volume of the influent oxygen, nitrate, and sulfate (M_{in}^{resp}/PV) is shown in Figure S4-5 a,b. The M_{in}^{resp}/PV comprised 10 % to 77 % of the total respiration in each pore volume (M_{bio}^{resp}/PV) in the bioreactors (Figure S4-5 c,d). This indicated that there were additional sources of oxygen in the bioreactors.

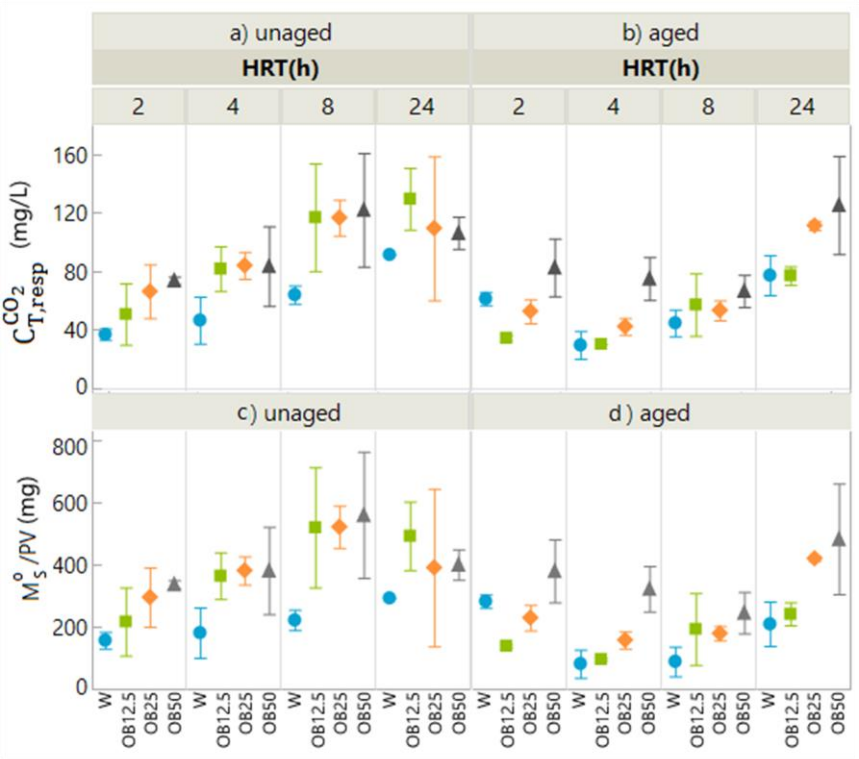

CO_2 concentration paired comparison			
substrate		unaged	aged ‡
●	W	a	a
■	OB12.5	b	ab
◆	OB25	b	b
▲	OB50	b	b

‡ excludes 2h HRT

CO_2 mass balance paired comparison			
substrate		unaged	aged ‡
●	W	a	a
■	OB12.5	b	ab
◆	OB25	b	bc
▲	OB50	b	c

‡ excludes 2h HRT

Figure 4-5 Respired CO_2 ($C^{CO_2}_{T,resp}$; Eq. 4-6) and oxygen source per pore volume (M^O_S/PV; Eq. 4-7) of the bioreactors filled with W (woodchip), OB12.5 (woodchip amended with 12.5% oxidized biochar), OB25 (woodchip amended with 25% oxidized biochar), and OB50 (woodchip amended with 50% oxidized biochar) at the four hydraulic retention times (HRT). a) $C^{CO_2}_{T,resp}$ of the unaged bioreactors, b) $C^{CO_2}_{T,resp}$ of the aged bioreactors, c) Oxygen source M^O_S/PV in unaged bioreactors and d) Oxygen source M^O_S/PV in aged bioreactors. The paired comparison for each group is shown to the right. The levels not connected with the same letter are significantly different.

Oxygen source in each pore volume (M^O_S/PV) of the bioreactors varied from 36 to 766 mg and increased with the biochar amendment level (Figure 4-5c,d). When unaged, the M^O_S/PV of the W bioreactor was 202.7 ± 27.1 mg which was significantly less than the OB bioreactors with the average M^O_S/PV varying from 398.6 to 421.3 mg ($p < 0.05$, Figure 4-5c).

The aged W had significantly less M_S^O/PV than the aged OB25 and OB50 bioreactors, while the difference between M_S^O/PV of the aged W and that of the aged OB12.5 bioreactors was not significant (Figure 4-5c,d). The only exception happened in 2 h HRT. At this HRT, the M_S^O/PV of the W bioreactor was significantly more than that of the OB12.5 bioreactors, while it was not different from that of the OB25 and OB50 bioreactors. On average, the W bioreactors had the least M_S^O/PV of 183.3 ± 23.2 mg among the bioreactors. The M_S^O/PV of the OB12.5, OB25, and OB50 in the bioreactors were 284.1± 46.6, 323.1± 40.7 and 390.2 ± 39.0 mg, respectively.

4.4.2 Field Bioreactors

The NO_3^-—N concentrations at the influent and the effluents of the field bioreactors over the 6 years are shown in Figure S4-6. The HRT (Eq. 4-2) of the woodchip (W) and fresh biochar amended (FB10) bioreactors was 1.6 ± 0.5 d and 1.7 ± 0.3 d, respectively. Because of this difference, NO_3^-—N removal rate (Eq. 4-1) was calculated for comparison of the two bioreactors. The NO_3^-—N removal rate of the bioreactors varied from 0 to 44.6 mg/L/d with an average of 4.5 mg/L/d. Figure 4-6a shows the NO_3^-—N removal rate of the bioreactors, excluding rate-limited points when effluent NO_3^-—N concentrations were lower than 0.5 mg/L.

During the first two years, in 2013 and 2014, the FB10 bioreactor removed 3.4 and 0.5 mg/L/d more NO_3^-—N than the W bioreactor ($p< 0.05$; Figure 4-6a). However, in the subsequent three years, there was not a significant difference between NO_3^-—N removal of the W and FB10 bioreactors. In 2018, however, the W bioreactor removed 0.5 mg/L/d more NO_3^-—N than the FB10 bioreactor ($p= 0.03$; Figure 4-6a). Over the whole period of

application, there was not a significant difference between the NO_3^-—N removal rate of W and FB10 bioreactors (p= 0.49).

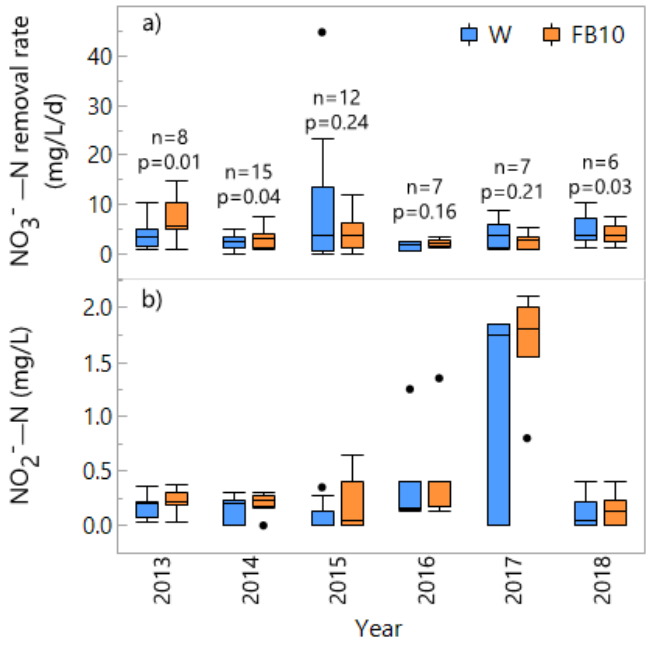

Figure 4-6 a) The NO_3^-—N removal rate in W (woodchip) and FB10 (woodchip with 10% biochar) field bioreactors over the 6 years of application. Each line on the box plot from top to bottom shows maximum, the first quartile, median, third quartile, and minimum values. P values and n, the number of sampling events in each year, are shown above the columns for each year. b) The nitrite-N concentrations at the effluent of the field bioreactors.

The nitrite (NO_2^-—N) concentrations of the W bioreactor at 0.22 ± 0.04 mg/L was significantly lower than those of the FB10 bioreactor at 0.29 ± 0.05 mg/L (p=0.009; Figure 4-6b). The NO_2^-—N concentrations varied from 0 to 2.1 mg/L with a maximum observed in the FB10 bioreactor in 2017. In 2017, the greatest concentrations of NO_2^-—N were observed in both reactors, but in 2018, after draining the bioreactors, those concentrations decreased. Effect of drying cycles requires further study (Maxwell et al., 2018).

In addition to sampling once a month, removal of NO_3^-—N of the W field bioreactor was compared to the FB10 bioreactor using high-frequency sampling for two weeks in May 2018. In this period, the inflow NO_3^-—N concentration was 8.5± 0.1 mg/L (Figure S4-7a) which reduced to 4.8± 0.1 and 5.1± 0.1 mg/L at the effluent of the W and FB10 bioreactor, respectively. The HRT of the W bioreactor was 12.7± 0.6 h, and that of the FB10 bioreactor was 18.1 ± 0.8 h. Thus, the NO_3^-—N removal rate for the W bioreactor was 7.2 ± 0.3 mg/L/d in comparison to 4.8 ± 0.2 mg/L/d for the FB10 bioreactor ($p < 0.0001$; Figure S4-7b).

The FB10 bioreactor had a significantly greater NO_2^-—N concentrations of 0.5 ± 0.06 mg/L compared to the W bioreactor of 0.3 ± 0.05 mg/L (Figure S4-7c; $p = 0.001$), despite removing less NO_3^-—N. On average, during this period, 4% of the inflow NO_3^-—N was transformed to NO_2^-—N in the W bioreactor and 6% in the FB10 bioreactor.

4.5 Discussion

4.5.1 Effect of Oxidized Biochar on Nitrate Removal and Respiration

In the literature, experiments with bioreactors found that biochar amendments had no effect (Christianson et al., 2011d) or small positive effect (Bock et al., 2014; Pluer et al., 2016) on NO_3^-—N removal. These results are consistent with our supplemental experiment on fresh biochar (section 4.8.1), which showed fresh biochar increased NO_3^-—N removal in denitrifying bioreactors.

Contrary to the previous studies, our laboratory study found that oxidized biochar (OB) adversely impacted NO_3^-—N removal (Figure 4-3). This happened while OB bioreactors had the same or more $C_{T,resp}^{CO_2}$ (respired CO_2), compared to W bioreactors

(Figure 4-5). Since the bioreactors were air-sealed, the source of oxygen for respiration was either from the influent or from the substrate. We calculated this oxygen source, M_S^O/PV, in the bioreactors (Eqs 4-3 to 4-7). The M_S^O/PV increased with the addition of oxidized biochar (Figure 4-5c,d), which was an indicator of the presence of an additional oxygen source in the OB bioreactors in comparison to W bioreactors. Thus, oxidized biochar acted as an electron acceptor and reduced denitrification (Kappler et al., 2014; Klüpfel et al., 2014; Chen et al., 2018).

Biochar produced at high temperatures, such as that used in the current study is redox-active (Klüpfel et al., 2014; Chen et al., 2018). Klüpfel et al. (2014) found carbon-oxygen double bond functional groups were major electron acceptors in oxidized biochar. We, too, observed Keto and carboxylic functional groups on biochar's surface one year after purchase as reported in Hassanpour et al. (2019). In addition to the formation of oxygen-rich functional groups, oxygen can be adsorbed in structural holes within condensed hexagonal planes of biochar (Swiatkowski et al., 2004). Biochar's role as electron shuttle is well known (Cayuela et al., 2013; Kappler et al., 2014; Yu et al., 2016), but its implications in engineered and natural systems are currently researched. Recently, Saquing et al. (2016) and Chen et al. (2018), showed oxidized biochar acted as an electron acceptor and reduced reduction of nitrate to ammonium and denitrification in aqueous anaerobic conditions containing acetate. Such an impact was observed in the current study, with woodchip as the substrate, as well.

The role of oxidized biochar in reducing NO_3^-—N removal was noticeable in mid-range HRT of 8 h, while in short HRTs of 2 and 4 h, the OB and W bioreactors removed NO_3^-—N similarly. This could be ascribed to electron transfer kinetics and the formation

of anoxic conditions (Klüpfel et al., 2014). Although the role of biochar in long HRT of 24 h was linked to NO_3^-—N limited conditions, the OB bioreactors removed less NO_3^-—N than the W bioreactors at this HRT as well (Figure 4-3a,b).

Our experiments showed an increased NO_3^-—N removal and a decreased $C_{T,resp}^{CO_2}$ with aging (Figures 4-3 and 4-5). This happened for two reasons. First, in the unaged experiment, the internal porosity of woodchip and biochar may not have been fully saturated. As a result, oxygen may have diffused to the pore water, thus reduced denitrification in the unaged bioreactors.

Second, prolonged anaerobic conditions impacted the electron-acceptor ability of the biochar during the aged experiments. This is reflected in the reduced $C_{T,resp}^{CO_2}$ of the aged OB12.5 bioreactors, with the lowest biochar amendment. The $C_{T,resp}^{CO_2}$ of the aged OB12.5 bioreactors was not significantly different from that of the aged W bioreactors (Figure 4-5). This, however, was not relevant in OB50 bioreactors, with a larger biochar amendment level. Thus, the electron-accepting ability of biochar might decrease over time, depending on the amendment level.

4.5.2 Environmental Implications

The trend observed in NO_3^-—N removal of the field bioreactors can be explained by the role of biochar as an electron shuttle. After launch, fresh biochar increased NO_3^-—N removal in field bioreactors (Figure 4-6), in agreement with the result of our supplemental experiment (section 4.8.1) and other research findings (Pluer et al., 2016). This is consistent with fresh biochar acting as an electron donor by chemisorbing oxygen (Bradbury and Shafizadeh, 1980; Klüpfel et al., 2014; Prévoteau et al., 2016). Indeed, in the aging of

biochar, according to Cheng et al. (2006) oxygenated functional group increase on the biochar surface. However, by aging for 6 years and going under a drying cycle, which led to an interaction with atmospheric oxygen, biochar acted as an electron acceptor and reduced NO_3^-—N removal in comparison to that of the W bioreactor (Klüpfel et al., 2014; Saquing et al., 2016).

Addition of both fresh and oxidized biochar led to increased concentrations of the intermediate products of denitrification in the bioreactors. In the field bioreactors, the effluent NO_2^-—N concentrations were greater in the biochar amended bioreactor (Figure 4-6b, S4-7). We did not measure N_2O—N concentrations in the field. However, in the laboratory, the most notable effect of oxidized biochar amendment on N_2O—N concentration was observed in aged OB50 bioreactors. The aged OB50 bioreactors had two orders of magnitude greater N_2O—N concentrations than the other aged or unaged bioreactors (Figure 4-4b). Similarly, Bock et al. (2018) found that the bioreactors amended with 30% biochar had the maximum N_2O—N emission in comparison to those with a lower level of biochar amendment or no amendment. Thus, it can be concluded that biochar reduced completion of denitrification.

4.6 Conclusion

In the current study, we showed that biochar could be both an electron donor and an electron acceptor in denitrifying bioreactors. Our supplemental and field experiment showed that fresh biochar increased denitrification by chemisorbing oxygen. However, oxidized biochar reduced denitrification by functioning as an electron acceptor. The adverse effect of biochar on NO_3^-—N removal by the bioreactors persisted over time,

although reduced significantly. The role of biochar as electron acceptor was also observed when in biochar aged in the field bioreactors for 6 years, which ultimately led to decreased NO_3^-—N removal in the 6th year, despite increasing NO_3^-—N removal in the initial years.

In summary, our study showed the electron-accepting ability of biochar could impact its function in anaerobic conditions and reduce NO_3^-—N removal. Finally, we suggest that biochar studies consider reporting the storage conditions of biochar as it may impact its characteristics.

4.7 Acknowledgment

This research was made possible by funding from USDA NIFA Northeast SARE# GNE17-151-31064, and USDA NIFA Hatch Accession #231333 and #1237429, and NRCS- Conservation Innovation Grant (CIG) 67-3A75-13-215. The authors would like to thank Karl Pendleton, who helped to construct the chambers, and Daniel F. May for his help in sample collection. Special thanks to Dr. Brian Richards for his suggestions.

4.8 Supplemental Material

4.8.1 supplemental Experiment on fresh biochar

4.8.1.1 Material and Methods

Cylindrical up-flow bioreactors with a volume of 12 L were constructed and filled with woodchips (W) and woodchip amended with fresh biochar (FB50; 1:1 by volume) in duplicates. Bottom of each bioreactor was equipped with a perforated sheet to avoid the preferential flow of water and solute to the W and FB50 media. Woodchips, acquired from a local sawmill, was from ash trees and were 1-5 cm long and 5 -6 mm wide. Biochar was

supplied from Biochar Now® and was produced by slow pyrolysis at temperatures of between 550 °C and 600 °C. It was from woody stocks mostly of pine (Pinus sp.) origin. The length of the biochar chips was around 1–2 cm.

Before the experiments started, bioreactors received 5 pore volume of water from our field bioreactor in Tompkins County, NY (Hassanpour et al., 2017) to be inoculated with denitrifying bacteria. The bioreactors were kept in saturated conditions for four months, and in each month, bioreactors received one series of tap water, each time for 56 h at the rate of 7.5 mL/min. Tap which had an original nitrate-N (NO_3^-—N) concentration of 2 mg/L was used. After 6 months of aging, tap water spiked to a concentration of 6.2 mg/L NO_3^-—N flowed through the bioreactors at the rate of 26 mL/min for 100 h. This flow rate corresponded with an HRT of 4.8 h. Immediately after, for 128 h, the influent reservoir's DO was reduced to 1.5 mg/L by putting nitrogen gas (Air gas, Ithaca, NY). It must be mentioned that one of each bioreactor type received 10 µg/L atrazine. The experiment was carried out in an ambient room temperature of 21° C. The NO_3^-—N, nitrite-N (NO_2^-—N), and the dissolved oxygen (DO) was monitored during the experiment.

4.8.1.2 Results and Discussion

Both bioreactors reduced NO_3^-—N from the influent water. With aerobic influent, after reaching to equilibrium, the average concentration of NO_3^-—N at the effluent of the W bioreactors was 5.1 mg/L in comparison to that at the effluent of the FB50 bioreactors which was 3.7 mg/L (Table S4-1, Figure S4-1a). This corresponded with NO_3^-—N removal of 18% (C/C_0=0.82) and 41% (C/C_0=0.59) in W and FB50 bioreactors, respectively (Table S4-1), and indicated that the biochar amendment improved NO_3^-—N removal. By switching

to the anaerobic influent, the NO_3^-—N removal of the W bioreactor increased by 20% while the FB50 bioreactors experienced only a 6% increase in NO_3^-—N removal. It is of note that with the reduced influent dissolved oxygen, the FB10 and W bioreactors eventually had the same NO_3^-—N removal rate (Figure S4-1b).

The increased NO_3^-—N removal in the FB50 bioreactors could be attributed to the role of biochar in chemisorbing dissolved oxygen (Bradbury and Shafizadeh, 1980). Figure S4-2 shows how the effluent dissolved oxygen of the W bioreactor reached 1.7 mg/L through the experiment, which decreased to a relatively constant value of about 0.5 mg/L after the influent dissolved oxygen was reduced. The FB50 bioreactors had low effluent dissolved oxygen of 0.5 mg/L during the whole experiment (with both aerobic and anaerobic influent). If FB10 bioreactors were removing the dissolved oxygen by increased respiration, the reduced dissolved oxygen in the influent should have increased NO_3^-—N removal like that of the W bioreactor (Figure S4-1a, b). This clearly was not the case. Thus, the increased NO_3^-—N removal of the FB10 bioreactors can be related to chemisorption of dissolved oxygen by the biochar. Thus, fresh biochar used in bioreactors for 6 months acted as an electron donor.

The effect of fresh biochar on nitrite (NO_2^-—N) is depicted in Figure S4-1c. The (FB 50) bioreactors had greater NO_2^-—N concentrations during the experiment. This indicated that the completion of denitrification was hindered by biochar.

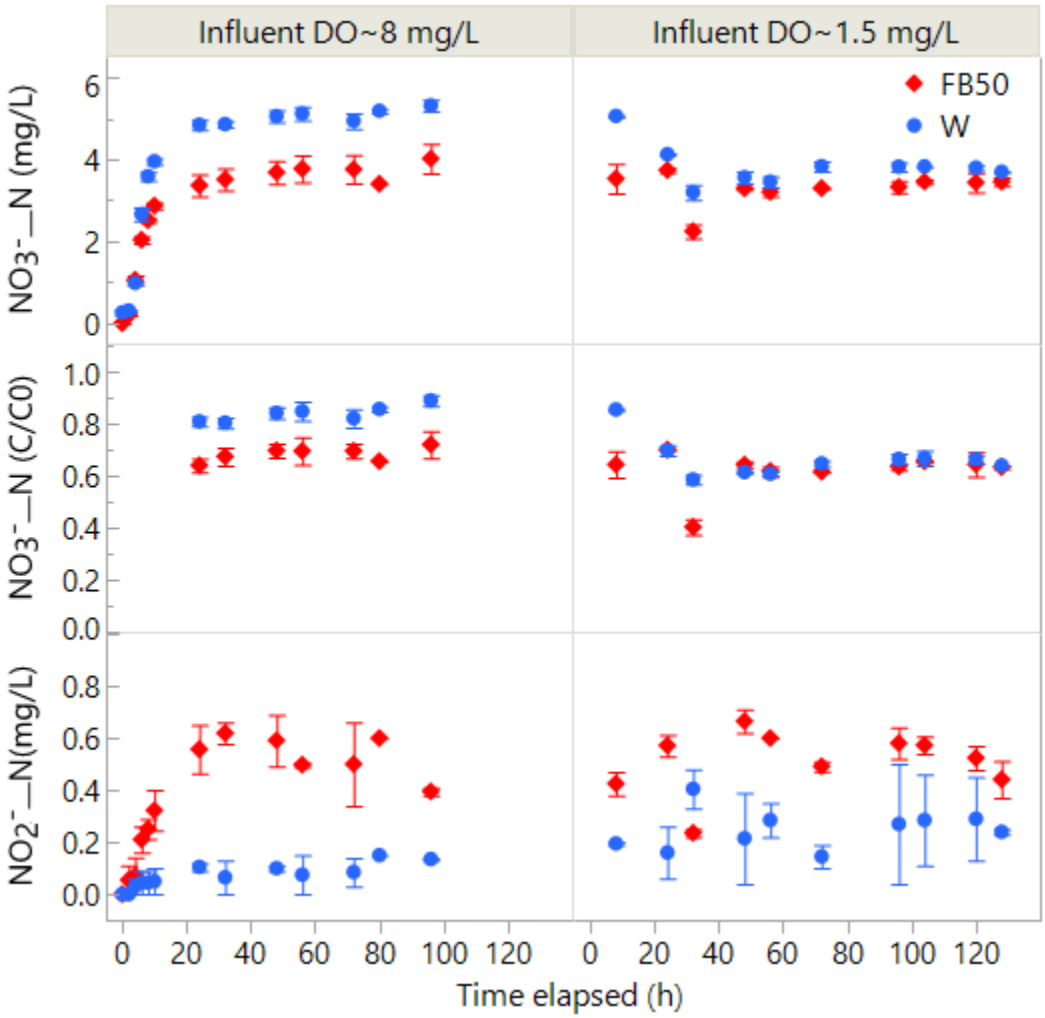

Figure S 4-1 a) effluent NO_3^-—N concentrations, b) the ratio of the effluent to influent NO_3^-—N concentrations (C/C_0), and c) effluent NO_2^-—N concentrations of the woodchips (W) and woodchips + 50% fresh biochar (FB50) bioreactors under varied influent dissolved oxygen (DO) of 8 and 1.5 mg/L.

Table S 4-1 The average effluent NO_3^-—N concentrations, average effluent NO_2^-—N concentrations, the C/C_o of NO_3^-—N (effluent concentration/influent concentration), NO_3^-—N removal rate and effluent dissolved oxygen (DO) of the woodchip (W) and woodchip + 50% biochar (FB50) bioreactors under varied influent aeration.

Experiment no	Bioreactor	Effluent NO_3^-—N ± std error (mg/L)	Effluent NO_2^-—N ± std error (mg/L)	NO_3^-—N (C/C_o) ± std error	NO_3^-—N removal rate ± std error (mg/L/d)	Effluent DO ± std error (mg/L)
Aerobic influent (DO≈8 mg/L)	W	5.1± 0.06	0.1± 0.01	0.82±0.01	5.8±0.27	1.17±0.1
	FB50	3.7± 0.10	0.5± 0.03	0.59±0.01	13.1±0.47	0.64±0.07
Anaerobic influent (DO≈1.5 mg/L)	W	3.8± 0.11	0.25±0.03	0.62±0.02	12.6±0.61	0.49±0.06
	FB50	3.3± 0.09	0.5±0.03	0.53±0.02	15.3±0.52	0.44±0.05

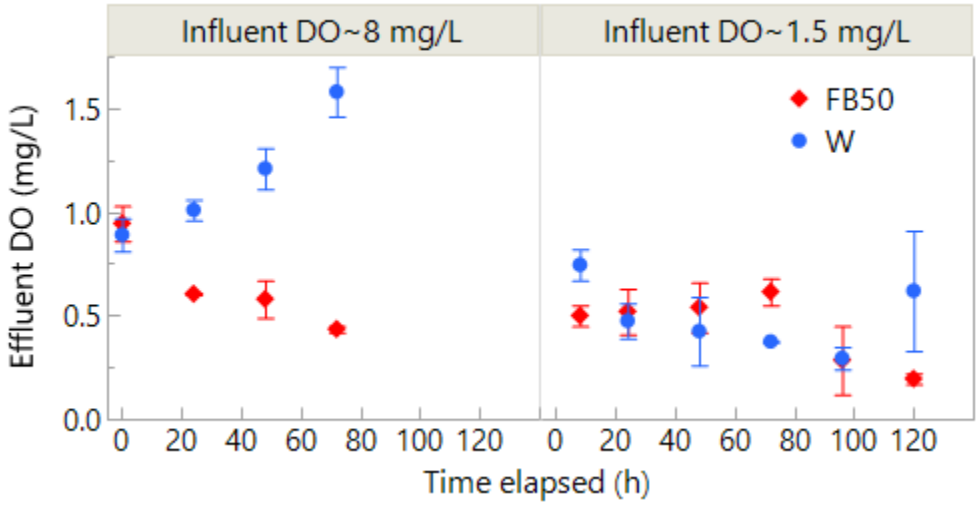

Figure S 4-2 the effluent dissolved oxygen of the woodchip (W) and woodchip + 50% fresh biochar (FB50) bioreactors over time under varied influent dissolved oxygen (DO) of 8 and 1.5 mg/L.

4.8.2 Additional Information: Laboratory Experiment on Oxidized Biochar

4.8.2.1 Measurement of Total Respiration

The EPA method (Hudson, 2004) for the gas analysis, the measured concentration of gas by the GC is converted to the concentration of gas in the aqueous and headspace, and the sum of both is the gas concentration of the original sample. In our study, we were interested in the total respired CO_2, thus HCO_3^- concentration was important since CO_2 is the converted to HCO_3^- in environmental pH. Wilhelm et al., (1977) suggested using equilibrium constant to calculate the sum of CO_2 and HCO_3^- in equilibrium with headspace gas. Thus, we adapted the EPA method as followed:

$$C_T^{CO_2} = C_{AH} + C_A + C_{AB} \qquad (S-1)$$

Where $C_T^{CO_2}$ is the total concentration of CO_2 in the original water sample (mg/L), including both CO_2 and HCO_3^-, C_{AH} is the aqueous gas concentration in headspace after equilibrium, C_A is the aqueous gas concentration in water after equilibrium, and C_{AB} is the HCO_3^- in the water after equilibrium. C_{AH} is calculated as followed:

$$C_{AH} = \frac{V_h}{V_w} \times C_g \times \rho \qquad (S-2)$$

Where C_g is the volume ratio measured by the gas chromatograph (gas volume/total volume) ,V_h is the headspace volume, V_w is the volume of the water sample, and ρ is the density of the gas (mg/L). The C_{AH} is expressed as mg/L. Then, the C_A is calculated as followed:

$$C_A = 55.5 \times \frac{C_g \times P_T}{H} \times M_W \qquad (S-3)$$

Where 55.5 is the molar concentration of water mol/L, P_T is the atmospheric pressure (1 atm), C_g is the the volume ratio measured by the gas chromatograph (gas volume/total volume), H is the Henry's constant (atm/mol) as described by Wilhelm et al. (1977), and Mw is the molar mass of gas (mg/L). The final concentration was expressed as mg/L.

For HCO_3^- concentration, the C_A concentration was converted to mol/L, and the following equilibrium equation was applied:

$$C_{HCO_3^-} = \frac{C_A \times K_1}{[H^+]} \qquad (S-4)$$

Where $[H^+]$ was acquired from the pH of the sample, and K_1 is the equilibrium constant of $10^{-6.3}$ for the carbonate system. Each mole of CO_2 produces 1 mole of HCO_3^-, thus the equivalent CO_2 concentration of $C_{HCO_3^-}$ was used for the $C_{AH,}$ in mg/L.

An example for such calculation is as followed:

$C_g = 4365.2\ (ppm) * 10^{-6}$

Aqueous gas concentration in headspace was calculated first:

$$C_{AH} = \frac{V_h}{V_w} \times C_g \times \rho$$

$$= \frac{45(ml\ headspace)}{15(ml\ water\ sample)} * 4365.2\ (ppm) * 10^{-6}$$

$$* \frac{10^3 * 44.01\ (\frac{mg\ CO_2}{mole})}{22.4\ (\frac{L}{mole})} * \frac{273.15}{273.15 + 24.3} = 24.02\ mg/L$$

Then the aqueous gas concentration in water after equilibrium was calculated:

$$\mathrm{C}_A = 55.5 \times \frac{C_g \times P_T}{H} \times M_W$$

$$= 55.5\ (\frac{mol\ water}{L}) * \left(\frac{4365(ppm) * 10^{-6} * 1(atm)}{1606\ \left(\frac{atm}{mol}\right)} \right) * 44.01$$

$$* 10^3(\frac{mg\ CO_2}{mol}) = 6.7 mg/L$$

Note: H is Henry's constant. For CO_2 gas, according to Wilhelm et al. (1977) H is:

$$H = \exp[-\left(-317.658 + \frac{1731.2}{T + 273.15} + 43.0607 * \ln(T + 273.15) - 0.00219107\right.$$

$$\left. * (T + 273.15) \right) / 1.987] = 1606\ atm/mol$$

The following is the concentration of HCO_3^- in the water after equilibrium in a sample with a pH of 7.14:

$$\mathrm{C}_{HCO_3^-}(equivalent\ CO_2) = \mathrm{C}_A \times \frac{K_1}{[H^+]} = \left(\frac{6.7 mg/L}{44.01(\frac{g\ CO_2}{mol})} \right) * \frac{10^{-6.3}}{10^{-7.14}} = 1.06\ mM$$

The following is the concentration of CO_2 that was converted to HCO_3^-

$$\mathrm{C}_{\mathrm{AB}}\ \left(\frac{\mathrm{mg}}{\mathrm{L}}\right) = \mathrm{C}_{HCO_3^-}(mM) \times 44.01\ \frac{gCO_2}{mol}$$

$$\mathrm{C}_{\mathrm{AB}}\ \left(\frac{\mathrm{mg}}{\mathrm{L}}\right) = 1.06 * 44.01\ \frac{gCO_2}{mol} = 46.7\ mg/L$$

$$C_T^{CO_2} = 46.7 + 6.7 + 24.02 = 77.44 \frac{mg}{L}$$

4.8.2.2 Influent CO_2 Content

The influent carbonate species $C_T^{CO_2}$concentration was calculated as followed:

$$C_{T,in}^{CO_2} = C_{in}^{CO_2} + C_{in}^{HCO_3^-} \qquad (s-5)$$

Where the $C_{in}^{CO_2}$ is the influent concentration of $CO_{2(aq)}$ (mg/L) and $C_{in}^{HCO_3^-}$ is the influent HCO_3^- concentration, expressed as the equivalent CO_2 in mg/L. The pH of the influent was 7.7. The following was used to calculate these concentrations.

$$C_{in}^{CO_2} = K_H \times P_{CO_2} = 10^{-1.5} \times 10^{-3.5} = 10^{-5}\, M \times 44.01\, \frac{g}{mol} \times 1000 = 0.44 \frac{mg}{L}$$

$$C_{in}^{HCO_3^-} = \frac{10^{-5} \times K_1}{[H^+]} = \frac{10^{-5} \times 10^{-6.3}}{10^{-7.7}}$$

$$= 10^{-3.6}\, M \times 44.01\, \frac{g\ (equivalent\ CO_2)}{mol} \times 1000 = 11.07\, mg/L$$

Thus, the $C_{T,in}^{CO_2}$ was 11.51 mg/L.

4.8.2.3 Carbon Dioxide Production Pathways

Table S 4-2 Stoichiometry of carbon dioxide production pathways

Aerobic respiration	$CH_2O + O_2 \rightarrow H_2O + CO_2$
Denitrification	$4/5\ H^+ + CH_2O + 4/5NO_3^- \rightarrow CO_2 + 2/5N_2 + 7/5H_2O$
Sulfate reduction	$H^+ + CH_2O + 1/2SO_4^{2-} \rightarrow CO_2 + 1/2H_2S + H_2O$
Nitrate reduction to nitrous oxide	$H^+ + CH_2O + NO_3^- \rightarrow CO_2 + 1/2N_2O + 3/2H_2O$
Carbonate system	$CO_2+H_2O \rightarrow HCO_3^-+H^+$

4.8.2.4 Nitrate-N Removal Rate

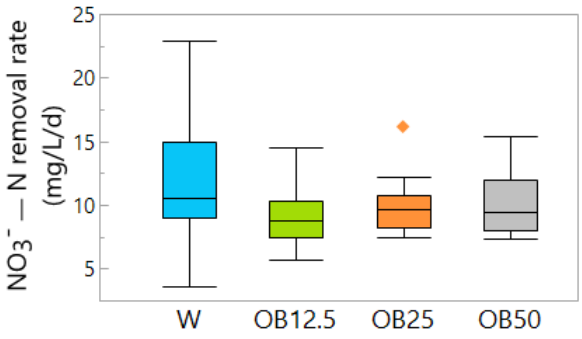

Figure S 4-3 NO_3^-—N removal rates of bioreactors filled with W (woodchip), OB12.5 (woodchip+12.5% oxidized biochar), OB25 (woodchip+25% oxidized biochar), and OB50 (woodchip+ 50% oxidized biochar).

4.8.2.5 Sulfate-S Reduction In the Bioreactors

The tap water contained sulfate (SO_4^{2-}—S). The SO_4^{2-}—S concentrations were 3.9 mg/L for the unaged experiments and 9.9 mg/L for the aged experiments. The SO_4^{2-}—S concentrations generally remained unchanged at the effluent of the bioreactors, except for the 24 h HRT when NO_3^-—N was present at low concentrations (Figure 4-4 a,b). In the unaged bioreactors, at 24 h retention time, 95 ± 0.4 % of the influent SO_4^{2-}—S was found at the effluent, which reduced to 90 ± 1 % in the aged bioreactors. This is consistent with the increased NO_3^-—N removal when bioreactors aged (Figure 4-4 a,b).

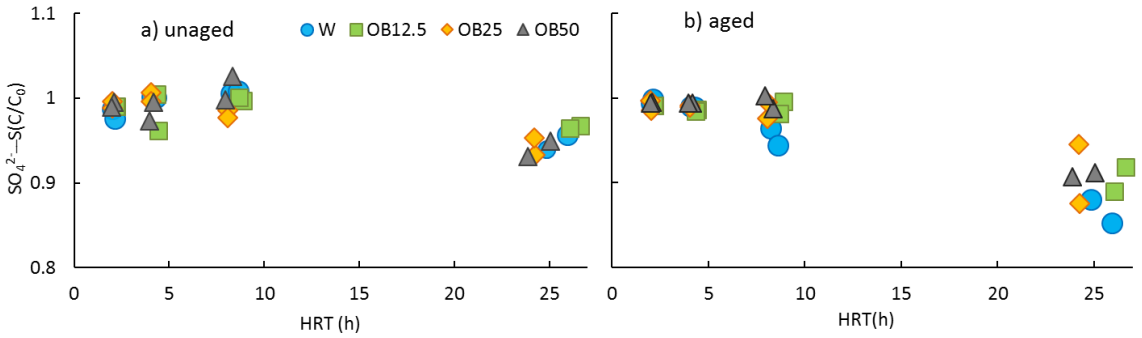

Figure S 4-4 C/C_0 (effluent concentration/influent concentration) of SO_4^{2-}—S for bioreactors containing W (woodchip), OB12.5 (woodchip amended with 12.5% oxidized biochar), OB25 (woodchip amended with 25% oxidized biochar), and OB50 (woodchip amended with 50% oxidized biochar) at different hydraulic retention times (HRT). a) C/C_0 of SO_4^{2-}—S in the unaged and, b) C/C_0 of SO_4^{2-}—S in the aged bioreactors

4.8.2.6 Respired CO_2 by the Reduction of Influent

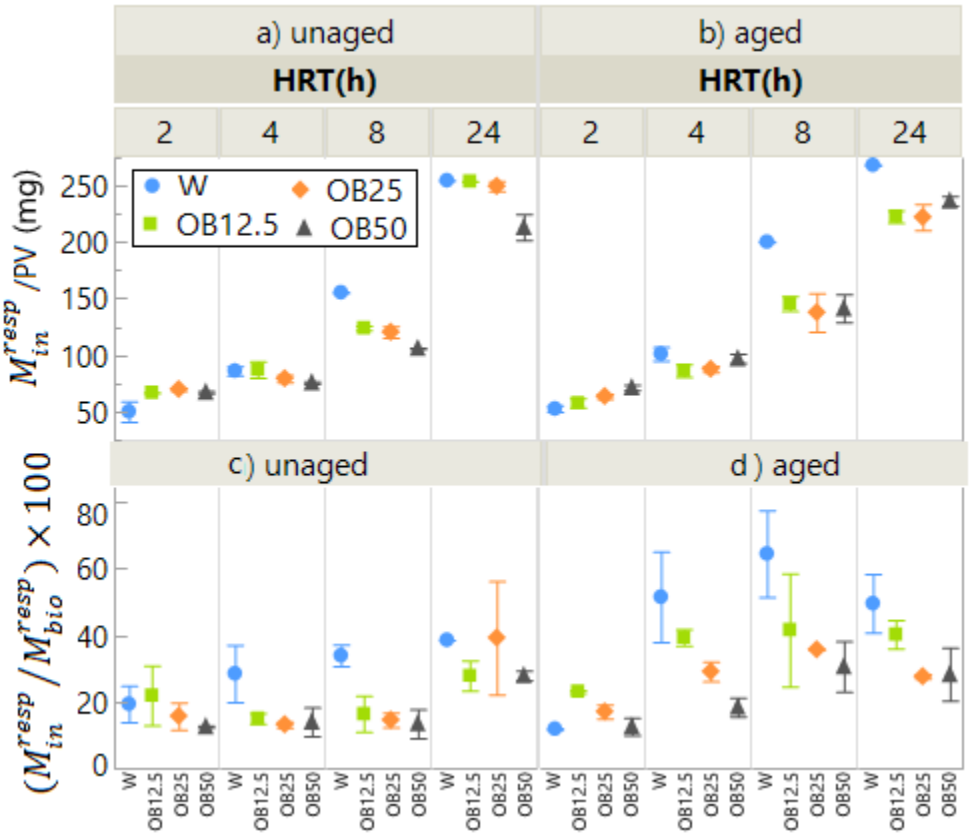

Figure S 4-5 M_{in}^{resp}/PV is the respired CO_2 (mg) per pore volume by the reduction of influent calculated using stoichiometry of the reduction reactions from Table S4-2. $(M_{in}^{resp}/M_{bio}^{resp}) \times 100$ is the percentage of contribution of M_{in}^{resp}/PV to the total respiration per pore volume. a) M_{in}^{resp}/PV in unaged bioreactors, b)M_{in}^{resp}/PV in aged bioreactors, c) M_{in}^{resp}/PV in unaged bioreactors, d) M_{in}^{resp}/PV in aged bioreactors.

4.8.3 Additional Information: Field Bioreactors

4.8.3.1 Nitrate-N Concentration of the Influent and Effluent of the Field Bioreactors

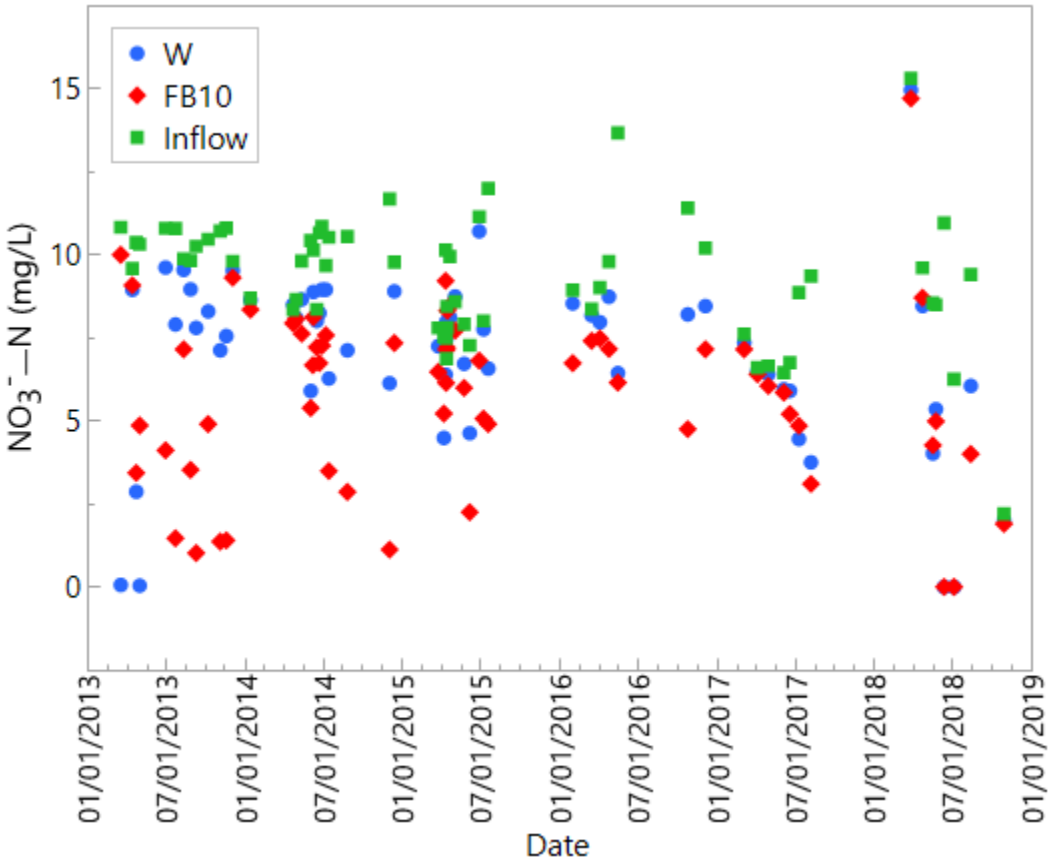

Figure S 4-6 NO_3^-—N concentrations at the influent and effluent of the field woodchip (W) and woodchips with 10% biochar (FB10) bioreactors over the 6 years of bioreactor use

4.8.3.2 Nitrate-N in Field Bioreactors in May 2018

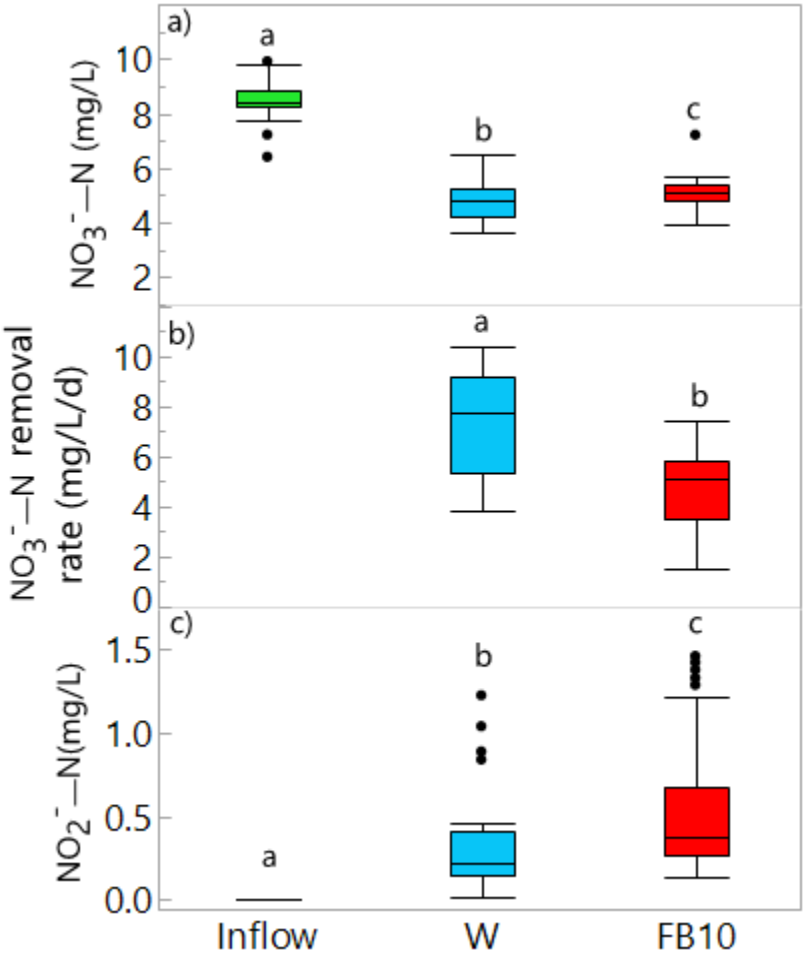

Figure S 4-7 the performance of the field bioreactors containing woodchip (W) and woodchips with 10% biochar (FB10) during the two weeks of high-frequency sampling in May 2018 a) NO_3^-—N concentrations at the influent and effluent of the bioreactors, b) The NO_3^-—N removal rate, and c) the NO_2^-—N concentrations of the bioreactors. Different letters in each graph indicate significant differences ($p < 0.05$).

CHAPTER 5:

PREDICTING THE FATE OF PREFERENTIALLY MOVING HERBICIDES

Adapted from: Hassanpour, B., B.K. Richards, L.D. Goehring, J. Parlange, and T.S. Steenhuis. 2019. Predicting the Fate of Preferentially Moving Herbicides. Vadose Zo. J. 18(1).

5.1 ABSTRACT

Simulation of preferential flow remains a challenge despite being a recognized phenomenon. With short-interval data, we adapted and tested the preferential flow model (PFM) to simulate the vertical transport of herbicides to lower soil layers. The PFM divides the soil profile into a top distribution zone and a conveyance zone below. The distribution zone acts as a reservoir, with an exponential loss of solutes to the conveyance zone. In the conveyance zone, water and solutes move as convective-dispersive flow through multiple flow paths—preferential and matrix—to shallow groundwater. Our field experiment was performed on a structured Hudson silty clay loam soil (a fine, illitic, mesic Glossaquic Hapludalf) that exhibits preferential flow. The site was instrumented with a variety of soil water samplers placed at depths of 60 cm to monitor the volume and quality of the leachate. Agronomic application of atrazine [6-chloro-N-ethyl-N'-(1-methylethyl)- 1,3,5-triazine-2,4-diamine] and 2,4-D [2-(2,4-dichlorophenoxy) acetic acid] was used, followed by 75 cm of controlled and natural rainfall over 100 d. In addition, Cl^- was applied as a conservative tracer. All samplers monitored during this period showed a fast breakthrough of solutes consistent with the occurrence of preferential flow, with two groups of

breakthrough curves observed. By fitting the Cl^- breakthrough curve for each group, PFM input parameters were estimated, including water velocity in preferential flow paths and the fraction of water moving through each flow path. With two additional parameters for herbicide adsorption and degradation rates, the model successfully simulated the extent of preferential flow of herbicides.

5.2 Introduction

It is well documented that groundwater and tile water is susceptible to pesticide contamination (Hallberg, 1989; Leistra and Boesten, 1989; Ghodrati and Jury, 1992; Flury, 1996; Guzzella et al., 2006; Vryzas et al., 2012; Toccalino et al., 2014; Vryzas, 2018). In structured soils, this is largely because of preferential flow through macropores, such as cracks, worm holes and root channels (Lawes et al., 1882; Beven and Germann, 1982, 2013; Gerke, 2006), and in coarse unstructured or water repellent soils, it is through unstable wetting fronts leading to rapid "fingered flow" (Hill and Parlange, 1972; Bauters et al., 1998; Li et al., 2018). Preferential flow allows a fast transport of water and solute to lower soil horizons by bypassing the soil matrix (Kung et al., 2000b; a). Preferential flow influences the transport of both absorbent and non-absorbent tracers in field conditions.

It is now generally accepted that preferential flow at the field scale is rather the rule than the exception (Vanclooster et al., 2000; Beven, 2018; Guo and Lin, 2018), especially in structured soils (Gerke, 2006; Köhne et al., 2009a; b). Preferential flow occurs in both tilled and non-tilled soils (Andreini and Steenhuis, 1990; Gish et al., 1995; Shalit and Steenhuis, 1996; Elliott et al., 2000). The BTCs were right skewed in no-tilth soils, which were attributed to the greater infiltration rate in such soils (Boll et al., 1997; Siczek et al.,

2008). Sanders et al. (2012) found that in an untilled agricultural silty clay loam soil, preferential flow comprised 34% to 99% of the infiltrated water. Most of the classical pesticide transport and fate models fall short because they are based on mass transfer (Queyrel et al., 2016) or the convective-dispersive equation (CDE), and do not allow for different velocities of water in the porous media (Richard and Steenhuis, 1988; Gärdenäs et al., 2006).

Given the importance of the preferential flow, numerous water and solutes transport models have emerged that consider preferential flow in the vadose zone (Köhne et al. 2009a, b; Jarvis et al. 2016), which include RZWQM (Kumar et al., 1998), MACRO (Larsbo et al., 2005; Jarvis and Larsbo, 2012), STICS-MACRO (Lammoglia et al., 2018), and HYDRUS (Simunek et al., 2005, 2009). Although these models have different complexities, they all assume that water and solute move faster in preferential pathways than in the matrix (Hutson and Wagenet, 1995; Köhne et al., 2009a; Jarvis et al., 2016). Among these models, dual region models are most common (Simunek et al., 2003). These models assign two flow pathways, preferential and matrix, for water and solute transport and usually rely on numerical solutions with multiple inputs to model the transport of water and chemicals (Gerke, 2006; Wu et al., 2014; Jarvis et al., 2016). Gärdenäs et al. (2006) compared four conceptually different models and concluded that dual porosity and permeability models successfully predicted drainage discharge and pesticide concentrations. Multi-region models that are conceptually similar to dual region models and better represent the porous media are used less often. The increased flexibility of multi-region models is generally offset by additional input parameters which are often poorly defined, or difficult to determine (Wu et al., 2004; Gerke, 2006; Zhang et al., 2018).

Kim et al. (2005) overcame the difficulty of applying multi-region models by providing the Preferential Flow Model (PFM) with input parameters that are easily defined. The PFM divides the soil profile into two layers, a distribution zone near the surface layer, and a conveyance zone below. These two distinct soil layers were observed previously in the profile of soils with preferential pathways (Steenhuis et al., 1994; Ritsema and Dekker, 1995; De Rooij and De Vries, 1996; Barry et al., 2013; Liu et al., 2018). The distribution zone behaves like a first order reservoir with an exponential loss of solutes to the conveyance zone (Steenhuis et al., 1994, 2001). Water and solute in the conveyance zone flow through multiple preferential pathways, obeying the convective-dispersion equation in each flow path. It is noteworthy that the PFM relies on an analytical solution for the transport of preferentially moving chemicals.

The PFM was used for simulating the transport of non-adsorbed solutes in undisturbed laboratory columns (Darnault et al., 2004; Kim et al., 2005). It was also used but not tested for locating landscape areas with a high risk of agrochemicals leaching (Sinkevich et al., 2005). Although the PFM has been used sparsely, it remains attractive because of its simplicity of modeling the preferential flow of pesticides in natural soils. Thus, its validation under field conditions is of interest. With the application of a multitude of field samplers including wick pan, gravity pan, pipe and suction cup samplers, BTCs of chloride, atrazine, and 2,4-D were measured in a structured soil. These samplers allowed investigation of the transport of chemicals in great detail because leached water was collected in entirety (Jarvis et al., 1995; Vanclooster et al., 2000; Köhne et al., 2009a).

Evaluation of the potential of pesticide contamination of groundwater requires a systematic approach through mathematical modeling coupled with field validation. The

objective of this study is, therefore, to adapt and test a multi-region model for predicting pesticide movement and validating it with the chloride and pesticide breakthrough curves (BTCs) determined in Peranginangin et al. (2009).

5.3 Material and Methods

5.3.1 Mathematical Modeling

The Preferential Flow Model (PFM) developed by Kim et al. (2005) was adapted to describe herbicide transport and degradation. It assumes that all percolating water and solutes mix uniformly in the upper distribution zone (Figure 5-1). Preferential flow occurs when water entering the soil exceeds the amount needed to saturate the distribution zone. Therefore, this zone acts as a linear reservoir, resulting in an exponential loss of solutes to the lower conveyance zone described as (Steenhuis et al., 1994):

$$C = C_0 \exp - (\int (\frac{Rdt}{W}) + \beta t) \qquad (5\text{-}1a)$$

where C is the solute concentration [ML^{-3}], R is the rainfall rate (LT^{-1}), β is the first order degradation rate of the chemical in the soil [T^{-1}], t is time [T], and W is the apparent water content of the distribution zone [L]; C_o is the initial solute concentration [ML^{-3}] which equals $C_o = \frac{M_0}{W}$, where M_0 is the mass of solute applied per unit of the surface area [ML^{-2}]. For non-adsorbed chemicals, W is simply the water content of the distribution zone per unit area. For adsorbed (desorbed) chemicals, W is calculated as:

$$W = d(\rho k_d + \theta_d) \qquad (5\text{-}1b)$$

where d is the depth of the distribution zone [L], ρ is the bulk density of the soil [ML^{-3}], k_d is the desorption partition coefficient [L^3M^{-1}], and θ_d is the moisture content of the distribution zone [L^3L^{-3}].

Under steady state conditions, Eq5-1a reduces to:

$$C = C_0 \exp[-(^{q}/_{W} + \beta)t] \quad (5\text{-}1c)$$

where q is the average steady-state rainfall rate [LT^{-1}].

When the distribution zone is near saturation, water and solutes are released to the subsoil via the conveyance zone as preferential and matrix flow. The transport in the conveyance zone can be described with a convective-dispersive equation for each flow path, i, with a sink term to describe the irreversible degradation/decay of pesticides. The governing equation for one-dimensional transport in the conveyance zone under steady state flow is:

$$\frac{\partial C_i}{\partial t} = D\,\frac{\partial^2 C_i}{\partial x^2} - v_i \frac{\partial C_i}{\partial x} - \beta C_i \quad (5\text{-}2)$$

where v_i is the velocity of water and solutes [LT^{-1}], x is the vertical distance from the source of input to the point of sampling [L], and β is the first-order decay rate [T^{-1}], and D is the dispersion coefficient [L^2T^{-1}]. It is worth mentioning that in the current study, β was assumed to be the same for both distribution and conveyance zones because of the shallow depth of the samplers. Eq 5-2 can be solved for boundary condition (1) using Laplace transforms for $\frac{4D(\frac{q}{W})}{v^2} < 1$ as (van Genuchten and Alves, 1984):

$$C_i = \frac{1}{2}\,\frac{M_0}{d(\rho K_a + \theta_d)} \exp\left[-\left(\frac{q}{w} + \beta\right)t\right] \left[\exp\left(\frac{V_i X}{2D_i}(1 - \alpha_i)\right) \operatorname{erfc}\left\{\frac{x - V_i t\alpha}{2\sqrt{D_i t}}\right\} + \exp\left(\frac{V_i X}{2D_i}(1 + \alpha_i)\right) \operatorname{erfc}\left\{\frac{x + V_i t\alpha}{2\sqrt{D_i t}}\right\}\right] \quad (5\text{-}3)$$

where $\alpha_i = \sqrt{1 - \frac{4D(\frac{q}{W} + \beta)}{{v_i}^2}}$.

Assuming that water and solutes in the flow paths do not mix, the average solute concentration at any point x can simply be expressed by summing the contributions of the various flow paths, e.g.:

$$C = \sum_{i=1}^{n} a_i C_i \qquad (5\text{-}4)$$

where a_i is the fraction of water moving through flow path i at a velocity of v_i.

Figure 5-1 The pattern of the preferential flow in Hudson soil. The top layer is the distribution zone, where the uniform flow of the dye is visible. The preferential flow pathways with a variety of patterns are visible in the beneath layer which is named the conveyance zone

5.3.2 Site Description

Experiments were carried out in Ithaca, New York at a field site instrumented with a range of soil water samplers. A worst-case scenario was created by applying cumulative rain and irrigation of 75 cm following herbicide application at typical agronomic rates. Two commonly used herbicides, atrazine and 2,4-D were chosen as model compounds with different adsorption and degradation characteristics in the soil. A conservative tracer,

chloride (KCl), was used to determine the transport properties of the soil above each sampler.

The site was located on long-term, regularly mowed grass sod comprised of a 70:30 mixture of perennial ryegrass (Lolium perenne L.) and creeping red fescue (Festuca rubra L.) within the Cornell University Orchards (Merwin and Stiles, 1994; Merwin et al., 1994). The soil was formed in clayey and silty lacustrine sediments and is fine-grained with a subangular blocky structure and hexagonal shaped peds of 0.2-0.3 m in diameter (Boll et al., 1997). It is mapped as Hudson silty clay loam (fine, illitic, mesic Glossaquic Hapludalf) with 7% sand, 71% silt, and 22% clay. The organic matter content of this soil was 53 g/kg (Merwin et al., 1994).

Field observation made while digging the observation pit for the current experiment showed that the depth of the horizon A was 10 cm. The top 10 cm was brown with a weak subangular blocky structure parting to granular- was broken down easily by hand- and had fine roots and small wormholes. The bottom layer was pale brown with firm subangular blocky structure and peds and contained vertical wormholes and few roots.

According to the Soil Survey (Neeley et al., 1965), the upper 25 cm permeability ranges from 40-120 cm/d, and for depths from 25-110 cm, the permeability is between 1 and 40 cm/d. Earlier experiments on this site included blue dye tracers to visualize preferential flow paths showing well-defined macropore networks and preferential flow between the peds (Steenhuis et al., 1994; Ogawa et al., 2000; Richards et al., 2000; Akhtar et al., 2003) (Figure 5-1).

5.3.3 Field Experiment

In conducting the leaching experiment, two wick pan samplers, one gravity pan sampler, two pipe samplers, and five suction cups, made of non-reactive material, were installed in a plot area of 2.4m × 6.6 m. The two wick pan samplers and one gravity pan sampler, each with the surface area of 1090 cm^2, were installed 1 m apart, 0.6 m below the soil surface in 0.7 m horizontal tunnels excavated laterally under the test plot. The samplers were pressed upward against the exposed face of undisturbed subsoil using wedges and blocks. Two pipe samplers with a diameter of 28 cm were excavated by inserting a pipe and hand excavating undisturbed soil columns and placing sample collectors below them. The soil columns were secured by being placed on a plastic screen and using expanding polyurethane foam around them. In addition, five suction cup samplers were installed at 60 cm depth. Below all samplers, at a depth of 0.9 to 1.05 m, backup tile drains were installed to prevent overflow into the wick and pan samplers. The details of each sampler and their installation are described in Peranginangin et al. (2009).

After approximate steady-state soil moisture conditions were established by applying irrigation at 2.6 cm/d for 4 consecutive days, a chloride (Cl^-) tracer solution was sprayed using a sprinkler at a rate of 441 Kg Cl^-/ha. Atrazine and 2,4-D were then applied on the same day, each at typical agronomic rates of 2 Kg/ha. Following herbicide application, irrigation was again applied with two sprinklers. During the first 4 days, an average of 2.6 cm of rain was applied daily at a mean rate of 1.6 cm/h. After the 4^{th} day (10.4 cm of cumulative rain), the rain was applied every 2 to 4 days at similar intensity and duration. When natural rainfall occurred, the irrigation amount was reduced accordingly to achieve approximately 2.6 cm of total rain per day. Percolating water was collected

immediately after rainfall simulation ceased and in the morning following rain application. The leachate volume from each sampler was also recorded. Final samples were collected when a cumulative rain and irrigation totaled 75 cm over the course of 100 d, composed of 31 cm natural rainfall, and 44 cm irrigated water. Two days after an accumulative rain of 63 cm, three duplicate soil cores were extracted to a depth of 90 cm, with samples were taken at depths of 15, 30, 45, 60, and 90 cm below the ground surface.

Leachate samples were analyzed for chloride content using a Buchler Instruments Model 442-5000 digital chloridometer. Enzyme-Linked Immunosorbent Assays (ELISA) from Strategic Diagnostics Inc. (Newark, DE), were used for the analysis of the herbicides in the samples. The detection limit for atrazine and 2,4-D were 0.04 and 0.7 μg L^{-1}, respectively. The corresponding quantification limits for these two herbicides were 0.1 and 0.7 μg L^{-1}. More details are provided elsewhere (Peranginangin et al., 2009).

5.3.4 Model Evaluation

To evaluate how well the model fits the observed data, both graphical displays and statistical criteria were used. Four numerical assessment criteria were used to evaluate model performance: (I) standard R-squared correlation method (R^2), (II) mean cumulative error (MCE: Perrin et al., 2001), (III) Nash-Sutcliffe model efficiency (E_f: Nash and Sutcliffe, 1970), and (IV) coefficient of determination (CD: Loague and Green, 1991). R^2 ranges from 0 to 1, MCE and E_f range from $-\infty$ to 1, and CD ranges from 0 to ∞, in all cases, 1 represents a perfect fit. These statistical quality measures are sensitive to a few large errors, especially in small data sets.

The MCE evaluates how well a model correctly reproduces the concentrations over the entire experimental period, given as (Perrin et al., 2001):

$$MCE = 1 - \left| \sqrt{\frac{\sum_{i=1}^{n} C_{sim,i}}{\sum_{i=1}^{n} C_{obs,i}}} - \sqrt{\frac{\sum_{i=1}^{n} C_{obs,i}}{\sum_{i=1}^{n} C_{sim,i}}} \right| \qquad (5\text{-}5)$$

where $C_{obs,i}$ is the observed concentration at the time i, and $C_{sim,i}$ is the model simulated concentration at time i.

The third criterion, E_f, is another indicator of model performance. If E_f is less than zero, the simulated values are worse than simply using the observed mean (Loague and Green, 1991). The E_f is given as (Nash and Sutcliffe, 1970):

$$E_f = 1 - \frac{\sum_{i=1}^{n} \left(C_{obs,i} - C_{sim,i}\right)^2}{\sum_{i=1}^{n} \left(C_{obs,i} - \overline{C_{obs}}\right)^2} \qquad (5\text{-}6)$$

where $\overline{C_{obs}}$ is mean observed concentration throughout the experiment and was calculated separately for each sampler.

The fourth criterion, CD, is a measure of the proportion of the total variance of observed data explained by the model simulated data, and is given as (Loague and Green, 1991):

$$CD = \frac{\sum_{i=1}^{n} \left(C_{obs,i} - \overline{C_{obs}}\right)^2}{\sum_{i=1}^{n} \left(C_{sim,i} - \overline{C_{obs}}\right)^2} \qquad (5\text{-}7)$$

All the above statistical criteria were applied to modeled data for the entire solute leaching experiment.

5.4 Results

Chloride breakthrough curves (BTCs) for various samplers are shown in Figures 5-2a to 5-6a. All samplers had a breakthrough of chloride during the application of the first

2.6 cm of rain. The peak concentration of chloride for the wick pan sampler A (wick A) was substantially greater compared to other samplers, with a maximum concentration of C = 502 mg/L in the first sample taken after the application of chloride on the soil surface (Figure 5-2a). Early peak concentrations were also observed with the pipe samplers but at a slightly lower value of C= 418 mg/L (Figure 5-3a). The peak concentration of chloride, C =190 mg/L of the wick pan sampler B (wick B) was relatively delayed and arrived at 10 cm cumulative rain, 4 days after pulse application (Figure 5-4a). Similarly, early peak concentrations of C= 157 mg/L and C= 180 mg/L were observed for the gravity pan sampler and suction cup samplers, respectively (Figures. 5-5a and 5-6a). At the end of the experiment (75 cm cumulative rain), 95.7%, 109%, 115 % and 75% of the applied chloride leached through Wick B, Wick A, gravity pan, and pipe samplers, respectively. Therefore, pipe samplers under-collected chloride. For all samplers, it was observed that secondary and tertiary peaks occurred at a cumulative rain application of 15 and 33 cm, respectively; suggesting the tracer traveled through different preferential flow paths. Pronounced tertiary peaks were observed in wick B and in the gravity pan sampler.

Overall, two groups of breakthrough curves were observed. Group 1 consisted of wick A and pipe samplers (Figures 5-2a, 5-3a) with sharp peaks observed that ceased quickly; and Group 2 consisted of wick B, gravity pan sampler, and suction cup samplers (Figures 5-4a to 5-6a) with rounded peaks and a gradual decline. The BTCs of atrazine, despite its possible adsorption to soil organic matter, closely followed those observed for chloride, especially in wick A and pipe samplers (Figures 5-2b, 5-3b), indicating rapid preferential transport which prevented solutes from being in full contact with the soil matrix. The observed peak concentration of atrazine in all the samplers varied from 195

µg/L in wick B to 1,214 µg/L in the pipe samplers. Despite similarities in the location of the peaks between the atrazine BTC of the gravity pan sampler and wick B, the concentrations of atrazine in the gravity pan sampler were two times greater than those of the wick B (Figures. 5-4b, 5-5b). The peak concentration of atrazine in the gravity pan sampler was 300 µg/L whereas it was 195 µg/L for the wick B, despite that these samplers observed relatively similar concentrations of chloride, (161 and 190 mg/L, in gravity pan sampler and wick B sampler, respectively). Similar values and trends to those of the gravity pan were observed in the suction cup samplers (Figure 5-6b).

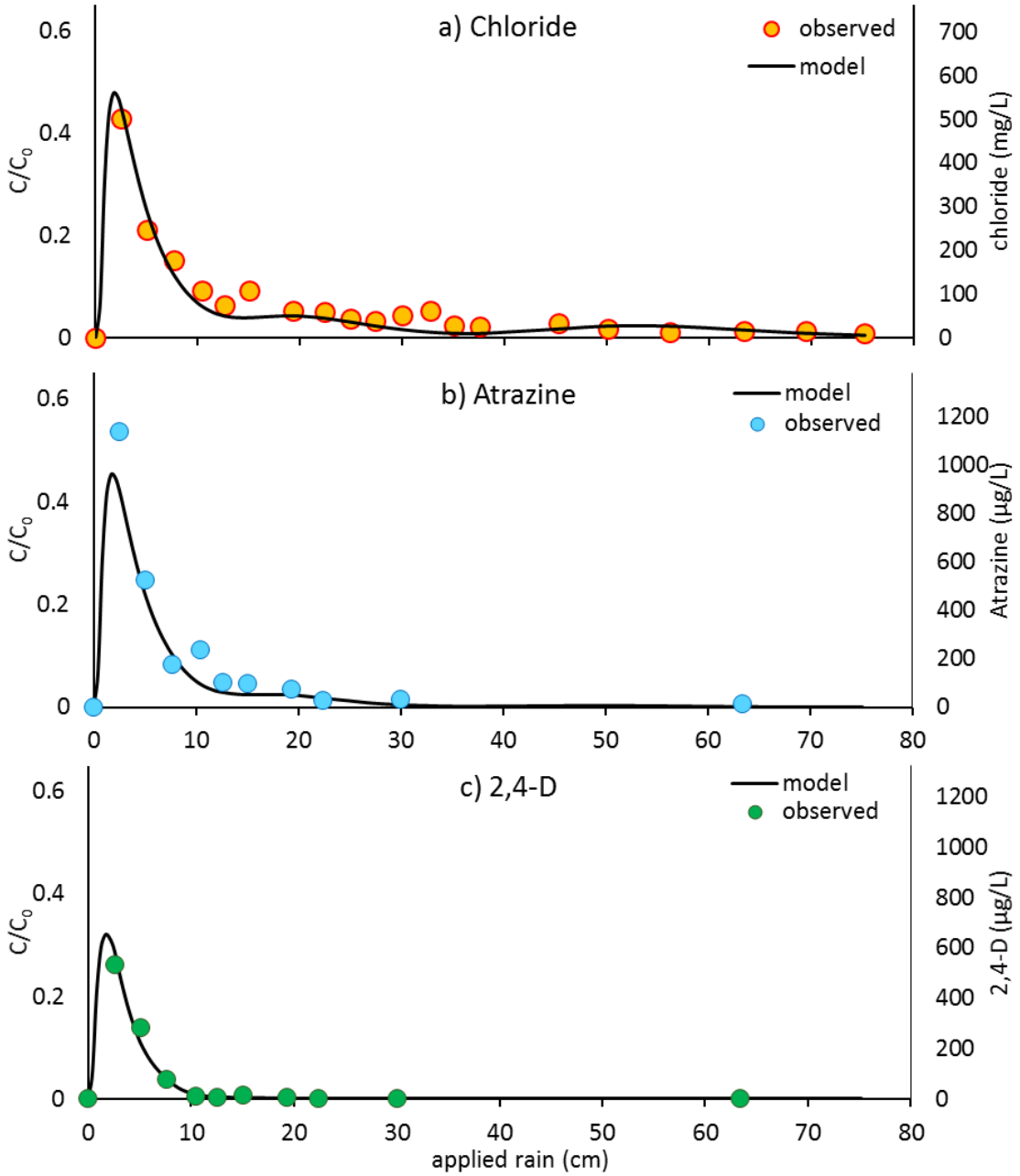

Figure 5-2 Wick pan sampler A (Wick A) breakthrough curves for a) chloride, b) atrazine and c) 2,4-D. The observed data points are shown with filled circles, and PFM simulated values are shown with black lined. Input parameters are given in Table 5-1. The C_o is calculated by Eq 5-1b and 5-1c.

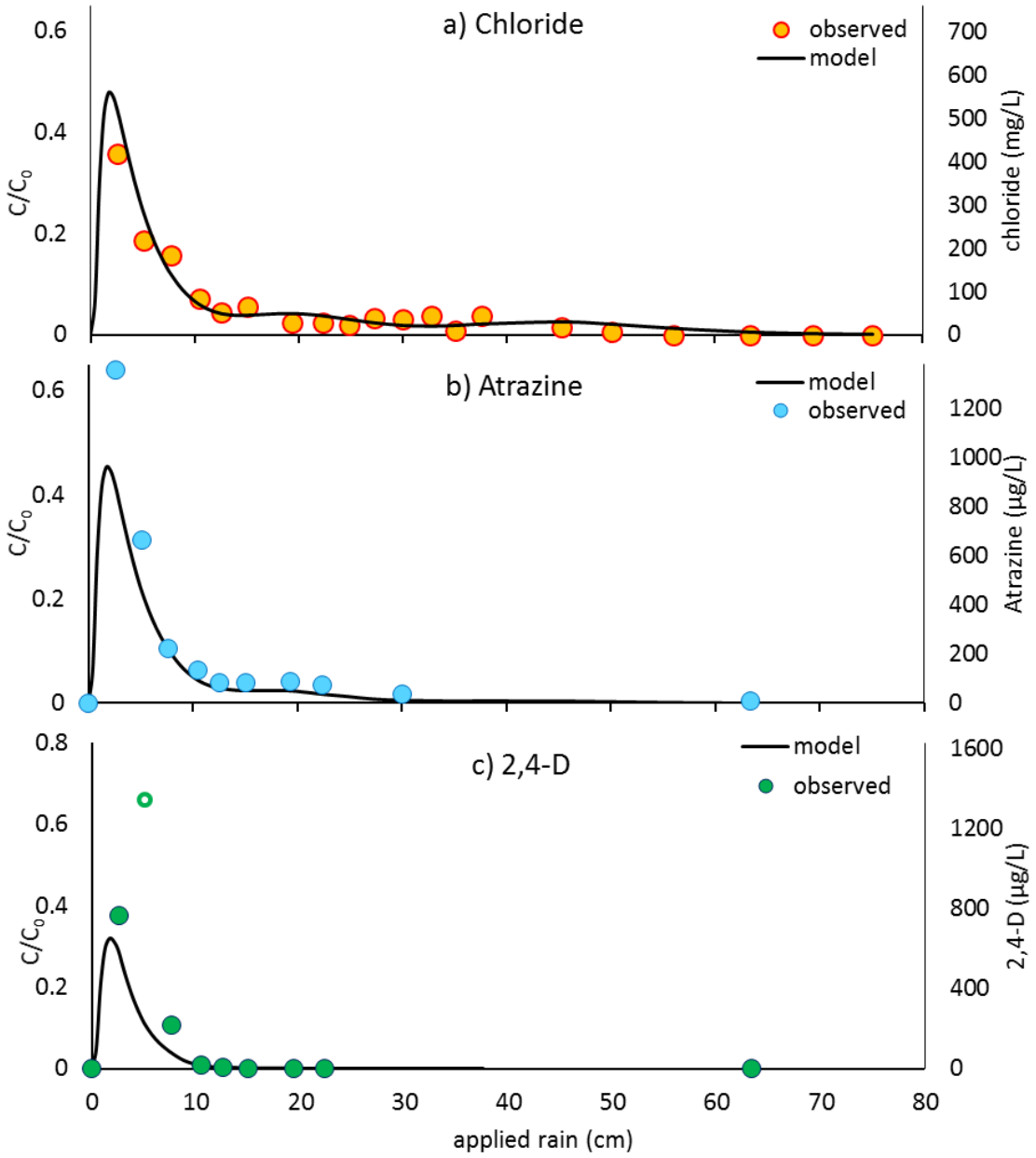

Figure 5-3 Pipe samplers sampler breakthrough curves for a) chloride, b) atrazine and c) 2,4-D. The observed data points are shown with filled circles, and PFM simulated values are shown with black lined. Input parameters are given in Table 5-1. The Co is calculated by Eq 5-1b and 5-1c.

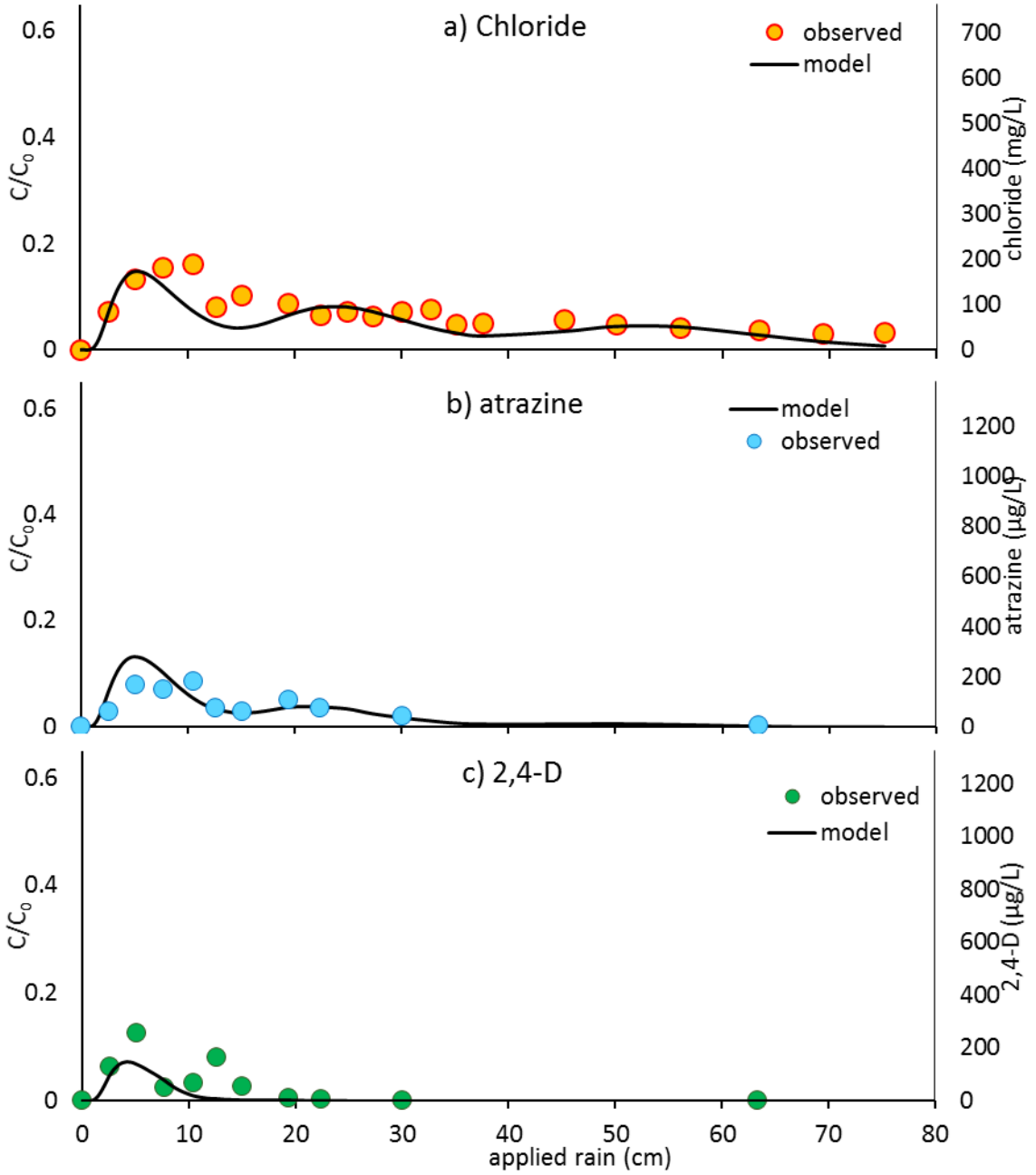

Figure 5-4 Wick pan sampler B (Wick B) breakthrough curves for a) chloride, b) atrazine and c) 2,4-D. The observed data points are shown with filled circles, and PFM simulated values are shown with black lined. Input parameters are given in Table 5-1. The Co is calculated by Eq 5-1b and 5-1c.

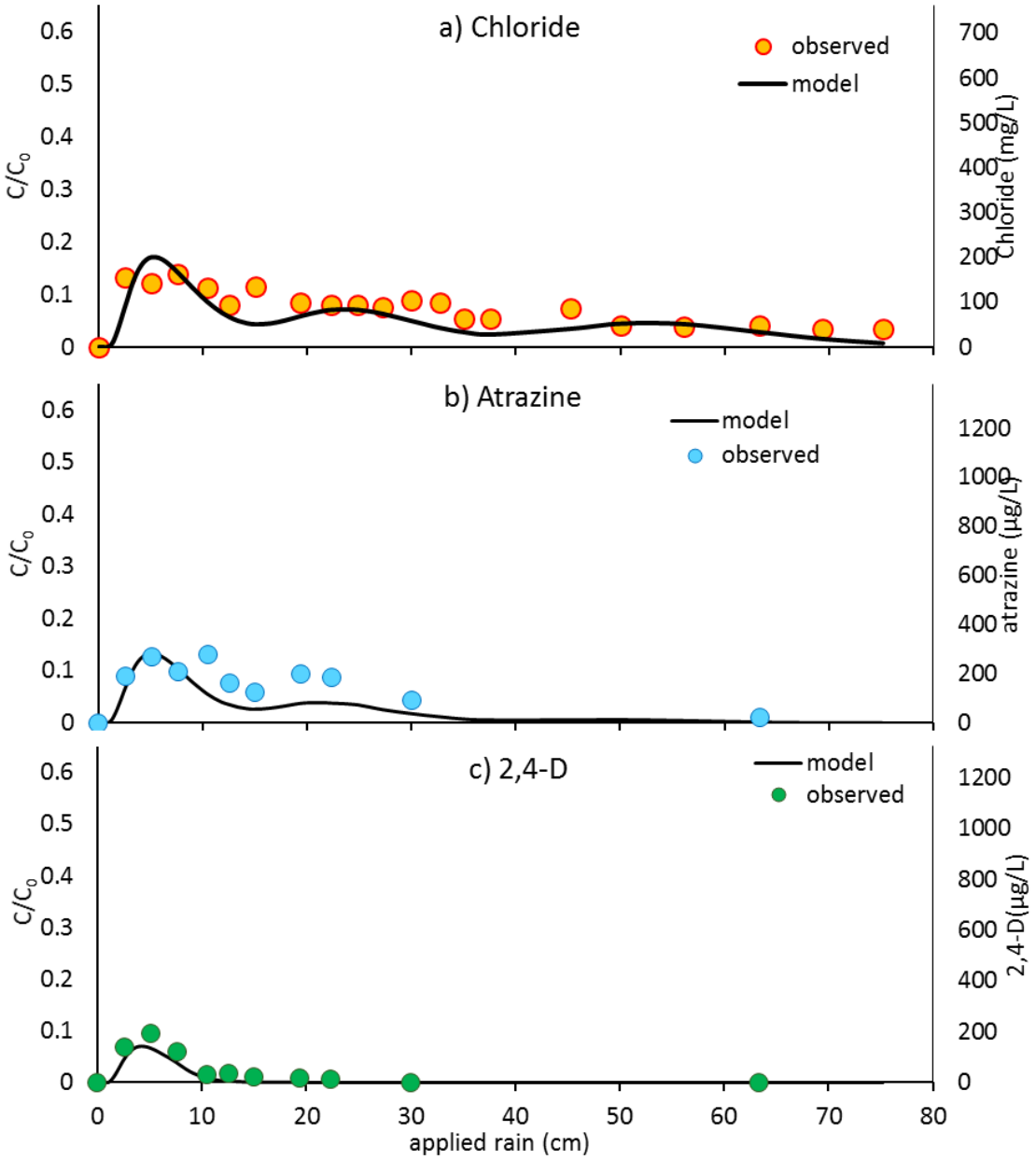

Figure 5-5 Gravity pan sampler breakthrough curves for a) chloride, b) atrazine and c) 2,4-D. The observed data points are shown with filled circles, and PFM simulated values are shown with black lined. Input parameters are given in Table 5-1. The Co is calculated by Eq 5-1b and 5-1c.

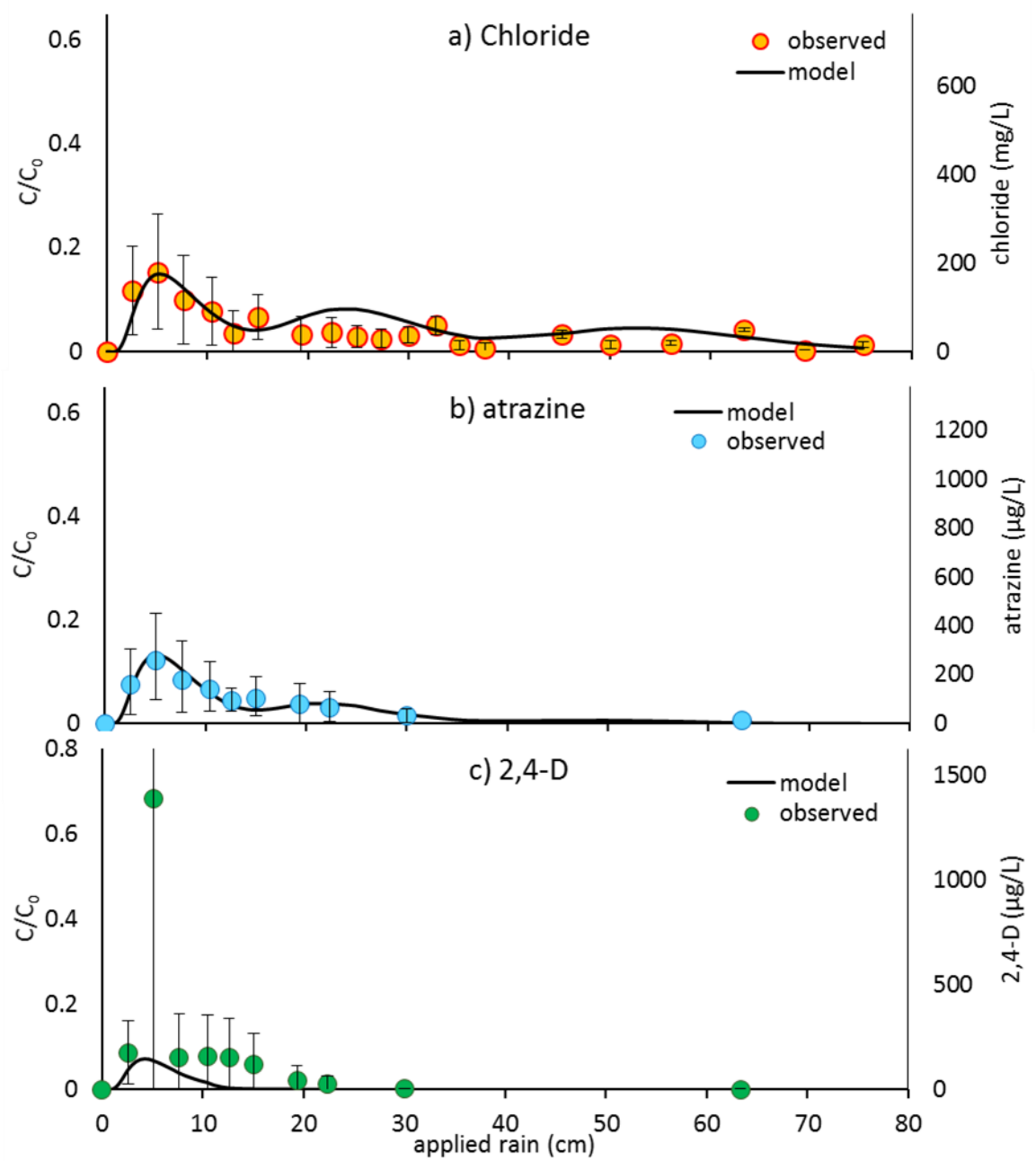

Figure 5-6 Suction cup samplers' breakthrough curves for a) chloride, b) atrazine and c) 2,4-D. The observed data points are shown with filled circles, and PFM simulated values are shown with black lined. Input parameters are given in Table 5-1. The error bars show standard deviation. The C_o is calculated by Eq 5-1b and 5-1c.

The BTCs for 2,4-D were generally similar to those of atrazine (Figures 5-2c-6c). Breakthroughs for all samplers were in the same order as atrazine and occurred either on

the day of or the day following application, except for suction cup samplers where the 2,4-D peak concentration was 1391 µg/L (Figure 5-6c), whereas the atrazine concentration was lower at 275 µg/L (Figure 5-6b). In addition, the peak concentration of 2,4-D in the pipe sampler occurred later than the atrazine peak (Figures. 5-3b and 5-3c).

As expected, observed 2,4-D concentrations declined more rapidly after the initial breakthroughs because of the rapid degradation in macropores, as shown by Pivetz and Steenhuis (1995). After 10 cm of cumulative rain, 2,4-D ceased to be detected in Wick A and the pipe samplers (Figures 5-2c, 5-3c), and it was not detected in the rest of the samplers after 30 cm of cumulative rain (Figures 5-4c to 5-6c). The soil moisture profile was taken 24 h after rain application (after a cumulative rain application of 63 cm) showed volumetric soil moisture contents of 0.37 in the top 15 cm of soil and about 0.26 in the subsoil. At these moisture contents, the rainfall intensity of 2.6 cm/d would conventionally be expected to result in pore water velocities of 7 to 10 cm/d. Accordingly, if all water and non-adsorbed tracer moved with this average velocity, we would expect the peak concentration to be observed at 60 cm soil depth 6 to 9 days after pulse application. For pesticides with an adsorption partition coefficient of about 0.45 cm^3/g, we would expect delayed peaks to appear at intervals 2.5 to 3 times longer than that (i.e., circa 20 days or more). Clearly, this did not occur in the Hudson soil, where solute was observed at 2.6 cm of cumulative applied rain, thus, confirming the dominant influence of preferential flow.

5.4.1 Modeling

The model requires the fitting of parameters related to the preferential flow through porous media. It is unfortunate that in soil physics, in-situ methods do not yet exist for

determining parameters for preferential flow models, and thus fitting is required. Malone et al., (2004) used 39 intact soil columns to estimate the number of percolate−producing macropores for the RZWQM model. The input parameters for the PFM are the depth and moisture of the distribution zone, d, and θ_d, the proportion a_i of water flowing with velocities, v_i, through the flow paths in the conveyance zone; and those specific to the solutes consisting of the dispersion coefficient, D, the adsorption partition coefficient of the pesticides, k_a, and first-order decay rate of the pesticides, β.

The porous media related parameters, d, a_i and v_i and the dispersion coefficient D (k_a, β equal zero) were determined first by fitting the chloride BTCS of the Wick A for the Group 1 and Wick B for the Group 2 (Table 5-1). Since two groups of BTCs were observed in this study, we utilized the same values of a_i, λ_i, v_i, and d with each group.

Our field observations showed that the depth of the horizon A was 10 cm, which had weak blocky subangular structure parting to granular. Assuming mixing happened in this layer, the depth of the distribution zone was 10 cm. This agrees with a prior field infiltration test using a blue dye. The volumetric moisture content of the top layer measured during the experiment was 0.37, which was used as the water content of the distribution zone. Since three chloride peaks were observed in the BTCs in the samplers (Figures 5-2a to 5-6a), we employed three flow paths. The fitted velocity of water and chloride moving through preferential flow paths (v_1) ranged from 35 cm/d for Group 2, to 120 cm/d for Group 1 (Table 5-1). The other fitted velocities, v_2, and v_3, were 6.8 and 3 cm/d for both groups (Table 5-1).

Table 5-1 the input parameters used for the model in different samplers. a_i is the fraction of water, λi the dispersivity of each fraction, V_i is the velocity of water moving through each fraction, d is the depth of the distribution zone, β is the first order decay rate, K_a is the adsorption partition coefficient.

Group*	a_1 %	a_2 %	a_3 %	$\lambda^{\ddagger}_1$ (cm)	λ_2 (cm)	λ_3 (cm)	V_1 cm /d	V_2 cm/ d	V_3 cm/ d	d cm	atrazine		2,4 D	
											β 1/d	k_a cm^3/g	β 1/d	k_a cm^3/g
Group 1	70	15	15	10	2	1	120	6.8	3	10	0.05	0.45	0.35	0.45
Group 2	35	35	30	10	2	1	35	6.8	3	10	0.05	0.45	0.35	0.45

* Group 1 comprise Wick A and pipe samplers, and Group 2 comprise Wick B, Gravity pan, and Suction cup samplers
‡ dispersivity(D/v)

After determining the values for the velocities using the nonreactive tracer, the values for adsorption and decay rates for atrazine and 2,4-D were determined by fitting with the BTC curves (Table 5-1, Figures 5-2b, c to 5-6b, c). The sorption and degradation parameters for each chemical were the same for all samplers because they were located in close proximity.

We first found the adsorption partition coefficients (K_a) for atrazine and 2,4-D for the Wick A sampler and used them to model solute transport in other samplers. The calibrated K_a of 0.45 for both atrazine and 2,4-D. The value of β for atrazine was 0.05 1/d corresponds with a half-life ($t_{1/2} = \ln 2/\beta$) of 14 d. The value used for the β value for 2,4-D was 0.35 1/d equal to the half-life of 2 d (Table 5-1).

Figures 5-2 to 5-6 show that the model fits with the observed data well. The model, however, did not predict the maximum concentrations of 2,4-D in pipe and suction cup samplers (Figures 5-3c, 5-6c).

Overall, the four evaluation criteria indicated that the model was in reasonable agreement with the observed data with R^2 values of 0.59-0.99, positive E_f values, and MCE values between 0.16 and 0.99 with the exception of the 2,4-D in the suction cup samplers (Table 5-2). Note that these values exclude the maximum concentration of 2,4-D in pipe samplers (Figure 5-3c; open circle). The model was able to match the data for most initial

peaks (Figures 5-2 to 5-6) with few under predictions- CD values over 1- or over predictions- CD values below 1- as indicated by CD values of 0.49 to 1.66 with the exception of 2,4-D in the suction cup (Table 5-2). Furthermore, the model adequately fit the significant asymmetry and tailing of the pesticide's BTCs obtained from field experiments.

It is of note that the greater the degree of preferential flow (i.e., the more progressive shifting of the BTC to the left), the better the model fits with the observed BTCs, as can be seen from the statistical results and fitting illustration of sampler Wick A and pipe samplers (Table 5-2, Figures 5-2, 5-3).

Table 5-2 the statistical qualities for the performance of the model for the different samplers. R-squared (R^2), mean cumulative error (MCE), Nash-Sutcliffe model efficiency (Ef), and coefficient of determination (CD)

Sampler	Chloride				Atrazine				2,4-D			
	R^2	MCE	E_f	CD	R^2	MCE	E_f	CD	R^2	MCE	E_f	CD
Wick A	0.94	0.82	0.94	0.85	0.97	0.74	0.92	1.47	0.97	0.98	0.97	0.88
Pipe samplers	0.96	0.90	0.90	0.68	0.99	0.61	0.84	2.15	0.97	0.63	0.90	1.66
Wick B	0.63	0.72	0.42	1.01	0.66	0.85	0.26	0.49	0.59	0.21	0.65	1.61
Gravity pan	0.62	0.69	0.20	0.64	0.63	0.54	0.16	0.73	0.97	0.47	0.80	1.60
Suction cup samplers	0.61	0.75	0.52	1.11	0.92	0.97	0.89	0.80	0.64	-1.16	-0.01	4.66

5.5 Discussion

Atrazine and 2,4-D were applied at agronomic rates on grass sod followed by 75 cm of rain of which 10.4 cm was applied on four consecutive days. The pesticide concentrations observed after the first four days are used in testing the model but are not likely to be found in the field under natural rainfall conditions.

Two groups of BTCs were observed. It is less likely that the type of sampling device impacted the observation of the two groups because the groups were observed across the samplers. In other words, the concentrations of tracer and herbicides observed in wick A were similar to those of the pipe sampler, and the BTC of the Wick B was similar to that of the gravity sampler. Peranginangin et al. (2009) in a discussion paper compared the performance of each sampler in comparison to others in details. They suggested that the pan samplers collected water at greater rates than other samplers. In addition, wick pan samplers behave better under decreased soil moisture and capturing matrix flow (Boll et al.,1997). However, both wick B and gravity pan samplers captured the long receding tail of the tracer concentrations as both had the same concentration of chloride.

The BTCs produced from the suction cup lysimeters were variable (Figure 5-6). Such erratic BTCs produced had been observed previously (Boll et al. 1997), and was attributed to the proximity of the local flow paths to their location. Therefore, individual cups were not able to capture the extent of the preferential flow or conversely exaggerated it. Whereas, in the wick pan samplers, the variation in preferential flow pathways within sampler was offset by variation between the different wicks because pan samplers can capture soil solution from a larger area of soil. Indeed, the pan samplers that are constructed in the field settings can best represent the local field conditions and, although expensive, have great utility investigating groundwater pollution risks (Boesten, 2007; Köhne et al., 2009a)" at least at the general soil class level. Our observation that pesticides are breaking through at the same time as the non-adsorbed tracers has been noticed by others (Kladivko et al., 1991; Flury, 1996; Kung et al., 2000b; Torrentó et al., 2018). Thus, the similarity of travel time independent of the sorption properties is largely due to the fast flow of water

and consequently, a short time that is available for adsorption to occur. This response does not allow for reaching equilibrium in the soil until the water stops flowing (Steenhuis et al., 1997; Kim et al., 2008; Liu et al., 2018). This preferential flow breakthrough pattern is distinctly different than that based on the convective-dispersive equation where adsorbed solutes move slower than non-adsorbed solutes (Smith et al., 1990; Kladivko et al., 1991; Ghodrati and Jury, 1992; Gerke, 2006; Jarvis, 2007; Köhne et al., 2009b).

While the velocities of the tracer and herbicides were comparable, the relative concentration (C/C_0) of the two herbicides collected by the samplers was generally less than C/C_0 of the non-adsorbed chloride tracer (Table 5-2, Figures 5-2 to 5-6).This was likely due to adsorption of the herbicides to the soil in the distribution zone and degradation of the herbicides in both distribution and conveyance zones. The 2,4-D concentrations ceased after application of 20 cm cumulative rain whereas atrazine was still detected due to its slower degradation rate. Mass balance shows that only 1% of the applied atrazine leached through the preferential flow paths, although this amount would be sufficient to exceed the drinking water standard concentration of 3 μg/L for atrazine and 70 μg/L for 2,4-D (according to the EPA) by two orders of magnitude (Figures 5-2 to 5-6).

The Preferential Flow Model (PFM) assumes a distribution zone that funnels water and dissolved pesticides in preferential flow paths to the conveyance zone below. Since field soils are heterogeneous, some input parameters cannot be determined *a priori*. In order to obtain the measured breakthrough curves, we used, therefore, a tracer to characterize and set the parameters for the number of flow paths including the velocity and proportion of water and the dispersion coefficient for each. A non-reactive tracer test is essential in identifying preferential flow parameters (Jarvis and Larsbo, 2012).

For predicting pesticide movement when breakthrough curves are not available, half a century after the first preferential flow experiments were done by Quisenberry and Phillips, (1976) and Beven and Germann, (1981) it may be feasible to develop a pedotransfer function for generalized preferential from the data available in the literature. A start has been made by Selker et al. (1992) who described the wetted area occupied by fingered flow as a ratio of maximum rainfall intensity and the soil saturation in sandy and water repellant soils. The advantage of the PFM model is that the number of parameters needed is manageable and physically-based.

The depth of the topsoil horizon was used to determine the depth of the distribution zone. A depth of 10 cm was within the range of that of earlier experiments (Steenhuis et al., 1994). The adsorption partition coefficient of 0.45 cm^3/g for both herbicides in the distribution zone, although within the range of published values (FAO and WHO, 1998; Moorman et al., 2001), is lower than that generally found in the literature for atrazine (Ahmad and Rahman, 2009). Given that the Hudson soil is rich in organic matter, the likely reason for a low K_a is that an adsorption equilibrium did not happen because topsoil was kept wet so that there was no intimate contact between the soil and the pesticides. In addition, due to the rapid water transport, chemical equilibrium may not have happened. Nonequilibrium adsorption was used previously in transport models and depended on the kinetics of the adsorption reaction (Leij et al., 1993; Köhne et al., 2009a; Celestino Ladu and Zhang, 2011).

In the conveyance zone, three different flow paths with different velocities were utilized to represent the initial breakthrough and the tailing. In a shorter duration experiment by Kim et al. (2005), two flow paths adequately predicted chloride BTCs

through undisturbed soil cores. Darnault et al., (2004), in an experiment in coarse sandy soil with fingered flow, showed one flow path was sufficient to predict Cryptosporidium parvum oocyst transport. In the current study, however, water and solutes travel time were 5-35 times faster through the macropores than through the slowest flow path, and multiple peaks were observed. The portion of the water flowing through preferential flow paths (a_1) for the wick A and pan sampler was 70% whereas it was only 40% for wick B and the gravity pan samplers (Table 5-1). This is expected because the soil above each sampler was undisturbed, and consequently, the soil structure was heterogeneous, causing various degrees of preferential flow that cannot be predicted very well beforehand; yet, the information was essential to model the herbicide loss well. Despite this variation, the estimated velocities were within the range of permeability previously characterized for the region (Neeley et al., 1965). The highest fitted velocity of 120 cm/d is the value of the highest infiltration rate found for the Hudson soil. Saturated hydraulic conductivity was previously used to describe the preferential flow in the MACRO model (Jarvis and Larsbo, 2012).

Fitted dispersivity values, λ, (the quotient of dispersion coefficient and solute velocity) in the preferential pathways varied from 1 cm in the matrix to 10 cm in preferential pathways, values that are within the observed dispersity values in field conditions according to Lal and Shukla (2005).

The decay rate values (β) of 0.05 1/d for atrazine and 0.35 1/d for 2,4-D (Table 5-2) agree with those previously observed in the literature. These decay rates correspond to half-lives of 14 d for atrazine and 2 d for 2,4-D. Such half-life for atrazine was observed previously in multiple studies (Jones et al., 1982; Vanderheyden et al., 1997; WHO, 2010),

although Seybold et al. (2001) indicated longer half-lives of atrazine. Taking into account that our experiment took place in organic-rich topsoil with macropores, observing values at the low end of the range reported in the literature is expected. A half-life of 2 d for 2,4-D is within the observed values by Wilson et al., (1997). Decay rates of 2,4-D being ten times faster than those of atrazine agree with the finding that 2,4-D disappearance time may be up to ten times earlier than atrazine (Hamaker, 1972).

The model predicted early sharp peaks better than rounded peaks with extended tails (Table 5-2). This is attributed to the utilization of the exponential loss of chemicals from the distribution layer, projecting a sharp decline in the solute leachate from the top layer. Therefore, in the case of rounded peaks with extended tails, the model assumption of simple conceptualization did not comport with field observations. Despite this, the locations of the peaks and the overall pattern of the BTCs are well identified as shown in the Figures 5-2 to 5-6.

5.6 Conclusion

The observed herbicide leaching mobility for an experiment on a well-structured Hudson silty clay loam soil in Ithaca, NY, was much faster than would be predicted by the convective-dispersive flow. This was attributed to preferential flow. The Preferential Flow Model (PFM) used seven input parameters (dispersivity, depth, and moisture of the distribution zone, the velocity of water, a portion in which water is transported at each velocity, adsorption coefficient, and degradation rate) to model the preferential flow. With realistic input values, the PFM described the early breakthroughs and the extensive tailings

of experimental breakthrough curves of non-adsorbed (chloride) and adsorbed (atrazine and 2,4-D) solutes under field conditions in the soil at or above field capacity.

5.7 Acknowledgments

This research was funded by the New York State Department of Environmental Conservation, Bureau of Pesticides Management, Ms. Luane Whitbeck, Project Manager. The authors would like to thank Mrs. Natalia Peranginangin for taking and analyzing the samples. We would like to extend our appreciation for the fieldwork assistance to Brett Bovee, Jeanne Lippincott, Renelle Sagana, and. Young-Jin Kim. We are grateful for the cooperation of Rick Reisinger (site permission), Gary Tennant, Rich Russell (site excavation), Peter Furdyna (confirming analyses) and Dan Van Vleet (pesticide applicator).

REFERENCES

Abate, G., J.C. Penteado, J.D. Cuzzi, G.C. Vitti, J. Lichtig, and J.C. Masini. 2004. Influence of humic acid on adsorption and desorption of atrazine, hydroxyatrazine, deethylatrazine, and deisopropylatrazine onto a clay-rich soil sample. J. Agric. Food Chem. 52(22): 6747–6754. doi: 10.1021/jf049229e.

Addy, K., A.J. Gold, L.E. Christianson, M.B. David, L.A. Schipper, and N.A. Ratigan. 2016. Denitrifying bioreactors for nitrate removal: A meta-analysis. J. Environ. Qual. 45(3): 873–881. doi: 10.2134/jeq2015.07.0399.

Ahmad, R., and A. Rahman. 2009. Sorption characteristics of atrazine and imazethapyr in soils of New Zealand: Importance of independently determined sorption data. J. Agric. Food Chem. 57(22): 10866–10875. doi: 10.1021/jf901365j.

Akhtar, M.S., B.K. Richards, P. a. Medrano, M. DeGroot, and T.S. Steenhuis. 2003. Dissolved phosphorus from undisturbed soil cores: Related to adsorption strength, flow rate, or soil structure? Soil Sci. Soc. Am. J. 67(2): 458–470.

Anderson, T.R., P.M. Groffman, S.S. Kaushal, and M.T. Walter. 2014a. Shallow groundwater denitrification in riparian zones of a headwater agricultural landscape. J. Environ. Qual. 43(2): 732. doi: 10.2134/jeq2013.07.0303.

Anderson, C.R., K. Hamonts, T.J. Clough, and L.M. Condron. 2014b. Biochar does not affect soil N-transformations or microbial community structure under ruminant urine patches but does alter relative proportions of nitrogen cycling bacteria. Agric. Ecosyst. Environ. 191(2): 63–72. doi: 10.1016/j.agee.2014.02.021.

Andreini, M.S., and T.S. Steenhuis. 1990. Preferential Paths of Flow under Conventional and conservation Tillage. Geoderma 46: 85–102.

Armstrong, D.E., G. Chesters, and R.F. Harris. 1967. Atrazine Hydrolysis in Soil. Soil Sci. Soc. Am. J. 31(1): 61. doi: 10.2136/sssaj1967.03615995003100010019x.

Ashoori, N., M. Teixido, S. Spahr, G.H. Lefevre, D.L. Sedlak, and R.G. Luthy. 2019. Evaluation of pilot-scale biochar-amended woodchip bioreactors to remove nitrate , metals , and trace organic contaminants from urban stormwater runoff. water Res. 154: 1–11.

Atwood, D., and C. Paisley-Jones. 2017. Pesticides Industry Sales and Usage; 2008-2012 Market Estimates.

Baghapour, M., S. Nasseri, and Z. Derakhshan. 2013. Atrazine Removal From Aqueous Solutions Using Submerged Biological Aerated Filter. J. Environ. Heal. Sci. Eng. 11(1): 6. doi: 10.1186/2052-336X-11-6.

Barry, D.A., G.C. Sander, S. Jomaa, L. Yeghiazarian, T.S. Steenhuis, and J.S. Selker. 2013. Solute and sediment transport at laboratory and field scale: Contributions of J.-Y. Parlange. Water Resour. Res. 49(10): 6111–6136. doi: 10.1002/wrcr.20510.

Bauters, T.W.J., T.S. Steenhuis, J.-Y. Parlange, and D.A. DiCarlo. 1998. Preferential flow in water-repellent sands. Soil Sci. Soc. Am. J. 62(5): 1185. doi: 10.2136/sssaj1998.03615995006200050005x.

Bayabil, H.K., C.R. Stoof, C. Mason, B.K. Richards, T.S. Steenhuis, A. Ploeger, S.S. Withanachchi, E. Koncagul, and Y. Zhang. 2016. Nitrous Oxide and Methane Fluxes from Smallholder Farms: A Scoping Study in the Anjeni Watershed. climate 4(62). doi: 10.3390/cli4040062.

Beven, K. 2018. A Century of Denial : Preferential and Nonequilibrium Water Flow in Soils, 1864-1984. Vadose Zo. J. 17(1). doi: 10.2136/vzj2018.08.0153.

Beven, K., and P. Germann. 1981. Water Flow in Soil Macropores II. A combined Flow Model. J. soil Sci. 32: 15–29.

Beven, K., and P.F. Germann. 1982. Macropores and water flows in soils. Water Resour. Res. 18(5): 1311–1325. doi: 10.1029/WR018i005p01311.

Beven, K., and P. Germann. 2013. Macropores and water flow in soils revisited. Water Resour. Res. 49(6): 3071–3092. doi: 10.1002/wrcr.20156.

Blann, K.L., J.L. Anderson, G.R. Sands, and B. Vondracek. 2009. Technology Effects of Agricultural Drainage on Aquatic Ecosystems : A Review Effects of Agricultural Drainage on Aquatic Ecosystems : A Review. Crit. Rev. Environ. Sci. Technol. 39: 909–1001. doi: 10.1080/10643380801977966.

Blasi, C. Di. 1993. Modeling and Simulation of Combustion Processes of Charring and Non-Charring Solid Fuels. Prog. Energy Combust. Sci. 19: 71–104. doi: 10.1016/0360-1285(93)90022-7.

Blowes, D.W., W.D. Robertson, C.J. Ptacek, and C. Merkley. 1994. Removal of agricultural nitrate from tile-drainage effluent water using in-line bioreactors. J. Contam. Hydrol. 15(3): 207–221. doi: 10.1016/0169-7722(94)90025-6.

Bock, E.M., B. Coleman, and Z.M. Easton. 2016. Effect of Biochar on Nitrate Removal in a Pilot-scale Denitrifying Bioreactor. J. Environ. Qual. 45(3): 762–771. doi: 10.2134/jeq2015.04.0179.

Bock, E.M., B.S.L. Coleman, and Z.M. Easton. 2018. Effect of biochar, hydraulic residence time, and nutrient loading on greenhouse gas emission in laboratory-scale denitrifying bioreactors. Ecol. Eng. 120: 375–383. doi: 10.1016/J.ECOLENG.2018.06.010.

Bock, E., N. Smith, M. Rogers, B. Coleman, M. Reiter, B. Benham, and Z.M. Easton. 2014. Enhanced Nitrate and Phosphate Removal in a Denitrifying Bioreactor with Biochar. J. Environ. Qual. 44(2): 605–613. doi: 10.2134/jeq2014.03.0111.

Boesten, J.J.T.I. 2007. Simulation of Pesticide Leaching in the Field and in Zero-Tension Lysimeters. Vadose Zo. J. 6(2004): 793–804. doi: 10.2136/2007.0067.

Boll, J., J.S. Selker, G. Shalit, and T.S. Steenhuis. 1997. Frequency distribution of water and solute transport properties derived from pan sampler data. Water Resour. Res. 33(12): 2655–2664. doi: 10.1029/97WR02588.

Bourke, J., M. Manley-Harris, C. Fushimi, K. Dowaki, T. Nunoura, and M.J. Antal. 2007. Do all carbonized charcoals have the same chemical structure? 2. A model of the chemical structure of carbonized charcoal. Ind. Eng. Chem. Res. 46(18): 5954–5967. doi: 10.1021/ie070415u.

Boussaid, F., G. Martin, J. Morvan, J.J. Collin, A. Landreau, and H. Talbo. 1988. Denitrification in-situ of groundwaters with solid carbon matter. Environ. Technol. Lett. 9(8): 803–816. doi: 10.1080/09593338809384636.

Boyer, E.W., R.W. Howarth, J.N. Galloway, F.J. Dentener, P.A. Green, and C.J. Vörösmarty. 2006. Riverine nitrogen export from the continents to the coasts. Global Biogeochem. Cycles 20(1): 1–9. doi: 10.1029/2005GB002537.

Bradbury, A.G.W., and F. Shafizadeh. 1980. Chemisorption of oxygen on cellulose char. Carbon N. Y. 18(2): 109–116. doi: 10.1016/0008-6223(80)90018-4.

Bradford, S.A., V.L. Morales, W. Zhang, W. Ronald, A.I. Packman, A. Mohanram, and C. Welty. 2013. Transport and fate of microbial pathogens in agricultural settings. Environ. Sci. Technol. 43(February): 775–893. doi: 10.1080/10643389.2012.710449.

Breitburg, D., L.A. Levin, A. Oschlies, M. Grégoire, F.P. Chavez, D.J. Conley, V. Garçon, D. Gilbert, D. Gutiérrez, K. Isensee, G.S. Jacinto, K.E. Limburg, I. Montes, S.W.A. Naqvi, G.C. Pitcher, N.N. Rabalais, M.R. Roman, K.A. Rose, B.A. Seibel, M. Telszewski, M. Yasuhara, and J. Zhang. 2018. Declining Oxygen in the Global Ocean and Coastal Waters. Science 359(6371): eaam7240. doi: 10.1126/science.aam7240.

Bridgham, S.D., R. Ye, R.D. DeLaune, K.R. Reddy, C.J. Richardson, and J.P. Megonigal. 2014. Organic Matter Mineralization and Decomposition. p. 385–406. *In* Methods in Biogeochemistry of Wetlands.

Brisson, N., B. Mary, D. Ripoche, M.H. Jeuffroy, F. Ruget, B. Nicoullaud, P. Gate, F. Devienne-Barret, R. Antonioletti, C. Durr, G. Richard, N. Beaudoin, S. Recous, X. Tayot, D. Plenet, P. Cellier, J.-M. Machet, J.M. Meynard, and R. Delécolle. 1998. STICS: a generic model for the simulation of crops and their water and nitrogen balances. I. Theory and parameterization applied to wheat and corn. Agronomie 18(1 998): 311–346. doi: 10.1051/agro:19980501.

Buhler, D.D., G.W. Randall, W.C. Koskinen, and D.L. Wyse. 1993. Atrazine and Alachlor Losses from Subsurface Tile Drainage of a Clay Loam Soil. J. Environ. Qual. 22(3): 583. doi: 10.2134/jeq1993.00472425002200030024x.

Burkart, M.R., and D.E. James. 1999. Agricultural-Nitrogen Contributions to Hypoxia in the Gulf of Mexico. J. Environ. Qual. 28(3): 850–859. doi: 10.2134/jeq1999.00472425002800030016x.

Cameron, S.G., and L. a. Schipper. 2010. Nitrate removal and hydraulic performance of organic carbon for use in denitrification beds. Ecol. Eng. 36(11): 1588–1595. doi: 10.1016/j.ecoleng.2010.03.010.

Cao, X., L. Ma, Y. Liang, B. Gao, and W. Harris. 2011. Simultaneous Immobilization of Lead and Atrazine in Contaminated Soils Using Dairy-Manure Biochar. Environ. Sci. Technol. 45(11): 4884–4889. doi: 10.1021/es103752u.

Cayuela, M.L., M.A. Sánchez-Monedero, A. Roig, K. Hanley, A. Enders, and J. Lehmann. 2013. Biochar and denitrification in soils: when, how much and why does biochar reduce N(2)O emissions? Sci. Rep. 3: 1732–1739. doi: 10.1038/srep01732.

Celestino Ladu, J.L., and D. Zhang. 2011. Modeling atrazine transport in soil columns with HYDRUS-1D. water Sci. Eng. 4(3): 258–269. doi: 10.3882/j.issn.1674-2370.2011.03.003.

Chapelle, F.H., P.M. Bradley, D.J. Goode, C. Tiedeman, P.J. Lacombe, K. Kaiser, and R. Benner. 2009. Biochemical indicators for the bioavailability of organic carbon in ground water. Ground Water 47(1): 108–121. doi: 10.1111/j.1745-6584.2008.00493.x.

Chefetz, B. 2003. Sorption of Phenanthrene and Atrazine by Plant Cuticular Fractions. Environ. Toxicol. Chem. 22(10): 2492–2498. doi: 10.1897/02-461.

Chen, J., H. Kim, and G. Yoo. 2015. Effects of Biochar Addition on CO2 and N2O Emissions following Fertilizer Application to a Cultivated Grassland Soil (RM Lehman, Ed.). PLoS One 10(5): e0126841. doi: 10.1371/journal.pone.0126841.

Chen, G., Z. Zhang, Z. Zhang, and R. Zhang. 2018. Redox-active reactions in denitrification provided by biochars pyrolyzed at different temperatures. Sci. Total Environ. 615: 1547–1556. doi: 10.1016/j.scitotenv.2017.09.125.

Cheng, C.H., and J. Lehmann. 2009. Ageing of black carbon along a temperature gradient. Chemosphere 75(8): 1021–1027. doi: 10.1016/j.chemosphere.2009.01.045.

Cheng, C.H., J. Lehmann, J.E. Thies, S.D. Burton, and M.H. Engelhard. 2006. Oxidation of black carbon by biotic and abiotic processes. Org. Geochem. 37(11): 1477–1488. doi: 10.1016/j.orggeochem.2006.06.022.

Christianson, L., A. Bhandari, and M.J. Helmers. 2011a. Pilot-Scale Evaluation of Denitrification Drainage Bioreactors: Reactor Geometry and Performance. J. Environ. Eng. 137(4): 213–220. doi: 10.1061/(ASCE)EE.1943-7870.0000316.

Christianson, L., A. Bhandari, and M. Helmers. 2011b. Potential Design Methodology for Agricultural Drainage Denitification Bioreactors. p. 2740–2748. *In* World Environmental and Water Resources Congress 2011:Bearing Knowledge for Sustainability © ASCE 2011. ASCE.

Christianson, L., A. Bhandari, and M.J. Helmers. 2012a. A Practice-oriented review of woodchip bioreactors for subsurface agricultural drainage. Appl. Eng. Agric. 28(6): 861–874. doi: 10.13031/2013.42479.

Christianson, L., A. Bhandari, M.J. Helmers, K. Kult, T. Sutphin, and R. Wolf. 2012b. Performance Evaluation of Four Field-Scale Agricultural Drainage Denitrification Bioreactors in Iowa. Trans. ASABE 55(6): 2163–2174. doi: 10.13031/2013.42508.

Christianson, L., R. Christianson, M. Helmers, C. Pederson, and A. Bhandari. 2013a. Modeling and calibration of drainage denitrification bioreactor design criteria. J. Irrig. Drain. Eng. © ASCE (139): 699–709. doi: 10.1061/(ASCE)IR.1943-4774.0000622.

Christianson, L., J.A. Hanly, and M.J. Hedley. 2011c. Optimized denitrification bioreactor treatment through simulated drainage containment. Agric. Water Manag. 99(1): 85–92. doi: 10.1016/j.agwat.2011.07.015.

Christianson, L., M. Hedley, M. Camps, H. Free, and S. Saggar. 2011d. Influence of biochar amendments on denitrification bioreactor performance. *In* Adding to the knowledge base for the nutrient manager from the 24th Annual Fertilizer and Lime Research Centre Workshop. Fertilizer and Lime Research Centre, Massey University, Palmerston North, New Zealand.

Christianson, L., M. Helmers, A. Bhandari, and T. Moorman. 2013b. Internal hydraulics of an agricultural drainage denitrification bioreactor. Ecol. Eng. 52(3): 298–307. doi: 10.1016/j.ecoleng.2012.11.001.

Christianson, L., and L. Schipper. 2016. Moving Denitrifying Bioreactors beyond Proof of Concept: Introduction to the Special Section. J. Environ. Qual. 45: 757–761. doi: 10.2134/jeq2016.01.0013.

Chun, J.A., R.A. Cooke, J.W. Eheart, and M.S. Kang. 2009. Estimation of flow and transport parameters for woodchip-based bioreactors: I. Laboratory-scale bioreactor. Biosyst. Eng. 104(3): 384–395. doi: 10.1016/j.biosystemseng.2009.06.021.

Chung, K.H., K.S. Ro, and D. Roy. 1995. Atrazine Biotransformation in Wetland Sediment Under Different Nutrient Conditions-I: Anaerobic. J. Environ. Sci. Heal. A 30(1): 109–120. doi: 10.1080/10934529509376189.

Chung, K.H., K.S. Ro, and D. Roy. 1996. Fate and Enhancement of Atrazine Biotransformation in Anaerobic Wetland Sediment. Water Res. 30(2): 341–346. doi: 10.1016/0043-1354(95)00164-6.

Clement, D.R. 2016. Does Phosphorus from Agricultural Tile Drains Fuel Algal Blooms ? Masters Th(Paper 807).

Clough, T.J., L.M. Condron, C. Kammann, and C. Müller. 2013. A Review of Biochar and Soil Nitrogen Dynamics. Agronomy 3: 275–293. doi: 10.3390/agronomy3020275.

Coleman, B.S.L., Z.M. Easton, and E.M. Bock. 2019. Biochar fails to enhance nutrient removal in woodchip bioreactor columns following saturation. J. Environ. Manage. 232(October 2018): 490–498. doi: 10.1016/j.jenvman.2018.11.074.

Dahlke, H.E., Z.M. Easton, S.W. Lyon, M. Todd Walter, G. Destouni, and T.S. Steenhuis. 2012. Dissecting the variable source area concept - Subsurface flow pathways and water mixing processes in a hillslope. J. Hydrol. 420–421: 125–141. doi: 10.1016/j.jhydrol.2011.11.052.

Darnault, C.J.G., T.S. Steenhuis, P. Garnier, Y.-J. Kim, M. Jenkins, W.C. Ghiorse, P. Baveye, and J.-Y. Parlange. 2004. Preferential flow and transport of Cryptosporidium parvum Oocysts through the vadose zone: Experiments and modeling. Vadose Zo. J. 3(2): 736–736. doi: 10.2113/3.2.736.

David, M.B., and L.E. Gentry. 2000. Anthropogenic Inputs of Nitrogen and Phosphorus and Riverine Export for Illinois, USA. J. Environ. Qual. 29: 494–508.

David, M.B., L.E. Gentry, K.M. Starks, and R.A. Cooke. 2003. Stream Transport of Herbicides and Metabolites in a Tile-Drained, Agricultural Watershed. J. Environ. Qual. 32: 1790–1801. doi: 10.2134/jeq2003.1790.

Delwiche, K.B., J. Lehmann, and M.T. Walter. 2014. Atrazine Leaching From Biochar-Amended Soils. Chemosphere 95: 346–352. doi: 10.1016/j.chemosphere.2013.09.043.

Derakhshan, Z., M.H. Ehrampoush, A.H. Mahvi, M. Dehghani, M. Faramarzian, M.T. Ghaneian, M. Mokhtari, A.A. Ebrahimi, and H. Fallahzadeh. 2018a. Evaluation Of A Moving Bed Biofilm Reactor For Simultaneous Atrazine , Carbon and Nutrients Removal From Aquatic Environments : Modeling And Optimization. J. Ind. Eng. Chem. 67: 219–230. doi: 10.1016/j.jiec.2018.06.032.

Derakhshan, Z., M.H. Ehrampoush, A.H. Mahvi, M.T. Ghaneian, S.M. Mazloomi, M. Faramarzian, M. Dehghani, H. Fallahzadeh, S. Yousefinejad, E. Berizi, and S. Bahrami. 2018b. Biodegradation of Atrazine From Wastewater Using Moving Bed Biofilm Reactor Under Nitrate-Reducing Conditions : A Kinetic Study. J. Environ. ma 212: 506–513.

Derakhshan, Z., A.H. Mahvi, M.T. Ghaneian, S.M. Mazloomi, M. Faramarzian, M. Dehghani, H. Fallahzadeh, S. Yousefinejad, E. Berizi, M.H. Ehrampoush, and S. Bahrami. 2018c. Simultaneous Removal of Atrazine and Organic Matter From Wastewater Using Anaerobic Moving Bed Biofilm Reactor : A Performance Analysis. J. Environ. Manage. 209: 515–524. doi: 10.1016/j.jenvman.2017.12.081.

Driel, P.W. Van, W.D. Robertson, and L.C. Merkley. 2006. Denitrification of Agricultural Drainage Using Wood-Based Reactors. Trans. ASABE 49(2): 565–574.

Dunigan, E.P., and T.H. McIntosh. 1971. Atrazine-Soil Organic Matter Interactions. weed Sci. 19(3): 279–283. http://www.jstor.org/stable/4041760.

Elgood, Z., W.D. Robertson, S.L. Schiff, and R. Elgood. 2010. Nitrate Removal and Greenhouse Gas Production in a Stream-bed Denitrifying bioreactor. Ecol. Eng. 36(11): 1575–1580. doi: 10.1016/j.ecoleng.2010.03.011.

Elliott, J.A., A.J. Cessna, W. Nicholaichuk, and L.C. Tollefson. 2000. Leaching Rates and Preferential Flow of Selected Herbicides through Tilled and Untilled Soil. J. Environ. Qual. 29: 1650–1656.

EPA. 1995. National Primary Drinking Water Regulations; Atrazine. 811-F-95-003 d-C.

EPA. 2005. Registration Eligibility Decision for 2,4-D. EPA 738-R-05-002 (June): 304.

EPA. 2006. Decision Documents for Atrazine. Washington, D.C.
EPA. 2015. A Compilation of Cost Data Associated with the Impacts and Control of Nutrient Pollution. EPA 820-F-15-096 (May). http://www2.epa.gov/sites/production/files/2015-04/documents/nutrient-economics-report-2015.pdf.
Ernstsen, V., P. Olsen, and A.E. Rosenbom. 2015. Long-Term Monitoring of Nitrate Transport to Drainage From Three Agricultural Clayey Till Fields. Hydrol. Earth Syst. Sci. 19(8): 3475–3488. doi: 10.5194/hess-19-3475-2015.
van Es, H.M., J.M. Sogbedji, and R.R. Schindelbeck. 2004. Effect of manure application timing, crop, and soil type on nitrate leaching. J. Environ. Qual. 35(2): 670–679. doi: 10.2134/jeq2005.0143.
FAO, and WHO. 1998. Pesticide residue in food 1998: Evaluation. Rome, Italy.
Flury, M. 1996. Experimental evidence of transport of pesticides through field soils—A review. J. Environ. Qual. 25(1): 25. doi: 10.2134/jeq1996.00472425002500010005x.
French, L., J. Wulforst, W. Broad, P. Bauter, and R. Guthrie. 1978. Soil Survey of Steuben County, New York. USDA, Washington. D.C.
Fuka, D., T.M. Walter, J. a. Archibald, T.S. Steenhuis, and Z.M. Easton. 2015. Package ' EcoHydRology .' : 34.
Galloway, J.N., F.J. Dentener, D.G. Capone, E.W. Boyer, R.W. Howarth, S.P. Seitzinger, G.P. Asner, C.C. Cleveland, P.A. Green, E.A. Holland, D.M. Karl, A.F. Michaels, J.H. Porter, A.R. Townsend, and C.J. Vo. 2004. Nitrogen Cycles: Past , Present , and Future. Biogeochemistry 70: 153–226.
Gamble, D.S., and S.U. Khan. 1985. Atrazine Hydrolysis in soils: Catalysis By the Acidic Functional Groups and Fulvic Acid. Can. J. Soil Sci. 443(1402): 435–443.
Gärdenäs, A.I., J. Šimůnek, N. Jarvis, and M.T. van Genuchten. 2006. Two-dimensional modelling of preferential water flow and pesticide transport from a tile-drained field. J. Hydrol. 329(3–4): 647–660. doi: 10.1016/j.jhydrol.2006.03.021.
Gaynor, J.D., D.C. MacTavish, and W.I. Findlay. 1992. Surface and subsurface transport of atrazine and alachlor from a Brookston clay loam under continuous corn production. Arch. Environ. Contam. Toxicol. 23(2): 240–245. doi: 10.1007/BF00212282.
Geisseler, D., W.R. Horwath, R.G. Joergensen, and B. Ludwig. 2010. Pathways of nitrogen utilization by soil microorganisms – A review. Soil Biol. Biochem. 42(12): 2058–2067. doi: 10.1016/j.soilbio.2010.08.021.
Geller, A. 1980. Studies on the Degradation of Atrazine by Bacterial Communities Enriched From Various Biotopes. Arch. Environ. Contam. Toxicol. 9(3): 289–305. doi: 10.1007/BF01057409.
Gentry, L.E., M.B. David, K.M. Smith-Starks, and D.A. Kovacic. 2010. Nitrogen Fertilizer and Herbicide Transport from Tile Drained Fields. J. Environ. Qual. 29(1): 232. doi: 10.2134/jeq2000.00472425002900010030x.
Gentry, L.E., M.B. David, K.M. Smith, and D.A. Kovacic. 1998. Nitrogen Cycling and Tile Drainage Nitrate Loss in a Corn/Soybean Watershed. Agric. Ecosyst. Environ. 68(1–2): 85–97. doi: 10.1016/S0167-8809(97)00139-4.
van Genuchten, M.T., and W.J. Alves. 1984. Analytical solutions of the one-dimensional convective-dispersive solute transport equation.
Gerke, H.H. 2006. Preferential flow descriptions for structured soils. J. Plant Nutr. Soil

Sci. 169(3): 382–400. doi: 10.1002/jpln.200521955.
Ghane, E., G.W. Feyereisen, C.J. Rosen, and U.W. Tschirner. 2018. Carbon Quality of Four-Year-Old Woodchips in a Denitrification Bed Treating Agricultural Drainage. Trans. ASABE 2018 61(3): 995–1000.
Ghodrati, M., and W.A. Jury. 1992. A field study of the effects of soil structure and irrigation method on preferential flow of pesticides in unsaturated soil. J. Contam. Hydrol. 11(1–2): 101–125. doi: 10.1016/0169-7722(92)90036-E.
Ghosh, P.K., L. Philip, and M. Bandyopadhyay. 2001. Anaerobic Treatment of Atrazine Bearing Wastewater. J. Environ. Sci. Heal. Part B 36(3): 301–316. doi: 10.1081/PFC-100103571.
Gilham, R.., and J.. Cherry. 1977. Field Evidence of Denitrification in Shallow Groundeater Flow Systems. Water Pollut. Resour. Canada 13.
Gilliom, R.J. 2007. Pesticides in U.S. Streams and Groundwater. Environ. Sci. Technol. 41(10): 3408–3414. doi: 10.1021/es072531u.
Gilliom, R.J., J.E. Barbash, C.G. Crawford, P. a. Hamilton, J.D. Martin, N. Nakagaki, L.H. Nowell, J.C. Scott, P.E. Stackelberg, G.P. Thelin, and D.M. Wolock. 2006. The Quality of Our nation's Waters-Pesticides in the Nation's Streams and Groundwater, 1992–2001.
Gish, T.J., A. Shirmohammadi, R. Vyravipillai, and B.J. Wienhold. 1995. Herbicide Leaching under Tilled and No-Tillage Fields. Soil Sci. Soc. Am. J. 59: 895–901.
Graymore, M., F. Stagnitti, and G. Allinson. 2001. Impacts of Atrazine in Aquatic Ecosystems. Environ. Int. 26(7–8): 483–495. doi: 10.1016/S0160-4120(01)00031-9.
Greenan, C.M., T.B. Moorman, T.C. Kaspar, T.B. Parkin, and D.B. Jaynes. 2006. Comparing carbon substrates for denitrification of subsurface drainage water. J. Environ. Qual. 35(3): 824–829. doi: 10.2134/jeq2005.0247.
Greenan, C.M., T.B. Moorman, T.B. Parkin, T.C. Kaspar, and D.B. Jaynes. 2009. Denitrification in Wood Chip Bioreactors at Different Water Flows. J. Environ. Qual. 38(4): 1664–1671. doi: 10.2134/jeq2008.0413.
Guo, L., and H. Lin. 2018. Addressing two bottlenecks to advance the understanding of preferential flow in soils. 1st ed. Elsevier Inc.
Guzzella, L., F. Pozzoni, and G. Giuliano. 2006. Herbicide Contamination of Surficial Groundwater in Northern Italy. Environ. Pollut. 142(2): 344–353. doi: 10.1016/j.envpol.2005.10.037.
Gwo, J.P., P.M. Jardine, G.V. Wison, and G.T. Yeh. 1995. A multiple-pore-region concept to modeling mass transfer in subsurface media. J. Hydrol. 164: 217–237.
Hallberg, G.R. 1989. Pesticides pollution of groundwater in the humid United States. Agric. Ecosyst. Environ. 26(3–4): 299–367. doi: 10.1016/0167-8809(89)90017-0.
Hamaker, J.W. 1972. Decomposition : Quantitative aspects. *In* Goring, C.A.., Hamaker, J.W. (eds.), Organic chemicals in the soil environments. Marcel Dekker, Inc, New York.
Hance, R.. 1974. Soil Organic Matter and the Adsorption and Decomposition of the Herbicides Atrazine and Linuron. Soil Biol. Biochem. 6: 39–42.
Harter, J., H.-M. Krause, S. Schuettler, R. Ruser, M. Fromme, T. Scholten, A. Kappler, and S. Behrens. 2014. Linking N2O emissions from biochar-amended soil to the structure and function of the N-cycling microbial community. ISME J. 8(3): 660–674. doi: 10.1038/ismej.2013.160.

Hassanpour, B., L.D. Geohring, A.R. Klein, S. Giri, L. Aristilde, and T.S. Steenhuis. 2019. Application of denitrifying bioreactors for the removal of atrazine in agricultural drainage water. J. Environ. Manage. 239(December 2018): 48–56. doi: 10.1016/j.jenvman.2019.03.029.

Hassanpour, B., S. Giri, W. Pluer, T.S. Steenhuis, and L. Geohring. 2016. Field performance of denitrifying bioreactors in the Northeastern United States. p. 1–9. *In* 10th International Drainage Symposium, American Society of Agricultural and Biological Engineers. Minneapolis, Minnesota.

Hassanpour, B., S. Giri, W.T. Pluer, T.S. Steenhuis, and L.D. Geohring. 2017. Seasonal Performance of Denitrifying Bioreactors in the Northeastern United States: Field Trials. J. Environ. Manage. 202: 242–253. doi: 10.1016/j.jenvman.2017.06.054.

Heitkötter, J., and B. Marschner. 2015. Interactive effects of biochar ageing in soils related to feedstock, pyrolysis temperature, and historic charcoal production. Geoderma 245–246: 56–64. doi: 10.1016/j.geoderma.2015.01.012.

Hergert, H.L. 1960. Infrared Spectra of Lignin and Related Compounds. II. Conifer Lignin and Model Compounds1,2. J. Org. Chem. 25(3): 405–413. doi: 10.1021/jo01073a026.

Hill, D.E., and J.-Y. Parlange. 1972. Wetting front instability in layered soils1. Soil Sci. Soc. Am. J. 36(5): 697. doi: 10.2136/sssaj1972.03615995003600050010x.

Hoover, N.L., A. Bhandari, M.L. Soupir, and T.B. Moorman. 2016. Woodchip Denitrification Bioreactors: Impact of Temperature and Hydraulic Retention Time on Nitrate Removal. J. Environ. Qual. 45(3): 803. doi: 10.2134/jeq2015.03.0161.

Hudson, F. 2004. Sample Preparation and Calculations for Dissolved Gas Analysis in Water Samples Using a GC Headspace Equilibration Technique.

Hunter, W.J., and D.L. Shaner. 2010. Biological Remediation of Groundwater Containing both Nitrate and Atrazine. Curr. Microbiol. 60(1): 42–46. doi: 10.1007/s00284-009-9499-3.

Hutson, J.L., and R.J. Wagenet. 1995. A multiregion model describing water flow and solute transport in heterogeneous soils. Soil Sci. Soc. Am. J. 59(3): 743. doi: 10.2136/sssaj1995.03615995005900030016x.

Ilhan, Z.E., S.K. Ong, and T.B. Moorman. 2011. Dissipation of Atrazine, Enrofloxacin, and Sulfamethazine in Wood Chip Bioreactors and Impact on Denitrification. J. Environ. Qual. 40(6): 1816. doi: 10.2134/jeq2011.0082.

Islam, F., J. Wang, M.A. Farooq, M.S.S. Khan, L. Xu, J. Zhu, M. Zhao, S. Muños, Q.X. Li, and W. Zhou. 2018. Potential impact of the herbicide 2,4-dichlorophenoxyacetic acid on human and ecosystems. Environ. Int. 111: 332–351. doi: 10.1016/J.ENVINT.2017.10.020.

Issa, S., and M. Wood. 2005. Degradation of Atrazine and Isoproturon in Surface and Sub-surface Soil Materials Undergoing Different Moisture and Aeration Conditions. Pest Manag. Sci. 61(2): 126–132. doi: 10.1002/ps.951.

Jahangir, M.M.R., P. Johnston, M.I. Khalil, J. Grant, C. Somers, and K.G. Richards. 2012. Evaluation of headspace equilibration methods for quantifying greenhouse gases in groundwater. J. Environ. Manage. 111: 208–212. doi: 10.1016/J.JENVMAN.2012.06.033.

Janssen, B.H. 1984. A simple method for calculating decomposition and accumulation of 'young' soil organic matter. Plant Soil 76(1–3): 297–304. doi: 10.1007/BF02205588.

Jarvis, N.J. 2007. A review of non-equilibrium water flow and solute transport in soil

macropores: Principles, controlling factors and consequences for water quality. Eur. J. Soil Sci. 58(3): 523–546. doi: 10.1111/j.1365-2389.2007.00915.x.

Jarvis, N.J., L.F. Bersgrom, and B. C.D. 1995. Pesticide leaching models and their use for management purposes. p. 196–220. *In* Roberts, T.R., Kearny, P.C. (eds.), Environmental behaviour of agrochemicals. John Wiley and Sons Ltd.

Jarvis, N., J. Koestel, and M. Larsbo. 2016. Understanding preferential flow in the vadose zone: Recent advances and future prospects. Vadose Zo. J. 15(12): 0. doi: 10.2136/vzj2016.09.0075.

Jarvis, N.J., and M. Larsbo. 2012. MACRO (V5.2): Model use, calibration and validation. Trans. ASABE 55: 1413–1423.

Jaynes, D.B., J.L. Hatfield, and D.W. Meek. 1999. Water Quality in Walnut Creek Watershed: Herbicides and Nitrate in Surface Waters. J. Environ. Qual. 28: 45–59.

Jindo, K., H. Mizumoto, Y. Sawada, M.A. Sanchez-Monedero, and T. Sonoki. 2014. Physical and Chemical Characterization of Biochars Derived From Different Agricultural Residues. Biogeosciences 11(23): 6613–6621. doi: 10.5194/bg-11-6613-2014.

Jones, T.W., W.M. Kemp, J.C. Stevenson, and J.C. Means. 1982. Degradation of Atrazine in Estuarine Water/Sediment Systems and Soils. J. Environ. Qual. 11(4): 632. doi: 10.2134/jeq1982.00472425001100040015x.

Kappler, A., M.L. Wuestner, A. Ruecker, J. Harter, M. Halama, and S. Behrens. 2014. Biochar as an Electron Shuttle between Bacteria and Fe(III) Minerals. Environ. Sci. Technol. Lett. 1(8): 339–344. doi: 10.1021/ez5002209.

Katz, I., C.G. Dosoretz, R.T. Mandelbaum, and M. Green. 2001. Atrazine Degradation Under Denitrifying Conditions in Continuous Culture of Pseudomonas ADP. Water Res. 35(13): 3272–3275. doi: 10.1016/S0043-1354(01)00009-4.

Kim, Y.J., C.J.G. Darnault, N.O. Bailey, J.Y. Parlange, and T.S. Steenhuis. 2005. Equation for describing solute transport in field soils with preferential flow paths. Soil Sci. Soc. Am. J. 69(2): 291–300. doi: 10.1084/jem.20070109.

Kim, Y.J., T.S. Steenhuis, and K. Nam. 2008. Movement of heavy metals in soil through preferential flow paths under different rainfall intensities. Clean - Soil, Air, Water 36(12): 984–989. doi: 10.1002/clen.200800141.

Kimetu, J.M., and J. Lehmann. 2010. Stability and Stabilization of Biochar and Green Manure in Soil With Different Organic Carbon Contents. Aust. J. Soil Res. 48: 577–585.

King, K.W., and J.C. Balogh. 2010. Chlorothalonil and 2,4-D losses in surface water discharge from a managed turf watershed. J. Environ. Monit. 12(8): 1601–1612. doi: 10.1039/c0em00030b.

Kladivko, E.J., J.R. Frankenberger, D.B. Jaynes, D.W. Meek, B.J. Jenkinson, and N.R. Fausey. 2004. Nitrate Leaching to Subsurface Drains as Affected by Drain Spacing. J. Environ. Qual. 33: 1803–1813.

Kladivko, E.J., G.E. Van Scoyoc, E.J. Monke, K.M. Oates, and W. Pask. 1991. Pesticide and Nutrient Movement Into Subsurface Tile Drains on a Silt Loam Soil in Indiana. J. Environ. Qual. 20(1): 264–270. doi: 10.2134/jeq1991.00472425002000010043x.

Klüpfel, L., M. Keiluweit, M. Kleber, and M. Sander. 2014. Redox properties of plant biomass-derived black carbon (biochar). Environ. Sci. Technol. 48(10): 5601–5611. doi: 10.1021/es500906d.

Köhne, J.M., S. Köhne, and J. Šimůnek. 2009a. A review of model applications for structured soils: b) Pesticide transport. J. Contam. Hydrol. 104(1–4): 36–60. doi: 10.1016/j.jconhyd.2008.10.003.

Köhne, J.M., S. Köhne, and J. Šimůnek. 2009b. A review of model applications for structured soils: a) Water flow and tracer transport. J. Contam. Hydrol. 104(1–4): 4–35. doi: 10.1016/j.jconhyd.2008.10.002.

Koivunen, M.E., K. Dettmer, R. Vermeulen, B. Bakke, S.J. Gee, and B.D. Hammock. 2006. Improved Methods For Urinary Atrazine Mercapturate Analysis-Assessment of an Enzyme-Linked Immunosorbent Assay (ELISA) and a Novel Liquid Chromatography-Mass Spectrometry (LC-MS) Method Utilizing Online Solid Phase Extraction (SPE). Anal. Chim. Acta 572(2): 180–189. doi: 10.1016/j.aca.2006.05.037.

Korom, S.F. 1992. Natural denitrification in the saturated zone: A review. Water Resour. Res. 28(6): 1657. doi: 10.1029/92WR00252.

Kröger, R., M.T. Moore, J.L. Farris, and M. Gopalan. 2011. Evidence for the use of low-grade weirs in drainage ditches to improve nutrient reductions from agriculture. Water. Air. Soil Pollut. 221(1–4): 223–234. doi: 10.1007/s11270-011-0785-x.

Krutz, L.J., S.A. Senseman, K.J. McInnes, D.A. Zuberer, and D.P. Tierney. 2003. Adsorption and Desorption of Atrazine, Desethylatrazine, Deisopropylatrazine, and Hydroxyatrazine in Vegetated Filter Strip and Cultivated Soil. J. Agric. Food Chem. 51(25): 7379–7384. doi: 10.1021/jf0348572.

Kulikova, N.A., and I. V. Perminova. 2002. Binding of Atrazine to Humic Substances From Soil, Peat, and Coal Related to Their Structure. Environ. Sci. Technol. 36(17): 3720–3724. doi: 10.1021/es015778e.

Kumar, A., R.S. Kanwar, and L.R. Ahuja. 1998. Evaluation of preferential flow component of RZWQM in simulating water and atrazine transport to subsurface drains. Trans. ASAE 41(1993): 627–637.

Kung, K.-J.S., E.J. Kladivko, T.J. Gish, T.S. Steenhuis, G. Bubenzer, and C.S. Helling. 2000a. Quantifying preferential flow by breakthrough of sequentially applied tracers: Silt loam soil. Soil Sci. Soc. Am. J. 64(4): 1296. doi: 10.2136/sssaj2000.6441296x.

Kung, K.-J.S., T.S. Steenhuis, E.J. Kladivko, T.J. Gish, G. Bubenzer, and C.S. Helling. 2000b. Impact of preferential flow on the transport of adsorbing and non-adsorbing tracers. Soil Sci. Soc. Am. J. 64(4): 1290. doi: 10.2136/sssaj2000.6441290x.

Lai, L., S. Kumar, E.G. Mbonimpa, C.O. Hong, V.N. Owens, and R.P. Neupane. 2016. Evaluating the impacts of landscape positions and nitrogen fertilizer rates on dissolved organic carbon on switchgrass land seeded on marginally yielding cropland. J. Environ. Manage. 171: 113–120. doi: 10.1016/j.jenvman.2016.01.028.

Lal, R., and M. Shukla. 2005. Principles of soil physics. New York. Basel.

Lammoglia, S.-K., F. Brun, T. Quemar, J. Moeys, E. Barriuso, B. Gabrielle, and L. Mamy. 2018. Modelling pesticides leaching in cropping systems: Effect of uncertainties in climate, agricultural practices, soil and pesticide properties. Environ. Model. Softw. doi: 10.1016/j.envsoft.2018.08.007.

Larsbo, M., S. Roulier, F. Stenemo, R. Kasteel, and N. Jarvis. 2005. An Improved Dual-Permeability Model of Water Flow and Solute Transport in the Vadose Zone. Vadose Zo. J. 4: 398–406. doi: 10.2136/vzj2004.0137.

Lavaire, T., L.E. Gentry, M.B. David, and R.A. Cooke. 2017. Fate of water and nitrate using drainage water management on tile systems in east-central Illinois. Agric. Water

Manag. 191: 218–228. doi: 10.1016/j.agwat.2017.06.004.
Lawes, J.B., J.H. Gilbert, and R. Warington. 1882. On the amount and composition of the rain and drainage water collected at Rothamstead. Williams Clowes and Sons,Ltd, London.
Lehmann, J., M.C. Rillig, J. Thies, C. a. Masiello, W.C. Hockaday, and D. Crowley. 2011. Biochar effects on soil biota - A review. Soil Biol. Biochem. 43(9): 1812–1836. doi: 10.1016/j.soilbio.2011.04.022.
Leij, F.J., N. Toride, and M.T. van Genuchten. 1993. Analytical solutions for non-equilibrium solute transport in three-dimensional porous media. J. Hydrol. 151: 193–228.
Leistra, M., and J.J.T.I. Boesten. 1989. Pesticide contamination of groundwater in western Europe. Agric. Ecosyst. Environ. 26(3–4): 369–389. doi: 10.1016/0167-8809(89)90018-2.
Lerch, R.N., E.M. Thurman, and P.E. Blanchard. 1999. Hydroxyatrazine in Soils and Sediments. Environ. Toxicol. Chem. 18(10): 2161. doi: 10.1897/1551-5028(1999)018<2161:HISAS>2.3.CO;2.
Lesaffre, B., and D. Zimmer. 1989. Subsurface drainage peak flows in shallow soil. Irrig. Drain. Eng. 114(3): 387–406. doi: 10.1061/(ASCE)0733-9437(1988)114:3(387).
Li, B., A.R. Pales, H.M. Clifford, S. Kupis, S. Hennessy, W.Z. Liang, S. Moysey, B. Powell, K.T. Finneran, and C.J.G. Darnault. 2018. Preferential flow in the vadose zone and interface dynamics: Impact of microbial exudates. J. Hydrol. 558: 72–89. doi: 10.1016/j.jhydrol.2017.12.065.
Lima, D.L.D., R.J. Schneider, H.W. Scherer, A.C. Duarte, E.B.H. Santos, and V.I. Esteves. 2010. Sorption desorption behavior of atrazine on soils subjected to different organic long-term amendments. J. Agric. Food Chem. 58(5): 3101–3106. doi: 10.1021/jf903937d.
Liu, N., A.B. Charrua, C.H. Weng, X. Yuan, and F. Ding. 2015. Characterization of Biochars Derived From Agriculture Wastes and Their Adsorptive Removal of Atrazine from Aqueous Solution: A Comparative Study. Bioresour. Technol. 198: 55–62. doi: 10.1016/j.biortech.2015.08.129.
Liu, M., L. Guo, J. Yi, H. Lin, S. Lou, H. Zhang, and T. Li. 2018. Characterising preferential flow and its interaction with the soil matrix using dye tracing in the Three Gorges Reservoir Area of China. Soil Res. doi: 10.1071/SR17238.
Loague, K., and R.E. Green. 1991. Statistical and graphical methods for evaluating solute transport models: Overview and application. J. Contam. Hydrol. 7(1–2): 51–73. doi: 10.1016/0169-7722(91)90038-3.
Lupul, I., J. Yperman, R. Carleer, and G. Gryglewicz. 2015. Adsorption of Atrazine on Hemp Stem-based Activated Carbons With Different Surface Chemistry. Adsorption 21(6–7): 489–498. doi: 10.1007/s10450-015-9689-1.
Ma, L., and H.M. Selim. 1996. Atrazine Retention and Transport in Soils. p. 129–173. *In* Ware, G.W., Gunther, F.A. (eds.), Reviews of Environmental Contamination and Toxicology. Springer New York, New York, NY.
Mackay, A.A., and P.M. Gschwend. 2000. Sorption of Monoaromatic Hydrocarbons to Wood. Environ. Sci. Technol. 34(5): 839–845. doi: 10.1021/es9900858.
Malone, R.W., B.T. Nolan, L. Ma, R.S. Kanwar, C. Pederson, and P. Heilman. 2014. Effects of Tillage and Application Rate on Atrazine Transport to Subsurface

Drainage: Evaluation of RZWQM Using a Six-year Field Study. Agric. Water Manag. 132(5): 10–22. doi: 10.1016/j.agwat.2013.09.009.
Malone, R.W., M.J. Shipitalo, and D.W. Meek. 2004. Relationship Between Herbicide Concentration In Percolate, Percolate Breakthrough Time and Number of Active Macropores. Trans. ASAE 47(5): 1453–1456.
Manassaram, D.M., L.C. Backer, and D.M. Moll. 2006. A Review of Nitrates in Drinking Water : Maternal Exposure and Adverse Reproductive and Developmental Outcomes. Environ. Health Perspect. 114(3): 320–327. doi: 10.1289/ehp.8407.
Mandelbaum, R.T., L.P. Wackett, and D.L. Allan. 1993. Rapid Hydrolysis of Atrazine to Hydroxyatrazine by Soil Bacteria. Environ. Sci. Technol. 27(9): 1943–1946. doi: 10.1021/es00046a028.
Marjerison, R.D., J. Melkonian, J.L. Hutson, H.M. van Es, S. Sela, L.D. Geohring, and J. Vetsch. 2016. Drainage and Nitrate Leaching from Artificially Drained Maize Fields Simulated by the Precision Nitrogen Management Model. J. Environ. Qual. 45(6): 2044. doi: 10.2134/jeq2016.04.0129.
Maxwell, B.M., F. Birgand, L.A. Schipper, L.E. Christianson, S. Tian, M.J. Helmers, D.J. Williams, G.M. Chescheir, and M.A. Youssef. 2018. Drying–Rewetting Cycles Affect Nitrate Removal Rates in Woodchip Bioreactors. J. Environ. Qual. 48(1): 93. doi: 10.2134/jeq2018.05.0199.
Mayer, B., E.W. Boyer, C. Goodale, N.A. Jaworski, N. Van Breemen, R.W. Howarth, S. Seitzinger, G. Billen, K. Lajtha, K. Nadelhoffer, D. Van Dam, L.J. Hetling, M. Nosal, and K. Paustian. 2002. Sources of Nitrate in Rivers Draining Sixteen Watersheds in the Northeastern U.S.: Isotopic Constraints. Biogeochemistry 57–58: 171–197. doi: 10.1023/A:1015744002496.
McCann, I.R., M.J. McFarland, and J.A. Witz. 1991. Near-surface bare soil temperature model for biopysical models. Trans. ASAE 34(3): 0748–0755. doi: 10.13031/2013.31726.
Mclatchey, G.P., and K.R. Reddy. 1998. Regulation of Organic Matter Decomposition and Nutrient Release in a Wetland Soil. J. Environmetnal Qual. 27: 1268–1274.
Merwin, I.A., and W.C. Stiles. 1994. Orchard Groundcover Management Impacts on Apple Tree Growth and Yield , and Nutrient Availability and Uptake. J. Am. Soc. Hortic. Sci. 119(2): 209–215.
Merwin, I.A., W.C. Stiles, and H.M. van Es. 1994. Orchard groundcover management impacts on soil physical properties. J. Am. Soc. Hortic. Sci. 119(2): 216–222.
Van Meter, K.J., N.B. Basu, J.J. Veenstra, and C.L. Burras. 2016. The nitrogen legacy: emerging evidence of nitrogen accumulation in anthropogenic landscapes. Environ. Res. Lett. 11(3): 035014. doi: 10.1088/1748-9326/11/3/035014.
Mills, M.S., and E.M. Thurman. 1992. Mixed-Mode Isolation of Triazine Metabolites from Soil and Aquifer Sediments Using Automated Solid-Phase Extraction. Anal. Chem. 64(17): 1985–1990. doi: 10.1021/ac00041a038.
Mohan, D., C.U. Pittman, and P.H. Steele. 2006. Pyrolysis of Wood/Biomass for Bio-oil: A Critical Review. Energy and Fuels 20(3): 848–889. doi: 10.1021/ef0502397.
Mohanty, B.P., R.S. Bowman, J.M.H. Hendrickx, J. Simunek, and M.T. Van Genuchten. 1998. Preferential Transport of Nitrate to a Tile Drain in an Intermittent-Flood-Irrigated Field: Model Development and Experimental Evaluation. Water Resour. Res. 34(5): 1061–1076.

Montzka, S.A., E.J. Dlugokencky, and J.H. Butler. 2011. Non-CO2 greenhouse gases and climate change. Nature 476(7358): 43–50. doi: 10.1038/nature10322.
Moorman, T.B., K. Jayachandran, and A. Reungsang. 2001. Adsorption and desorption of atrazine in soils and subsurface sediments. Soil Sci. 166(12): 921–929. doi: 10.1097/00010694-200112000-00006.
Moorman, T.B., T.B. Parkin, T.C. Kaspar, and D.B. Jaynes. 2010. Denitrification activity, wood loss, and N2O emissions over 9 years from a wood chip bioreactor. Ecol. Eng. 36(11): 1567–1574. doi: 10.1016/j.ecoleng.2010.03.012.
Myrold, D.D., and N.R. Posavatz. 2007. Potential importance of bacteria and fungi in nitrate assimilation in soil. Soil Biol. Biochem. 39(7): 1737–1743. doi: 10.1016/J.SOILBIO.2007.01.033.
Nash, J.E., and J. V Sutcliffe. 1970. River flow forecasting through conceptual models Part I-a discussion of principles. J. Hydrol. 10: 282–290. doi: 10.1016/0022-1694(70)90255-6.
Neeley, J., E. Giddings, and C. Pearson. 1965. Soil Survey Tompkins County, New York. USDA, Washington. D.C.
Ochoa-Herrera, V., G. León, Q. Banihani, J.A. Field, and R. Sierra-Alvarez. 2011. Toxicity of Copper(II) Ions to Microorganisms in Biological Wastewater Treatment Systems. Sci. Total Environ. 412–413: 380–385. doi: 10.1016/j.scitotenv.2011.09.072.
Ogawa, S., P. Baveye, C.W. Boast, J.-Y. Parlange, and T. Steenhuis. 2000. Surface fractal characteristics of preferential flow patterns in field soils: evaluation and effect of image processing. Fractals soil Sci. 88(1999): 19–46. doi: 10.1016/S0166-2481(00)80004-5.
Paré, D., R. Boutin, G.R. Larocque, and F. Raulier. 2006. Effect of temperature on soil organic matter decomposition in three forest biomes of eastern Canada. Can. J. Soil Sci. 86(Special Issue): 247–256. doi: 10.4141/S05-084.
Pearson, C., R. Parsons, N. Hulbert, and W. Williams. 1973. Soil Survey of Chemung County, New York. USDA, Washington. D.C.
Peranginangin, N.P., B.K. Richards, and T.S. Steenhuis. 2009. Assessment of vadose zone sampling methods for detection of preferential herbicide transport. Hydrol. Earth Syst. Sci. Discuss. 6(6): 7247–7285. doi: 10.5194/hessd-6-7247-2009.
Perrin, C., C. Michel, and V. Andréassian. 2001. Does a large number of parameters enhance model performance? Comparative assessment of common catchment model structures on 429 catchments. J. Hydrol. 242(3–4): 275–301. doi: 10.1016/S0022-1694(00)00393-0.
Pfaff, J. 1993a. Method 300.0 Determination of Inorganic Anions by Ion Chromatography. EPA Doc. #. USEPA Environmental Monitoring Systems Lab, Cincinnati, OH.
Pfaff, J. 1993b. Methods for the Determination of Inorganic Substances in Environmental Samples (EPA/600/R-93/100). Method 300.0.
Pivetz, B.E., and T.S. Steenhuis. 1995. Soil matrix and macropore biodegradation of 2,4-D. J. Environ. Qual. 24(4): 564. doi: 10.2134/jeq1995.00472425002400040002x.
Pluer, W., L. Geohring, T.S. Steenhuis, T.M. Walter, and M. Todd Walter. 2016. Controls Influencing the Treatment of Excess Agricultural Nitrate With Denitrifying Bioreactors. J. Environ. Qual. 45: 772–778. doi: 10.2134/jeq2015.06.0271.
Pluer, W.T., C.K. Morris, M.T. Walter, and L.D. Geohring. 2019. Denitrifying bioreactor response during storm events. Agric. Water Manag. 213(January): 1109–1115. doi:

10.1016/j.agwat.2018.12.004.
Porter, M.D., J.M. Andrus, N.A. Bartolerio, L.F. Rodriguez, Y. Zhang, J.L. Zilles, and A.D. Kent. 2015. Seasonal patterns in microbial community composition in denitrifying bioreactors treating subsurface agricultural drainage. Microb. Ecol. 70(3): 710–723. doi: 10.1007/s00248-015-0605-8.
Potter, B.B., and J.C. Wimsatt. 2009. Method 415.3 Determination of total organic carbon and specific UV absorbance at 254nm in source water and drinking water. EPA Doc. #EPA/600/R-09/122: 415.1-1: 415.3-56.
Prévoteau, A., F. Ronsse, I. Cid, P. Boeckx, and K. Rabaey. 2016. The electron donating capacity of biochar is dramatically underestimated. Sci. Rep. 6(June): 1–11. doi: 10.1038/srep32870.
Queyrel, W., F. Habets, H. Blanchoud, D. Ripoche, and M. Launay. 2016. Pesticide fate modeling in soils with the crop model STICS: Feasibility for assessment of agricultural practices. Sci. Total Environ. 542: 787–802. doi: 10.1016/j.scitotenv.2015.10.066.
Quisenberry, V.L., and R.E. Phillips. 1976. Percolation of Surface-applied Water in the Field. Soil Sci. Soc. Am. J. 40(75): 484–489.
Rana, R., R. Langenfeld-Heyser, R. Finkeldey, and A. Polle. 2010. FTIR Spectroscopy, Chemical and Histochemical Characterisation of Wood and Lignin of Five Tropical Timber Wood Species of the Family of Dipterocarpaceae. Wood Sci. Technol. 44(2): 225–242. doi: 10.1007/s00226-009-0281-2.
Randall, G.W., J.A. Vetsch, and J.R. Huffman. 2003. Nitrate losses in subsurface drainage from a corn-soybean rotation as affected by time of nitrogen application and use of nitrapyrin. J. Environ. Qual. 32: 1764–1772.
Reddy, K.R., and D.R. Delaune. 2008. Biogeochemistry of Wetlands; Science and Applications. Taylor& Francis Group, LLC, Boca Raton, FL.
Rice, C.W., and J.M. Tiedje. 1989. Regulation of nitrate assimilation by ammonium in soils and in isolated soil microorganisms. Soil Biol. Biochem. 21(4): 597–602. doi: 10.1016/0038-0717(89)90135-1.
Richard, T.L., and T.S. Steenhuis. 1988. Tile drain sampling of preferential flow on a field scale. J. Contam. Hydrol. 3(2–4): 307–325. doi: 10.1016/0169-7722(88)90038-1.
Richards, B.K., T.S. Steenhuis, J.H. Peverly, and M.B. McBride. 2000. Effect of sludge-processing mode, soil texture and soil pH on metal mobility in undisturbed soil columns under accelerated loading. Environ. Pollut. 109(2): 327–346. doi: 10.1016/S0269-7491(99)00249-3.
Ritsema, C.J., and L.W. Dekker. 1995. Distribution flow: A general process in the top layer of water repellent soils. Water Resour. Res. 31(5): 1187–1200. doi: 10.1029/94WR02979.
Ro, K.S., and K.H. Chung. 1995. Atrazine Biotransformation in Wetland Sediment Under Different Nutrient Conditions-II: Aerobic. J. Environ. Sci. Heal. A 30(1): 121–131. doi: 10.1080/10934529509376190.
Robertson, W.D. 2010. Nitrate removal rates in woodchip media of varying age. Ecol. Eng. 36(11): 1581–1587. doi: 10.1016/j.ecoleng.2010.01.008.
Robertson, W.D., J.L. Vogan, and P.S. Lombardo. 2008. Nitrate removal rates in a 15-Year-Old permeable reactive barrier treating septic system nitrate. Gr. Water Monit. Remediat. 28(3): 65–72. doi: 10.1111/j.1745-6592.2008.00205.x.

Rocha, C., E.A. Pappas, and C. Huang. 2008. Determination of trace triazine and chloroacetamide herbicides in tile-fed drainage ditch water using solid-phase microextraction coupled with GC- MS. Environ. Pollut. 152. doi: 10.1016/j.envpol.2007.04.029.

De Rooij, G.H., and P. De Vries. 1996. Solute leaching in a sandy soil with a water-repellent surface layer: A simulation. Geoderma 70(2–4): 253–263. doi: 10.1016/0016-7061(95)00081-X.

Rothstein, E., T.S. Steenhuis, J.H. Peverly, and L.D. Geohring. 1996. Atrazine Fate on a Tile Drained Field in Northern New York: A Case Study. Agric. Water Manag. 31(3): 195–203. doi: 10.1016/0378-3774(96)01250-4.

Saia, S.M., P.J. Sullivan, J.M. Regan, H.J. Carrick, A.R. Buda, N.A. Locke, and M.T. Walter. 2017. Evidence for Polyphosphate Accumulating Organism (PAO)-Mediated Phosphorus Cycling in Stream Biofilms Under Alternating Aerobic/Anaerobic Conditions. Freshw. Sci. 36(2): 284–296. doi: 10.1086/691439.

Sánchez-Sánchez, R., D. Ahuatzi-Chacón, J. Galíndez-Mayer, N. Ruiz-Ordaz, and A. Salmerón-Alcocer. 2013. Removal of Triazine Herbicides From Aqueous Systems By a Biofilm Reactor Continuously or Intermittently Operated. J. Environ. Manage. 128: 421–426. doi: 10.1016/j.jenvman.2013.05.050.

Sanders, E.C., M.R. Abou Najm, R.H. Mohtar, E. Kladivko, and D. Schulze. 2012. Field method for separating the contribution of surface-connected preferential flow pathways from flow through the soil matrix. Water Resour. Res. 48(4): 1–8. doi: 10.1029/2011WR011103.

Saquing, J.M., Y. Yu, and P.C. Chiu. 2016. Wood-Derived Black Carbon (Biochar) as a Microbial Electron Donor and Acceptor. Environ. Sci. Technol. Lett. 3(2): 62–66. doi: 10.1021/acs.estlett.5b00354.

Sass, J.B., and A. Colangelo. 2006. European Union Bans Atrazine, While the United States Negotiates Continued Use. Int. J. Occup. Environ. Health 12(3): 260–267. doi: 10.1179/oeh.2006.12.3.260.

Saunders, L., M. Koontz, and R. Pezeshki. 2013. Root-Zone Glyphosate Exposure Adversely Affects Two Ditch Species. Biology (Basel). 2(4): 1488–1496. doi: 10.3390/biology2041488.

Schipper, L.A., G.F. Barkle, and M. Vojvodic-Vukovic. 2005. Maximum Rates of Nitrate Removal in a Denitrification Wall. J. Environ. Qual. 34(4): 1270. doi: 10.2134/jeq2005.0008.

Schipper, L.A., W.D. Robertson, A.J. Gold, D.B. Jaynes, and S.C. Cameron. 2010. Denitrifying Bioreactors—An Approach For Reducing Nitrate Loads to Receiving Waters. Ecol. Eng. 36(11): 1532–1543. doi: 10.1016/j.ecoleng.2010.04.008.

Schipper, L., and M. Vojvodić-Vuković. 1998. Nitrate Removal From Groundwater Using a Denitrification Wall Amended With Sawdust: Field Trial. J. Environ. Qual. 27(3): 664. doi: 10.2134/jeq1998.00472425002700030025x.

Seitzinger, S., J. Harrison, J. Bohlke, A. Bouwman, R. Lowrance, B. Peterson, C. Tobias, and G. Van Drecht. 2006. Denitrification across landscaes and waterscapes: a synthesis. Ecol. Appl. 16(6): 2064–2090. doi: 10.1890/1051-0761(2006)016[2064:DALAWA]2.0.CO;2.

Selker, J., J.-Y. Parlange, and T. Steenhuis. 1992. Fingered Flow in Two Dimentions 2. Predicting Finger Moisture Pofile. 28(9): 2523–2528.

Seybold, C.A., W. Mersie, and C. Mcnamee. 2001a. Anaerobic Degradation of Atrazine and Metolachlor and Metabolite Formation in Wetland Soil and Water Microcosms. J. Environ. Qual. 30: 1271–1277.

Seybold, C.A., W. Mersie, and C. McNamee. 2001b. Anaerobic degradation of atrazine and metolachlor and metabolite formationin wetland soil and water research. J. Environ. Qual. 30(4): 1271–1277.

Shalit, G., and T. Steenhuis. 1996. A simple mixing layer model predicting solute flow to drainage lines under preferential flow. J. Hydrol. 183: 139–149.

Shimabukuro, R.H., and H.R. Swanson. 1969. Atrazine metabolism, selectivity, and mode of action. J. Agric. Food Chem. 17(2): 199–205. doi: 10.1021/jf60162a044.

Shipitalo, M.J., R.W. Malone, L. Ma, B.T. Nolan, R.S. Kanwar, D.L. Shaner, and C.H. Pederson. 2016. Corn stover harvest increases herbicide movement to subsurface drains - Root Zone Water Quality Model simulations. Pest Manag. Sci. 72(6): 1124–1132. doi: 10.1002/ps.4087.

Shirmardi, M., N. Alavi, E.C. Lima, A. Takdastan, A.H. Mahvi, and A.A. Babaei. 2016. Removal of atrazine as an organic micro-pollutant from aqueous solutions : a comparative study. Process Saf. Environ. Prot. 103: 23–35. doi: 10.1016/j.psep.2016.06.014.

Siczek, A., U. Kotowska, J. Lipiec, and A. Nosalewicz. 2008. Macro-porosity and leaching of atrazine in tilled and orchard loamy soils. Chemosphere 70(11): 1973–1978. doi: 10.1016/j.chemosphere.2007.09.038.

Simunek, J., M.T. van Genuchten, and M. Senja. 2005. The HYDRUS-1D software package for simulating the one-dimensional movement of water, heat, and multiple solutes in variably-saturated media. Version 3. Dep. Environ. Sci., Univ. Calif., Riverside. (April): 270.

Simunek, J., N.J. Jarvis, M.T. van Genuchten, and A. Gardenas. 2003. Review and comparison of models for describing non-equilibrium and preferential flow and transport in the vadose zone. J. Hydrol. 272(1–4): 14–35. doi: 10.1016/S0022-1694(02)00252-4.

Simunek, J., M. Sejna, H. Saito, M. Sakai, and M.T. van Genuchten. 2009. The HYDRUS-1D software package for simulating the one-dimensional movement of water, heat, and multiple solutes in variably-saturated media. Version 4.08. Dep. Environ. Sci., Univ. Calif., Riverside. (January): 332. doi: 10.1007/SpringerReference_28001.

Singh, B.P., B.J. Hatton, S. Balwant, A.L. Cowie, and A. Kathuria. 2009. Influence of biochars on nitrous oxide emission and nitrogen leaching from two contrasting soils. J. Environ. Qual. 39(4): 1224–1235. doi: 10.2134/jeq2009.0138.

Sinkevich, M.G., M.T. Walter, A.J. Lembo, B.K. Richards, N. Peranginangin, S.A. Aburime, and T.S. Steenhuis. 2005. A GIS-based ground water contamination risk assessment tool for pesticides. Gr. Water Monit. Remediat. 25(4): 82–91. doi: 10.1111/j.1745-6592.2005.00055.x.

Smith, G.A., B.V. Pepich, and D.J. Munch. 2007. Determination of Triazine Pesticides and Their Degradates in Drinking Water by Liquid Chromatography Elestrospray Ionization Tandem Mass Spectrometry (LC/ESI-MS/MS). : 1–32.

Smith, M.C., D.L. Thomas, A.B. Bottcher, and K.L. Campbell. 1990. Measurement of pesticide transport to shallow ground water. Trans. ASAE 33(5): 1573–1582.

Smith, V.H., G.D. Tilman, and J.C. Nekola. 1999. Eutrophication : Impacts of Excess

Nutrient Inputs on Freshwater , Marine , and Terrestrial Ecosystems. environmnetal Pollut. 100: 179–196.

Soares, M.I.M., and A. Abeliovich. 1998. Wheat straw as substrate for water denitrification. Water Res. 32(12): 3790–3794. doi: 10.1016/S0043-1354(98)00136-5.

De Souza, M.L., M.J. Sadowsky, and L.P. Wackett. 1996. Atrazine chlorohydrolase from Pseudomonas sp. Strain ADP: Gene sequence, enzyme purification, and protein characterization. J. Bacteriol. 178(16): 4894–4900. doi: 10.1128/jb.178.16.4894-4900.1996.

Spokas, K.A., W.C. Koskinen, J.M. Baker, and D.C. Reicosky. 2009. Impacts of Woodchip Biochar Additions on Greenhouse Gas Production and Sorption/Degradation of Two Herbicides in a Minnesota Soil. Chemosphere 77(4): 574–581. doi: 10.1016/j.chemosphere.2009.06.053.

Steenhuis, T.S., C.E. Baver, B. Hasanpour, C.R. Stoof, D.A. DiCarlo, and J.S. Selker. 2013. Pore scale consideration in unstable gravity driven finger flow. Water Resour. Res. 49(11): 7815–7819. doi: 10.1002/2013WR013928.

Steenhuis, T.S., M. Bodnar, L.D. Geohring, S.-A. Aburime, and R. Wallach. 1997. A simple model for predicting solute concentration in agricultural tile lines shortly after application. Hydrol. Earth Syst. Sci. 1(4): 823–833. doi: 10.5194/hess-1-823-1997.

Steenhuis, T.S., J. Boll, G. Shalit, J.S. Selker, and I. a. Merwin. 1994. A Simple equation for predicting preferential flow solute concentrations. J. Environ. Qual. 23(5): 1058. doi: 10.2134/jeq1994.00472425002300050030x.

Steenhuis, T.S., Y.J. Kim, J.Y. Parlange, M.. Akhtar, B.K. Richards, K.-J.S. Kung, T.J. Gish, L.W. Dekker, C.J. Ritsema, and S.. Aburime. 2001. An Equation for Describing Solute Transport in Field Soils with Preferential Flow Paths. p. 137–140. *In* Bosch, D., King, K. (eds.), Preferential Flow Water: Movement and Chemical Transport in the Environment, Proc. 2nd Intl.Symp . Honolulu, Hawaii, USA.

Steenhuis, T.S., W. Staubitz, M.S. Andreini, J. Surface, T.L. Richard, R. Paulsen, N.B. Pickering, J.R. Hagerman, and L.D. Geohring. 1990. Preferential Movement of Pesticides and Tracers in Agricultural Soils. J. Irrig. Drain. Eng. 116(1): 50–66. doi: 10.1061/(ASCE)0733-9437(1990)116:1(50).

Stevenson, F.J. 1972. Organic Matter Reactions Involving Herbicides in Soil1. J. Environ. Qual. 1(4): 333. doi: 10.2134/jeq1972.00472425000100040001x.

Swiatkowski, A., M. Pakula, S. Biniak, and M. Walczyk. 2004. Influence of the surface chemistry of modified activated carbon on its electrochemical behaviour in the presence of lead (II) ions. Carbon N. Y. 42: 3057–3069. doi: 10.1016/j.carbon.2004.06.043.

Taylor, J.M., M.T. Moore, and J.T. Scott. 2015. Contrasting Nutrient Mitigation and Denitrification Potential of Agricultural Drainage Environments with Different Emergent Aquatic Macrophytes. J. Environ. Qual. 44(4): 1304. doi: 10.2134/jeq2014.10.0448.

Tillitt, D.E., D.M. Papoulias, J.J. Whyte, and C.A. Richter. 2010. Atrazine reduces reproduction in fathead minnow (Pimephales promelas). Aquat. Toxicol. 99(2): 149–159. doi: 10.1016/j.aquatox.2010.04.011.

Tindall, J.A., and W.K. Vencill. 1995. Transport of atrazine, 2,4-D, and dicamba through preferential flowpaths in an unsaturated claypan soil near Centralia, Missouri. J.

Hydrol. 166(1–2): 37–59. doi: 10.1016/0022-1694(94)02603-9.
Toccalino, P.L., R.J. Gilliom, B.D. Lindsey, and M.G. Rupert. 2014. Pesticides in Groundwater of the United States: Decadal-scale Changes, 1993-2011. Ground Water 52: 112–125. doi: 10.1111/gwat.12176.
Torrentó, C., V. Prasuhn, E. Spiess, A. Melsbach, C. Lihl, T.B. Hofstetter, M. Elsner, and D. Hunkeler. 2018. Adsorbing vs . Nonadsorbing Tracers for Assessing Pesticide Transport in Arable Soils. Vadose Zo. J. 17(1). doi: 10.2136/vzj2017.01.0033.
Tsaboula, A., G. Menexes, E. Papadakis, Z. Vryzas, A. Kotopoulou, K. Kintzikoglou, and E. Papadopoulou-mourkidou. 2019. Science of the Total Environment Assessment and management of pesticide pollution at a river basin level part II : Optimization of pesticide monitoring networks on surface aquatic ecosystems by data analysis methods. Sci. Total Environ. 653: 1612–1622. doi: 10.1016/j.scitotenv.2018.10.270.
Vanclooster, A., J.J.T.I. Boesten, and M. Trevisan. 2000. Mathematical modeling for assessing pesticide leaching in agricultural soils at the field scale. p. 407–430. *In* Pesticide/soil interactions some current reseach methods. Institut National De La Recherche Agronomique (INRA), Paris.
Vanderheyden, V., P. Debongnie, and L. Pussemier. 1997. Accelerated Degradation and Mineralization of Atrazine in Surface and Subsurface Soil Materials. Pestic. Sci. 49(3): 237–242. doi: 10.1002/(SICI)1096-9063(199703)49:3<237::AID-PS511>3.0.CO;2-4.
van Verseveld, W.J., J.J. McDonnell, and K. Lajtha. 2009. The role of hillslope hydrology in controlling nutrient loss. J. Hydrol. 367(3–4): 177–187. doi: 10.1016/j.jhydrol.2008.11.002.
Van Verseveld, W.J., J.J. McDonnell, and K. Lajtha. 2008. A mechanistic assessment of nutrient flushing at the catchment scale. J. Hydrol. 358(3–4): 268–287. doi: 10.1016/j.jhydrol.2008.06.009.
Vryzas, Z. 2018. Pesticide fate in soil-sediment-water environment in relation to contamination preventing actions. Curr. Opin. Environ. Sci. Heal. 4: 5–9. doi: 10.1016/j.coesh.2018.03.001.
Vryzas, Z., E.N. Papadakis, G. Vassiliou, and E. Papadopoulou-Mourkidou. 2012. Occurrence of pesticides in transboundary aquifers of North-eastern Greece. Sci. Total Environ. 441: 41–48. doi: 10.1016/j.scitotenv.2012.09.074.
Wang, G.-S. 2005. Effects of Natural Organic Matter on Adsorption Capacity For Atrazine by Activated Carbon. J. Chinese Inst. Environ. Eng. 15(2): 81–89.
Warneke, S., L.A. Schipper, D.A. Bruesewitz, and W.T. Baisden. 2011a. A comparison of different approaches for measuring denitrification rates in a nitrate removing bioreactor. Water Res. 45(14): 4141–51. doi: 10.1016/j.watres.2011.05.027.
Warneke, S., L. a. Schipper, D. a. Bruesewitz, I. McDonald, and S. Cameron. 2011b. Rates, Controls and Potential Adverse Effects of Nitrate Removal in a Denitrification Bed. Ecol. Eng. 37(3): 511–522. doi: 10.1016/j.ecoleng.2010.12.006.
Warneke, S., L.A. Schipper, M.G. Matiasek, K.M. Scow, S. Cameron, D. a Bruesewitz, and I.R. McDonald. 2011c. Nitrate Removal, Communities of Denitrifiers and Adverse Effects in Different Carbon Substrates for Use in Denitrification Beds. Water Res. 45(17): 5463–5475. doi: 10.1016/j.watres.2011.08.007.
Warnemuende, E.A., J.P. Patterson, D.R. Smith, and C. Huang. 2007. Effects of Tilling No-till Soil on Losses of Atrazine and Glyphosate to Runoff Water Under Variable

Intensity Simulated Rainfall. J. Soil Tillage Res. 95: 19–26. doi: 10.1016/j.still.2006.09.001.

WHO. 2010. Atrazine and Its Metabolites in Drinking-water; Background Document For Development of WHO Guidelines For Drinking-Water Quality. WHO/HSE/WSH/10.01/11. http://www.who.int/entity/water_sanitation_health/dwq/chemicals/Fourth_Edition_Atrazine_Document_Draft.doc.

Wilhelm, E., R. Batting, and R.J. Wilcock. 1977. Low-pressure Solubility of gases in liquid water. Chem. Rev. 77(2). doi: 10.1021/cr60306a003.

Williams, M.R., K.W. King, and N.R. Fausey. 2015. Contribution of tile drains to basin discharge and nitrogen export in a headwater agricultural watershed. Agric. Water Manag. 158: 42–50. doi: 10.1016/j.agwat.2015.04.009.

Wilson, R.D., J. Geronimo, and J.A. Armbruster. 1997. 2,4-D dissipation in field soils after applications of 2,4-D dimethylamine salt and 2,4-D 2-ethylhexyl ester. Environ. Toxicol. Chem. 16(6): 1239–1246. doi: 10.1002/etc.5620160620.

Woli, K.P., M.B. David, R.A. Cooke, G.F. McIsaac, and C.A. Mitchell. 2010. Nitrogen balance in and export from agricultural fields associated with controlled drainage systems and denitrifying bioreactors. Ecol. Eng. 36(11): 1558–1566. doi: 10.1016/j.ecoleng.2010.04.024.

Wu, L., B. Gao, Y. Tian, and R. Muñoz-Carpena. 2014. Analytical and experimental analysis of solute transport in heterogeneous porous media. J. Environ. Sci. Heal. - Part A Toxic/Hazardous Subst. Environ. Eng. 49(3): 338–343. doi: 10.1080/10934529.2014.846686.

Wu, Y.S., H.H. Liu, and G.S. Bodvarsson. 2004. A triple-continuum approach for modeling flow and transport processes in fractured rock. J. Contam. Hydrol. 73(1–4): 145–179. doi: 10.1016/j.jconhyd.2004.01.002.

Xu, H., X. Wang, H. Yao, J. Su, H. Li, and Y.-G. Zhu. 2014. Biochar impacts soil microbial community composition and nitrogen cycling in an acidified soil planted with rape. Environ. Sci. Technol. 17(i): 9391–9399. doi: 10.1021/es5021058.

Yu, L., Y. Wang, Y. Yuan, J. Tang, and S. Zhou. 2016. Biochar as Electron Acceptor for Microbial Extracellular Respiration. Geomicrobiol. J. 33(6): 530–536. doi: 10.1080/01490451.2015.1062060.

Zhang, Z.B., X. Peng, H. Zhou, H. Lin, and H. Sun. 2015. Characterizing preferential flow in cracked paddy soils using computed tomography and breakthrough curve. Soil Tillage Res. 146(PA): 53–65. doi: 10.1016/j.still.2014.05.016.

Zhang, P., H. Sun, L. Yu, and T. Sun. 2013. Adsorption and Catalytic Hydrolysis of Carbaryl and Atrazine on Pig Manure-derived Biochars: Impact of Structural Properties of Biochars. J. Hazard. Mater. 244–245: 217–224. doi: http://dx.doi.org/10.1016/j.jhazmat.2012.11.046.

Zhang, N., Y. Wang, Q. Sun, and Y. Wang. 2018. Multiscale mass transfer coupling of triple-continuum and discrete fractures for flow simulation in fractured vuggy porous media. Int. J. Heat Mass Transf. 116: 484–495. doi: 10.1016/j.ijheatmasstransfer.2017.09.046.

Zhang, G., Q. Zhang, K. Sun, X. Liu, W. Zheng, and Y. Zhao. 2011. Sorption of Simazine to Corn Straw Biochars Prepared at Different Pyrolytic Temperatures. Environ. Pollut. 159(10): 2594–2601. doi: 10.1016/j.envpol.2011.06.012.

Zou, X.M., H.H. Ruan, Y. Fu, X.D. Yang, and L.Q. Sha. 2005. Estimating soil labile organic carbon and potential turnover rates using a sequential fumigation-incubation procedure. Soil Biol. Biochem. 37(10): 1923–1928. doi: 10.1016/j.soilbio.2005.02.028.